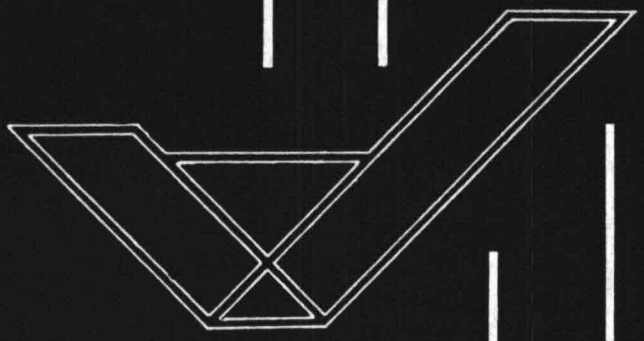

# Fully developed laminar flow in curved ducts

H.J. de Vriend

Internal report no. 2-78

Laboratory of Fluid Mechanics

Department of Civil Engineering

Delft University of Technology

H.J. Gruel
78-602

# Fully developed laminar flow in curved ducts

H.J. de Vriend

Internal report no. 2-78
Laboratory of Fluid Mechanics
Department of Civil Engineering
Delft University of Technology
Delft, The Netherlands

Contents

LIST OF FIGURES

21. Separate computation of the vertical distribution of the main velocity
22. Analysis of the mean velocity redistribution
23. Analysis of the vertical redistribution of the main velocity
24. Influence of secondary flow inertia on the flow in a shallow channel
25. Influence of neglecting all radial derivatives in the stream-fuction equation in case of a given main velocity distribution
26. Successive approximation of the main velocity by low Dean number perturbations in the whole cross-section
27. Basic solution for the central region
28. Successive approximation of the main velocity in the central region
29. Solution of $\bar{u}$ from depth-averaged equations derived from the low Dean number expansion (zero order approximation of the secondary flow)
30. Solution of depth-averaged equations derived from the low Dean number expansion (secondary flow updated in each iteration step)
31. Similarity solution

LIST OF SYMBOLS

| | |
|---|---|
| $a$ | radius of circular pipe cross-section |
| $A$ | cross-sectional area |
| $B$ | channel width |
| $C$ | Chezy's factor |
| $d$ | depth of flow |
| $De = Re\sqrt{d/R_c}$ | Dean number |
| $De_T$ | Dean number based on the turbulence viscosity |
| $e$ | normalized energy head |
| $E = p + \frac{1}{2}\epsilon^2 Re\ (v^2 + w^2)$ | |
| $Eq_k$ | k-th order perturbation of the longitudinal momentum equation |
| $f$ | vertical distribution function of the main velocity |
| $f' = f \ast \overline{f'}$ | |
| $f_0$ | vertical distribution function of u in a straight channel |
| $f_{1,1}$, $f_{1,2}$ | vertical distribution functions in $u_{1,1}$ and $u_{1,2}$ |
| $f_1(\zeta), f_2(\zeta)$ | polynominals in the first order perturbation of u |
| $g$ | acceleration due to gravity |
| $g$ | vertical distribution function of the streamfunction $\psi$ |
| $g' = g \ast \overline{g'}$ | |
| $i$ | vertical nodal point index in the computational grid |
| $j$ | horizontal nodal point index in the computational grid |
| $k$ | perturbation index |
| $k_1, k_2$ | constants in the inviscid core solution of u |
| $M$ | horizontal number of meshes of the computational grid |
| $n$ | iteration index |
| $N$ | vertical number of meshes of the computational grid |
| $p$ | pressure |
| $p'$ | normalized pressure |
| $p$ | normalized total pressure |
| $Q$ | discharge |
| $r$ | normalized radial coordinate |
| $R$ | radial coordinate |
| $R_c$ | radius of curvature of the channel axis |
| $R_{in}$ | radius of curvature of the inner wall |
| $R_{ou}$ | radius of curvature of the outer wall |

| | |
|---|---|
| $Re = \frac{Vd}{\nu}$ | Reynoldsnumber |
| $s = R\phi$ | longitudinal coordinate |
| $s'$ | normalized longitudinal coordinate |
| $u$ | normalized main velocity component |
| $\bar{u}$ | depth-averaged main velocity |
| $u' = u/\imath$ | |
| $u_k$ | k-th order perturbation of u |
| $u_{1,0}, u_{1,1}, u_{1,2}$ | constituents of $u_1$ |
| $v$ | normalized velocity-component |
| $V = Q/Bd$ | velocity scale |
| $v_R, v_\phi, v_z$ | velocity components in the cylindrical coordinate system (R,$\phi$,z |
| $w$ | normalized vertical velocity component |
| $y = R - R_{in}$ | transverse coordinate |
| $z$ | vertical coordinate |
| $z_b$ | vertical coordinate of the bottom |

| | |
|---|---|
| $\alpha$ | damping factor |
| $\alpha_i$ | direction of the main velocity isovels |
| $\alpha_s$ | direction of the streamlines of the secondary flow |
| $\delta$ | small constant in the termination criterion |
| $\Delta\zeta$ | vertical mesh size of the computational grid |
| $\Delta\xi$ | horizontal mesh size of the computational grid |
| $\frac{\delta}{\delta\zeta}, \frac{\delta}{\delta\xi}$ | finite difference representation of $\frac{\partial}{\partial\zeta}$ and $\frac{\partial}{\partial\xi}$ |
| $\zeta$ | normalized vertical coordinate |
| $\eta$ | dynamic viscosity of the fluid |
| $\imath$ | longitudinal slope factor |
| $\imath_o$ | longitudinal slope factor in the equivalent straight channel flow |
| $\nu$ | kinematic viscosity of the fluid |
| $\nu_T$ | kinematic turbulence viscosity |
| $\xi$ | normalized transverse coordinate |
| $\rho$ | mass density of the fluid |
| $\phi$ | angular coordinate |
| $\phi'$ | normalized angular coordinate |
| $\psi$ | normalized stream function of the secondary flow |
| $\bar{\psi}$ | depth-averaged value of $\psi$ |

$\hat{\psi}$ maximum of $\psi$

$\psi' = \psi \times Re$

$\omega$ normalized secondary flow vorticity

$\omega = \omega_2 \times Re$

$$\nabla^2 = \frac{\partial^2}{\partial \xi^2} + \frac{\partial^2}{\partial \zeta^2} + \frac{\varepsilon}{r}\frac{\partial}{\partial \xi} - \frac{\varepsilon^2}{r^2}$$

$\nabla^2$ finite difference representation of $\nabla^2$

SUMMARY

A mathematical model of steady, fully developed laminar flow in curved ducts is developed and used to derive a simplified computation method to be applied in another mathematical model predicting the flow in river bends. The laminar flow model is verified by comparing its results with analytical, numerical and experimental results reported in the literature. A series of shallow channel computations is made and the results are analysed, both from a mathematical and from a physical point of view. Various simplified computation methods are considered, most of which yield no satisfactory results when the advective influence of the secondary flow on the main velocity is important. Only a method based on similarity approximation sufficiently accurate to be applied further.

## 1. Introduction

The flow and the bed topography in curved alluvial river channels play a promiment part in several aspects of river engineering, such as navigability, bank protection and dispersion of pollutants. Hitherto, engineering problems concerning river bends are mostly investigated using physical scale models, even though the complex character of the flow may give rise to scale effects making the model data hard to interpret in prototype terms. The increased facilities of electronic computers, however, make mathematical models attractive to be developed. They would facilitate the understanding of the physical phenomena and could be used together with or even instead of physical models.
As it is impossible to reliably predict the bed topography without knowing the flow field, an adequate model of the flow in a curved channel with an uneven bed topography must be developed first. Assuming disturbances of the flow to travel at a much higher celerity than disturbances of the bed, as is the case in most of the navigable alluvial rivers, the bed can be considered as being fixed when computing the flow. In addition, the flow can be assumed to be steady, which is allowable under many practical conditions.
The development of a mathematical model of steady flow in river bends with a fixed uneven bed forms one of the research projects of the Laboratory of Fluid Mechanics of the Delft University of Technology, as a part of the river bend project of the joint hydraulic research programme T.O.W.*)

---

*) "Toegepast Onderzoek Waterstaat", in which Rijkswaterstaat, the Delft Hydraulics Laboratory and the Delft University of Technology collaborate.

## 2. The present problem

### 2.1. General outline

When straight channel flow enters a curved section, a transverse pressure gradient develops. Under the influence of this pressure gradient, the low velocity streamlines near the bottom are more sharply curved than the streamlines of the depth-averaged flow, whereas the high velocity streamlines near the free surface have a smaller curvature than these depth-averaged flow streamlines. The resultant flow field can be considered as being composed of a "main flow" tangential to the depth-averaged flow streamlines and a "secondary flow" perpendicular to these streamlines.
In the central part of the channel this secondary flow is directed inward (i.e. towards the centre of curvature of the main flow streamlines) near the bottom and outward near the free surface. Near the sidewalls, the secondary flow is vertical, upward near the inner wall and downward near the outer wall. Consequently, the curved flow field has a helical character.
In the curved channel, the main flow is redistributed over the cross-section, partly as a consequence of the redistribution of the longitudinal pressure gradient, partly under the influence of the secondary flow. This secondary flow gives rise to an advective transport of longitudinal momentum in the transverse plane, causing longitudinal accelerations of the main flow and hence a redistribution of the main velocity.
If the curvature and the cross-sectional geometry of the channel are constant over a sufficiently long distance, the redistribution of the main velocity goes on until the transverse flux of longitudinal momentum due to advection by the secondary flow and due to the redistribution of the longitudinal pressure gradient is balanced by an opposite flux due to additional shear stresses raised by the redistributed main velocity. Then the flow has reached its fully developed stage and it has become axisymmetric.

The main velocity redistribution plays an important part in curved flows, so it must be adequately incorporated in the mathematical model to be developed. Little is known, however, about how its mechanism works exactly and about what is important and what is not in the mathematical formulation of this mechanism. Therefore the present work deals with the analysis of the main velocity redistribution in curved flows. To that end axisymmetric laminar flow is considered since it is mathematically more accessible than developing flow or turbulent flow, while the redistribution mechanism acts as well.

After the redistribution has been analysed, it will be attempted to develop a simplified computation method for curved flows that yields a satisfactory description of fully developed curved flows and that is likely to do so for developing flows, either laminar or turbulent.

## 2.2. Previous work

Fluid flow through curved channels and pipes, with its striking helical character, has engaged research workers since a long time. As early as 1868, BOUSSINESQ gave a mathematical description of the velocity components in axisymmetric laminar flow through coiled pipes with a shallow, rectangular cross-section. This was the start of an extensive series of publications on the flow in curved channels and pipes, a full review of which would become far too long. Therefore only publications that are closely connected with the present problem will be considered.

The first method widely used to solve axisymmetric laminar flow problems was a perturbation method with the Dean number $Re\sqrt{d/R_c}$ *) as a perturbation parameter (DEAN, 1927 & 1928 and ADLER, 1934 for circular pipes; ITŌ, 1951 and CUMING, 1952 for elliptic and rectangular pipes). The mostly analytical solutions obtained in this way hold good for small values of the Dean number.

---

*) Here d denotes a linear dimension of the cross-section

In another group of publications, both on laminar and on turbulent curved flows, perturbation methods are used with the geometric ratio $d/R_c$ as a perturbation parameter (ANANYAN, 1965 (1957) & 1967 for axisymmetric flow in river bends of arbitrary cross-section; ROZOVSKII, 1961 (1957) for axisymmetric flow in bends of shallow channels; DE VRIEND, 1973a & b for axisymmetric laminar flow in shallow rectangular pipes and channels; DE VRIEND, 1976 & 1977 for turbulent flow in shallow river bends). In case of axisymmetric flow, however, the series of expansions forming the solution of the problem can be reduced to Dean number expansions equivalent to those resulting from a low Dean number perturbation.

In contrast with the low Dean number theories mentioned above, several authors presented an analytical high Dean number approach of the axisymmetric laminar flow problem, assuming the secondary flow and the main velocity gradients due to viscous effects to be concentrated in thin layers along the fixed boundaries and the flow outside these boundary layers to be inviscid (ADLER, 1934 and ITŌ, 1969 for circular pipes; MORI, UCHIDA AND UKON, 1971 for square pipes; SMITH, 1976 for pipes of arbitrary cross-sectional shape; MURAMOTO, 1965 for the inviscid core flow in rectangular open channels).

At intermediate Dean numbers no important approximate simplifications are possible: the complete set of balance equations for mass and momentum, either reformulated in terms of stream function and vorticity or not, has to be solved. Although attempts have been made to do this more or less analytically (McCONALOGUE AND SRVISTAVA, 1968, applied an iterative method using Fourier series to a circular pipe), most authors used numerical methods (for rectangular pipes: CHENG AND AKIYAMA, 1970; JOSEPH, SMITH AND ADLER, 1975; CHENG, LIN AND OU, 1976).

Experiments on axisymmetric laminar flow were mostly executed in air, which requires small dimensions of the pipe in order to have sufficiently small Reynolds numbers combined with sufficiently high velocities. These small dimensions make velocity measurements quite difficult, so that most experimental data concern the pressure losses rather than the velocity field

(for square pipes: LUDWIEG, 1951, presenting friction factors; MORI, UCHIDA AND UKON, 1971, giving friction factors and main velocity distributions; JOSEPH, SMITH AND ADLER, 1975, using flow visualization to investigate the changes of the secondary flow for increasing Dean numbers). A quite different type of experiment was reported by BAYLIS (1971), who investigated the friction factor in electromagnetically driven mercury flow in a toroidal channel of square cross-section.

A most important development in the mathematical description of curved flows lies in the application of more general three-dimensional flow computation methods, such as those developed at Imperial College, London (see, for instance, PATANKAR AND SPALDING, 1972 and PRATAP AND SPALDING, 1976) for "parabolic" flows, in which the velocity and the pressure in a cross-section are not influenced by what happens further downstream, and "partially parabolic" flows, in which upstream influencing through the pressure occurs.

When applied to axisymmetric curved flow in circular pipes of not too sharp curvature, the method yields results that agree very well with measured data, both for laminar and for turbulent flow (see PATANKAR, PRATAP AND SPALDING, 1974 and 1975, respectively). Not only axisymmetric curved flow can be predicted, however, also for developing flow very satisfactory results are obtained (PRATAP AND SPALDING, 1975, for turbulent flow in a rather sharply curved pipe of shallow cross-section; HUMPHREY, TAYLOR AND WHITELAW, 1977, for laminar flow in a sharply curved square pipe; McGUIRK, 1978, for turbulent flow in a rather sharply curved open channel). The aforementioned "parabolic" flow approximation was also used by GHIA AND SOKHEY (1977), who investigated laminar flow in curved ducts of regular (circular, but mostly rectangular) cross-section.

In not too sharply curved ducts where the "parabolic" flow approximation holds good, these three-dimensional computation methods yield good predictions of the flow field at low expenses (RODI, 1978). If the flow is "patially parabolic", however, like in sharply curved ducts, where the influence of the bend is perceptible in the flow field and the pressure distribution upstream (McGUIRK, 1978), the predictions are still good, but the expenses are high. Therefore, it is still

worthwhile to investigate the possibility of simplified computation methods for the flow in river bends.

In river problems, considerations are often limited to shallow channels, which provides the possibility of applying a depth-averaged mathematical model, thus reducing the number of dimensions in the mathematical problem (LESCHZINER, 1978). In addition, a free surface and an uneven bed can easily be accounted for in such depth-averaged models. The dispersion terms generated by integrating the nonlinear momentum equation over the depth of flow, however, play an important part in curved flow, where the advective influence of the secondary flow on the main flow is important. This becomes evident from depth-averaged curved flow computations in which the dispersion terms representing this advective influence were neglected (DE VRIEND, 1976 & 1977). The results of these computations show important errors, especially in the second part of the bend and further downstream (see also DE VRIEND AND KOCH, 1977 & 1978). So in order to make depth-averaged equations suited to describe curved flow in shallow channels, a closer investigation of the dispersion terms is necessary.

## 3. Mathematical model of axisymmetric laminar flow

### 3.1. Mathematical formulation of the problem

Incompressible laminar flow is described mathematically by the Navier Stokes equations, the equation of continuity and a relevant set of boundary and initial conditions. In a cylindrical coordinate system (R, $\phi$, z) with vertical z-axis (figure 1) the Navier Stokes equations for axisymmetric, incompressible steady flow read

$$v_R \frac{\partial v_\phi}{\partial R} + v_z \frac{\partial v_\phi}{\partial z} + \frac{v_R v_\phi}{R} = - \frac{1}{\rho} \frac{1}{R} \frac{\partial p}{\partial \phi} + \frac{\eta}{\rho} \left( \frac{\partial^2 v_\phi}{\partial z^2} + \frac{\partial^2 v_\phi}{\partial R^2} + \frac{1}{R} \frac{\partial v_\phi}{\partial R} - \frac{v_\phi}{R^2} \right) \qquad (3.1)$$

$$v_R \frac{\partial v_R}{\partial R} + v_z \frac{\partial v_R}{\partial z} - \frac{v_\phi^2}{R} = - \frac{1}{\rho} \frac{\partial p}{\partial R} + \frac{\eta}{\rho} \left( \frac{\partial^2 v_R}{\partial z^2} + \frac{\partial^2 v_R}{\partial R^2} + \frac{1}{R} \frac{\partial v_R}{\partial R} - \frac{v_R}{R^2} \right) \qquad (3.2)$$

$$v_R \frac{\partial v_z}{\partial R} + v_z \frac{\partial v_z}{\partial z} = - g - \frac{1}{\rho} \frac{\partial p}{\partial z} + \frac{\eta}{\rho} \left( \frac{\partial^2 v_z}{\partial z^2} + \frac{\partial^2 v_z}{\partial R^2} + \frac{1}{R} \frac{\partial v_z}{\partial R} \right) \qquad (3.3)$$

in which

$v_R$, $v_\phi$, $v_z$ = velocity components in R, $\phi$ and z-direction, respectively

p = pressure

$\rho$ = mass density of the fluid

$\eta$ = dynamic viscosity of the fluid

g = acceleration due to gravity

The equation of continuity for axisymmetric flow reads

$$\frac{\partial v_R}{\partial R} + \frac{v_R}{R} + \frac{\partial v_z}{\partial z} = 0 \qquad (3.4)$$

and the integral condition of continuity becomes

$$\iint_A v_\phi dA = Q \tag{3.5}$$

in which

A = cross-sectional area
Q = discharge

As the shape of the cross-section is not expected to play an essential part in the mechanism of velocity redistribution under the influence of curvature, only rectangular cross-sections are considered with a horizontal bottom and vertical sidewalls.
The free surface is replaced by a frictionless rigid plate parallel to the bottom at distance d, which exterts only normal stresses upon the fluid. In free surface flow, this schematization is allowed for low Froude numbers.
The boundary conditions at the bottom and the sidewalls, arising from the impermeability of these walls and the no-slip conditions there, are

$$v_R = 0;\ v_\phi = 0;\ v_z = 0 \qquad \text{at } z = z_b,\ R = R_{in} \text{ and } R = R_{ou} \tag{3.6}$$

in which

$z_b$ = the vertical coordinate of the bottom
$R_{in}$ = the radial coordinate of the inner sidewall
$R_{ou}$ = the radial coordinate of the outer sidewall

The boundary conditions at the "surface" arise from the impermeability of this boundary and the zero tangent shear stress:

$$v_z = 0;\ \frac{\partial v_\phi}{\partial z} = 0;\ \frac{\partial v_R}{\partial z} = 0 \qquad \text{at } z = z_b + d \tag{3.7}$$

The free surface condition p = 0 is not applicable here, since the surface plate exerts normal stresses upon the fluid.

In case of axial symmetry, equation (3.2) and (3.3) lead to:

$$\frac{\partial}{\partial\phi}\left(\frac{\partial p}{\partial R}\right) = 0 \quad \text{and} \quad \frac{\partial}{\partial\phi}\left(\frac{\partial p}{\partial z}\right) = 0 \quad \text{whence} \quad \frac{\partial p}{\partial\phi} = \text{constant} \tag{3.8}$$

## 3.2. Normalization

In order to find out which parameters play a part in the mathematical model, the system is normalized, such that each term in the differential equations and the boundary conditions (3.1) - (3.7) is written as the product of a constant scale-factor and a variable dimensionless quantity of the order of magnitude 0 (1)*)
It seems appropriate to carry out this normalization by adopting an adequate scale-factor for each variable, either dependent or independent. So a function f of the variable x is normalized by

$$f(x) = F * f(x) \qquad \text{and} \quad x = X * x \tag{3.9}$$

F and X being constant scale-factors. Applying this rule to the first derivative of f with respect to x yields:

$$\frac{df}{dx} = \frac{F}{X} * \frac{df}{dx} \quad \text{with} \quad \frac{df}{dx} = 0(1) \tag{3.10}$$

As the value of X is the same throughout the system of equations and boundary conditions, (3.10) is not necessarily correct for all derivatives with respect to x of all dependent variables in the system.

This kind of problem is encountered in the present case when attempting to normalize the radial coordinate R, which occurs in two types of terms:

---

* A quantity f is of the order $0(\varepsilon^n)$ if $\lim_{\varepsilon \downarrow 0} \frac{f}{\varepsilon^n}$ exists.

a. terms introduced by the use of curvilinear coordinates (in general: all terms containing $\frac{1}{R}$, except for the longitudinal pressure gradient term in (3.1))
b. terms containing radial derivatives that are not essentially due to curvature, such as for instance the viscous term in (3.1)

$$\frac{\eta}{\rho}\frac{\partial^2 v_\phi}{\partial R^2}$$

If R tends to infinity, the terms of the former type vanish, whereas the terms of the latter type do not. Hence normalizing R by

$$R = R_c * r \tag{3.11}$$

in which $R_c$ denotes the radius of curvature of the channel axis, is correct for the first type of terms, but it is not for the second. Applying (3.11) to the viscous term mentioned above, for instance, and normalizing $v_\phi$ by

$$v_\phi = V\,u \quad \text{with } V = \frac{Q}{Bd} \text{ and } u = O(1) \tag{3.12}$$

this term would then become

$$\frac{\eta}{\rho}\frac{\partial^2 v_\phi}{\partial R^2} = \frac{\eta}{\rho}\frac{V}{R_c^2}\frac{\partial^2 u}{\partial r^2} \tag{3.13}$$

As the term does not vanish if $R_c$ goes to infinity, the normalized quantity $\frac{\partial^2 u}{\partial r^2}$ can not be of the order O(1) for all values of $R_c$, which is in conflict with the starting-point of the normalization. In order to cope with this problem, an additional radial coordinate y is defined by:

$$R = R_c + y \tag{3.14}$$

yielding $\frac{\partial}{\partial R} = \frac{\partial}{\partial y}$ . This makes it possible to normalize the

two types of terms independently, the first type using

$$\frac{1}{R} = \frac{1}{R_c}\frac{1}{r} \qquad \text{with } \frac{1}{r} = 0(1) \tag{3.15}$$

As the terms of the second type are mainly due to friction, d is an adequate scale-factor for y as long as the cross-section is not deep and narrow, so in terms of the second type the normalization can be carried out using

$$y = d\xi \qquad \text{and } \frac{\partial}{\partial R} = \frac{1}{d}\frac{\partial}{\partial \xi} \qquad \text{with } \frac{\partial}{\partial \xi} = 0(1) \tag{3.16}$$

For the same reason, d is chosen as a scale-factor for z:

$$z = d\zeta \qquad \text{and } \frac{\partial}{\partial z} = \frac{1}{d}\frac{\partial}{\partial \zeta} \quad \text{with } \frac{\partial}{\partial \zeta} = 0(1) \tag{3.17}$$

The secondary flow ($v_R$, $v_z$) is a consequence of the main flow curvature: if $R_c$ tends to infinity, the secondary flow vanishes. Additionally, the intensity of the secondary flow increases as the depth of flow increases (except for narrow deep channels). Therefore the secondary velocity components are normalized by:

$$v_R = V\frac{d}{R_c}v \; ; \; v_z = V\frac{d}{R_c}w \tag{3.18}$$

The pressure p and the longitudinal coordinate $s = R\phi$ should be normalized such that the longitudinal pressure gradient in (3.1) is appropriately represented. In the limit case of steady straight channel flow, equation (3.1) reduces to

$$0 = -\frac{1}{\rho}\frac{\partial p}{\partial s} + \frac{\eta}{\rho}\left(\frac{\partial^2 v_\phi}{\partial z^2} + \frac{\partial^2 v_\phi}{\partial y^2}\right) \tag{3.19}$$

The pressure gradient term and the viscous terms are equally important in this equations and there is no reason why they should not be so in curved flow. Therefore p and s should be normalized such that:

$$\frac{\partial p}{\partial s} = \frac{V\eta}{d^2} \frac{\partial p'}{\partial s'} \quad \text{with } \frac{\partial p'}{\partial s'} = 0(1) \tag{3.20}$$

The three normalized Navier Stokes equations become consistent if s is normalized by

$$s = d\, r\, \phi' \quad \text{whence } \phi = \frac{d}{R_c}\, \phi' \tag{3.21}$$

In order to eliminate g from the normalized system, the "total pressure" $p + \rho gz$ is normalized instead of p. Regarding (3.20) and (3.21),

$$p + \rho gz = \frac{V\eta}{d} p = \frac{\rho V^2}{Re} p \tag{3.22}$$

in which Re is the Reynolds number based on the main velocity scale V and the depth of flow d.

Defining $\varepsilon = d/R_c$ and substituting the normalizations (3.12), (3.15)-(3.18), (3.21)-(3.22), into the system of differential equations and boundary conditions (3.1)-(3.7) yields the following normalized system:

$$\varepsilon Re \left(v \frac{\partial u}{\partial \xi} + w \frac{\partial u}{\partial \zeta} + \varepsilon \frac{uv}{r}\right) = -\frac{1}{r} \frac{\partial p}{\partial \phi'} + \frac{\partial^2 u}{\partial \zeta^2} + \frac{\partial^2 u}{\partial \xi^2} + \frac{\varepsilon}{r} \frac{\partial u}{\partial \xi} - \frac{\varepsilon^2}{r^2} u \tag{3.23}$$

$$\varepsilon^2 Re \left(v \frac{\partial v}{\partial \xi} + w \frac{\partial v}{\partial \zeta}\right) - \varepsilon Re \frac{u^2}{r} = -\frac{\partial p}{\partial \xi} + \varepsilon \left(\frac{\partial^2 v}{\partial \zeta^2} + \frac{\partial^2 v}{\partial \xi^2} + \frac{\varepsilon}{r} \frac{\partial v}{\partial \xi} - \frac{\varepsilon^2}{r^2} v\right) \tag{3.24}$$

$$\varepsilon^2 Re \left(v \frac{\partial w}{\partial \xi} + w \frac{\partial w}{\partial \zeta}\right) = -\frac{\partial p}{\partial \zeta} + \varepsilon \left(\frac{\partial^2 w}{\partial \zeta^2} + \frac{\partial^2 w}{\partial \xi^2} + \frac{\varepsilon}{r} \frac{\partial w}{\partial \xi}\right) \tag{3.25}$$

$$\frac{\partial v}{\partial \xi} + \frac{\varepsilon}{r} v + \frac{\partial w}{\partial \zeta} = 0 \tag{3.26}$$

$$\int_{-B/2d}^{B/2d} d\xi \int_{-1}^{0} u\, d\zeta = \frac{B}{d} \qquad \left(\xi = -\frac{B}{2d} \text{ at the inner sidewall, } \xi = \frac{B}{2d} \text{ at the outer sidewall}\right) \tag{3.27}$$

$$w = 0, \ \frac{\partial u}{\partial \zeta} = 0; \ \frac{\partial v}{\partial \zeta} = 0 \quad \text{at } \zeta = 0 \tag{3.28}$$

$$u = 0; \quad v = 0, \quad w = 0 \quad \text{at } \zeta = -1 \text{ and at } \xi = \pm \frac{B}{2d} \tag{3.29}$$

### 3.3. Stream function and vorticity of the secondary flow

The equation of continuity (3.26) only contains the two secondary velocity components, so a scalar stream function $\psi'$ can be defined, such that this equation is satisfied:

$$v = -\frac{1}{r}\frac{\partial \psi'}{\partial \zeta} \quad ; \quad w = \frac{1}{r}\frac{\partial \psi'}{\partial \xi} \tag{3.30}$$

It should be noted that other definitions of the stream function also satisfying (3.26) are possible. By adopting (3.30), however, lines of constant stream function represent streamlines of the secondary flow

$$\left.\frac{d\zeta}{d\xi}\right|_{d\psi' = 0} = -\frac{\partial \psi'}{\partial \xi} \Big/ \frac{\partial \psi'}{\partial \zeta} = w/v \tag{3.31}$$

Elimination of the pressure gradient terms from (3.24) and (3.25) by differentiating (3.24) with respect to $\zeta$ and (3.25) with respect to $\xi$ and subtracting yields

$$\varepsilon Re \left(v \frac{\partial \omega'}{\partial \xi} + w \frac{\partial \omega'}{\partial \zeta} - \frac{\varepsilon}{r} v\omega'\right) + Re \frac{\partial}{\partial \zeta}\left(\frac{u^2}{r}\right) = \nabla^2 \omega' \tag{3.32}$$

where $\nabla^2 = \frac{\partial^2}{\partial \xi^2} + \frac{\partial^2}{\partial \zeta^2} + \frac{\varepsilon}{r}\frac{\partial}{\partial \xi} - \frac{\varepsilon^2}{r^2}$ and $\omega'$ denotes the vorticity of the secondary flow defined by

$$\omega' = \frac{\partial w}{\partial \xi} - \frac{\partial v}{\partial \zeta} = \frac{1}{r}\left(\frac{\partial^2 \psi'}{\partial \zeta^2} + \frac{\partial^2 \psi'}{\partial \xi^2} - \frac{\varepsilon}{r}\frac{\partial \psi'}{\partial \xi}\right) \tag{3.33}$$

Considering the vorticity transport equation (3.32) , the only source of secondary flow vorticity appears to be the vertical derivative of the centrifugal force; if this term is dropped, the secondary flow is identically equal to zero. For small values of Re, when u is independent on Re as can be seen from (3.23), the source term in (3.32) is proportional to Re. This suggests the secondary flow to be proportional to Re for small values of Re. So defining

$$\psi' = Re\ \psi \quad ; \quad \omega' = Re\ \omega \tag{3.34}$$

$\psi$ and $\omega$ can be expected not to depend on Re if Re is small. Then it is useful to rewrite the normalized system (3.23)-(3.29) as follows:

$$\varepsilon Re^2 \left\{ -\frac{1}{r}\frac{\partial\psi}{\partial\zeta}\left(\frac{\partial u}{\partial\xi} + \frac{\varepsilon}{r}u\right) + \frac{1}{r}\frac{\partial\psi}{\partial\zeta}\frac{\partial u}{\partial\zeta}\right\} = -\frac{1}{r}\frac{\partial p}{\partial\phi'} + \nabla^2 u \tag{3.35}$$

$$\varepsilon Re^2 \left\{ -\frac{1}{r}\frac{\partial\psi}{\partial\zeta}\left(\frac{\partial\omega}{\partial\xi} - \frac{\varepsilon}{r}\omega\right) + \frac{1}{r}\frac{\partial\psi}{\partial\zeta}\frac{\partial\omega}{\partial\xi}\right\} + \frac{\partial}{\partial\zeta}\left(\frac{u^2}{r}\right) = \nabla^2\omega \tag{3.36}$$

$$\nabla_1^2\psi = \omega r \qquad \text{with } \nabla_1^2 = \frac{\partial^2}{\partial\zeta^2} + \frac{\partial^2}{\partial\xi^2} - \frac{\varepsilon}{r}\frac{\partial}{\partial\xi} \tag{3.37}$$

$$\int_{-B/2d}^{B/2d} d\xi \int_{-1}^{0} u\,d\zeta = \frac{B}{d} \tag{3.38}$$

$$u = 0 \quad \text{at } \zeta = -1 \text{ and at } \xi = \pm\frac{B}{2d} \; ; \; \frac{\partial u}{\partial\zeta} = 0 \text{ at } \zeta = 0 \tag{3.39}$$

$$\psi = 0 \text{ and } \frac{\partial\psi}{\partial\zeta} = 0 \quad \text{at } \zeta = -1; \; \psi = 0 \text{ and } \frac{\partial^2\psi}{\partial\zeta^2} = 0 \quad \text{at } \zeta = 0 \tag{3.40}$$

$$\psi = 0 \text{ and } \frac{\partial\psi}{\partial\xi} = 0 \quad \text{at } \xi = \pm\frac{B}{2d} \tag{3.41}$$

$$v = -\frac{Re}{r}\frac{\partial\psi}{\partial\zeta} \; ; \quad w = \frac{Re}{r}\frac{\partial\psi}{\partial\xi} \tag{3.42}$$

The three normalized velocity components u, v and w and the normalized longitudinal pressure gradient $\frac{\partial p}{\partial\phi'}$, can be solved from this system of differential equations and boundary conditions as well as from (3.23)-(3.29). The advantage of the present system is that the transverse pressure distribution needs not be solved in order to obtain the velocity field. As (3.36) and (3.37) can easily be reduced to one fourth order equations in $\psi$, this implies that three equations with two unknown functions $(u,\psi)$ and one unknown constant $(\frac{\partial p}{\partial\phi'})$ have to be solved simultaneously here, whereas (3.23)-(3.29)

requires the simultaneous solution of five equations with four unknown functions (u, v, w, $p$) and one unknown constant $(\frac{\partial p}{\partial \phi},)$. In the present system, the velocity components being known, the transverse pressure distribution $p(\xi,\zeta)$ can be solved from (3.24) or (3.25) or from a combination of these two equations obtained by differentiating (3.24) with respect to $\xi$ and (3.25) with respect to $\zeta$ and adding the results to (3.25) multiplied by $\frac{\varepsilon}{r}$. This yields

$$(\frac{\partial^2}{\partial \xi^2} + \frac{\partial^2}{\partial \zeta^2} + \frac{\varepsilon}{r}\frac{\partial}{\partial \xi})\ (p + \varepsilon^2 Re\ \frac{v^2+w^2}{2}) = \varepsilon^2\ Re(w\ \frac{\partial \omega}{\partial \xi} + \frac{\varepsilon}{r}\ w\omega - v\ \frac{\partial \omega}{\partial \zeta} + \omega^2)$$
$$+ \frac{\varepsilon Re}{r}\frac{\partial}{\partial \xi}\ (u^2) \qquad (3.43)$$

The relevant boundary conditions can be derived from (3.24) and (3.25) and the boundary conditions for v and w:

$$\frac{\partial p}{\partial \xi} = \varepsilon\ \frac{\partial^2 v}{\partial \zeta^2} \quad \text{at } \zeta = -1\ ;\ \frac{\partial p}{\partial \zeta} = 0 \quad \text{at } \zeta = 0 \qquad (3.44)$$

$$\frac{\partial p}{\partial \zeta} = \varepsilon(\frac{\partial^2 w}{\partial \xi^2} + \frac{\varepsilon}{r}\frac{\partial w}{\partial \xi}) \text{ at } \xi = \pm \frac{B}{2d} \qquad (3.45)$$

From equations (3.36) and (3.37) it becomes evident that the parameter indicating the importance of the advective terms with respect to the viscous and the pressure gradient terms is $\varepsilon Re^2$, both in the longitudinal momentum equation (3.36) and in the vorticity transport equation (3.37).
DEAN (1928) and ADLER (1934) have shown that the resistance of low Reynolds number flow in coiled circular pipes of moderate curvature can be expressed as a power series expansion of the parameter

$$(\frac{1}{\rho}\frac{1}{R_c}\frac{\partial p}{\partial \phi})^2\ \frac{a^7}{\nu^4 R_c} = De^2 \qquad (3.46)$$

in which a denotes the radius of the pipe cross-section. The

parameter De is called the Dean number. Carrying out a normalization as applied to the present model, this number can be rewritten as

$$\frac{V^2}{aRe'} \quad \frac{a^{7/2}}{\nu^2 R_c^{1/2}} = Re' \sqrt{\frac{a}{R_c}} \tag{3.47}$$

in which $Re' = \frac{Va}{\nu}$ . Hence the resistance parameter $De^2$ is equivalent to the secondary flow advection parameter $\varepsilon Re^2$ derived here. Therefore $Re\sqrt{\varepsilon}$ will be referred to as the Dean number hereafter.

## 3.4. Solution procedure

The non-linear system of differential equations and boundary conditions (3.37)-(3.41) has to be solved iteratively to yield approximations of u, $\frac{\partial p}{\partial \phi}$, and $\psi$ in each iteration step. The essential point of the iteration procedure is that the stream function of the secondary flow $\psi$ is supposed to be known when figuring in the advective terms in (3.35) and (3.36). It is estimated by its solution in the foregoing iteration step.
If n is the iteration index, $u^{(n)}$ and $\frac{\partial p}{\partial \phi}^{(n)}$ are solved from the longitudinal momentum equation (3.35), the integral condition of continuity (3.38) and the boundary conditions (3.40). As shown before, $\frac{\partial p}{\partial \phi}$, is a constant in axysymmetric flow. It will be indicated by $-\imath$ hereafter.
Defining

$$u = \imath u' \tag{3.48}$$

equation (3.35) can be reduced to:

$$\varepsilon Re^2 \left\{ -\frac{1}{r}\frac{\partial \psi}{\partial \zeta}\left(\frac{\partial u'}{\partial \xi} + \frac{\varepsilon}{r}u'\right) + \frac{1}{r}\frac{\partial \psi}{\partial \xi}\frac{\partial u'}{\partial \zeta}\right\} = \frac{1}{r} + \nabla^2 u' \tag{3.49}$$

As $\psi$ is considered as a known function here, this is a linear differential equation in u' with the known source term $-\frac{1}{r}$. The boundary conditions for u' are the same as those for u, so u' can be solved without knowing $\iota$, which is subsequently solved from

$$\iota = \frac{B/d}{\int_{-B/2d}^{B/2d} d\xi \int_{-1}^{0} u' d\zeta} \tag{3.50}$$

The stream function of the secondary flow $\psi$ is solved from the fourth order partial differential equation obtained by combining (3.36) and (3.37). Estimating the secondary velocity-components in the advective terms of the vorticity transport equations at their values in the foregoing iteration step, this combined fourth order equations reads

$$\varepsilon Re^2 \{-\frac{1}{r}\frac{\partial\psi^{(n-1)}}{\partial\zeta}\left(\frac{\partial^3\psi}{\partial\xi\partial\zeta^2}\right) + \frac{\partial^3\psi}{\partial\xi^3} - 2\frac{\varepsilon}{r}\frac{\partial^2\psi}{\partial\zeta^2} - 3\frac{\varepsilon}{r}\frac{\partial^2\psi}{\partial\xi^2} + 3\frac{\varepsilon^2}{r^2}\frac{\partial\psi}{\partial\xi}\Big)^{(n)} +$$

$$+\frac{1}{r}\frac{\partial\psi^{(n-1)}}{\partial\xi}\left(\frac{\partial^3\psi}{\partial\zeta^3} + \frac{\partial^3\psi}{\partial\xi^2\partial\zeta} - \frac{\varepsilon}{r}\frac{\partial^2\psi}{\partial\xi\partial\zeta}\right)^{(n)}\} + \frac{\partial}{\partial\zeta}(u^2)^{(n)} =$$

$$\{\frac{\partial^4\psi}{\partial\xi^4} + 2\frac{\partial^4\psi}{\partial\xi^2\partial\zeta^2} + \frac{\partial^4\psi}{\partial\zeta^4} - 2\frac{\varepsilon}{r}\left(\frac{\partial^3\psi}{\partial\xi^3} + \frac{\partial^3\psi}{\partial\xi\partial\zeta^2}\right) + 3\frac{\varepsilon^2}{r^2}\frac{\partial^2\psi}{\partial\xi^2} - 3\frac{\varepsilon^3}{r^3}\frac{\partial\psi}{\partial\xi}\}^{(n)} \tag{3.51}$$

As $\psi^{(n-1)}$ is a known function, this a linear equation in $\psi^{(n)}$, with $\frac{\partial}{\partial\zeta}(u^2)^{(n)}$ as a known source term. This equation can be solved with the boundary conditions (3.39)-(3.41).
The iteration is started by setting $\psi^{(0)} = 0$, such that in the first iteration step the advective terms in (3.49) and (3.51) drop out. The iteration is stopped when the following termination criterion is satisfied in every point of the cross-section:

$$|u^{(n)} - u^{(n-1)}| < \delta \qquad \text{with } \delta << 1 \tag{3.52}$$

As by definition the overall mean value of $u^{(n)}$ equals 1 for all n, this absolute criterion can be used instead of a relative one.

If only a fraction of the changes in u from one iteration step to another is accounted for, the convergence of the iteration procedure can be improved. Therefore

$$u^{(n)} = \frac{1}{\alpha} \{ \imath^{(n)} u'^{(n)} + (\alpha-1)\, u^{(n-1)} \} \qquad \text{with } \alpha \geq 1 \tag{3.53}$$

is used rather than

$$u^{(n)} = \imath^{(n)}\, u'^{(n)} \tag{3.54}$$

This does not influence the consistency of the solution procedure, (3.53) being equivalent to (3.54) if $u^{(n-1)} = u^{(n)}$. The termination criterion, however, must be corrected for $\alpha$:

$$|u^{(n)} - u^{(n-1)}| < \frac{\delta}{\alpha} \tag{3.55}$$

## 3.5. Numerical solution

In each iteration step the system of differential equations and boundary conditions (3.49)-(3.51), (3.53), (3.39)-(3.41) is solved numerically using an implicit second order finite difference method. The equations are discretized on an N by M rectangular grid of mesh size $\Delta\zeta \times \Delta\xi$, where $\Delta\zeta = 1/N$ and $\Delta\xi = 1/(Md)$ (see figure 2). Throughout the system central differences are used for discretization, except near the boundaries, where forward or backward differencing is applied. This is always done such that the truncation error is at least second order (see Appendix I). Adopting a shorthand notation in which $\frac{\delta}{\delta\zeta}$, $\frac{\delta}{\delta\xi}$ and $\nabla^2$ denote the finite difference representations

of $\frac{\partial}{\partial \zeta}$ , $\frac{\partial}{\partial \xi}$ and $\nabla^2$, respectively, the discretized longitudinal momentum equation in a grid point (i, j) reads:

$$\frac{\varepsilon Re^2}{r_j}\left[-\frac{\delta\psi^{(n-1)}_{i,j}}{\delta\zeta}\left\{\frac{\delta u'^{(n)}_{i,j}}{\delta\xi}+\frac{\varepsilon}{r_j}\,u'^{(n)}_{i,j}\right\}+\frac{\delta\psi^{(n-1)}_{i,j}}{\delta\xi}\,\frac{\delta u'^{(n)}_{i,j}}{\delta\zeta}\right]=-\frac{1}{r_j}+\nabla^2\,u'^{(n)}_{i,j} \tag{3.56}$$

The derivatives of $u'^{(n)}_{i,j}$ are evaluated by the usual 3-point formulae, whereas the derivatives of $\psi^{(n-1)}_{i,j}$ in the advection terms are evaluated using 5-point formulae in order to avoid artificial viscosity effects. For the same reason the possibility of using upwind difference schemes for the advection terms was rejected (ROACHE, 1972).

The discretized stream function equation reads:

$$\varepsilon Re^2\left[-\frac{\delta\psi^{(n-1)}_{i,j}}{\delta\zeta}\left\{\frac{\delta}{\delta\xi}\left(\frac{1}{r_j}\nabla_1^2\psi^{(n)}_{i,j}\right)-\frac{\varepsilon}{r_j^2}\nabla_1^2\psi^{(n)}_{i,j}\right\}+\frac{\delta\psi^{(n-1)}_{i,j}}{\delta\xi}\,\frac{\delta}{\delta\zeta}\left(\frac{1}{r_j}\nabla_1^2\psi^{(n)}_{i,j}\right)\right]+$$

$$+\,2\,u^{(n)}_{i,j}\,\frac{\delta u^{(n)}_{i,j}}{\delta\zeta}=r_j\,\nabla^2\left(\frac{1}{r_j}\nabla_1^2\psi^{(n)}_{i,j}\right) \tag{3.57}$$

The derivatives of $\psi^{(n)}_{i,j}$ in this equation are evaluated using second order finite difference schemes. For accuracy reasons (artificial viscosity), however, the derivatives of $\psi^{(n-1)}_{i,j}$ in the advection terms and the vertical derivative of $u^{(n)}_{i,j}$ in the source term of this equation are discretized by fourth order schemes. In Appendix I it is shown that the lower derivatives with respect to $\xi$ in the viscosity terms and with respect to $\xi$ and $\zeta$ in the advection terms (see also (3.51)) will give rise to artificial viscosity or similar numerical inaccuracies. Moreover, if the mesh size of the computational grid is too large with respect to the boundary layer thickness at the fixed walls, spurious spatial oscillations will occur in the finite difference solution of u (ROACHE, 1972). All these numerical inaccuracies are suppressed or are negligible if

$$\varepsilon Re|v_{i,j}| \frac{\Delta\xi}{2} < 1 \quad \text{and} \quad \varepsilon Re|w_{i,j}| \frac{\Delta\zeta}{2} < 1 \tag{3.58}$$

$$\frac{\varepsilon}{r_j} \Delta\xi << 1 \tag{3.59}$$

throughout the flow.

The discretization of equations (3.49) and (3.51) is described in detail in Appendix I. The resulting two sets of linear equations, viz. (M-1)*N equations in $u'^{(n)}_{i,j}$ and (M-1)*(N-1) equations in $\psi^{(n)}_{i,j}$, are solved using a matrix decomposition procedure (WILKINSON AND REINSCH, 1971). The integrations needed to determine $\iota$ from (3.50) are executed using Simpson's rule. The termination criterion for the iteration procedure being satisfied, the total pressure $p$ is solved from a rewritten version of (3.43) with $p$ given at all boundaries. The discretization of the pressure equation and the treatment of the boundary conditions are described in Appendix I.

## 4. Verification of the model

### 4.1. Comparison with analytical results

The results for low Dean numbers of the numerical solution method described in the foregoing paragraphs have been compared with analytical low Dean number solutions reported by ITŌ (1951), CUMING (1952) and DE VRIEND (1973a, b). In the first two publications the main velocity component and the stream function of the secondary flow are determined by successive approximations with the Dean number as a perturbation parameter. As a result, the main velocity and the stream function are expressed as power series expansions of $De^2$. Although derived for shallow channels of mild curvature, the analytical results for the main velocity and the stream function of the secondary flow reported by the third author can be reduced to power series expansions of the Dean number that are applicable to relatively deeper cross-sections as well.

All three authors have solved essentially the same differential equations *), Cuming stopping the analysis after having determined the first non-zero term of each series expansion, the other two authors also giving the second term of the main velocity expansion.

In figures 3 and 4, the analytical solutions of the normalized main velocity u and the normalized stream function of the secondary flow $\psi$ are compared with the results of the present model for $\varepsilon = 0.01$ and $Re = 50$, i.e. $De = 5$, both for $d/B = 0.5$ (in terms of pipe flow: square cross-section) and $d/B = 0.1$ (in terms of pipe flow: rectangular cross-section with aspect ratio 0.2). The numerical and the analytical solutions appear to agree well, both for the main velocity and for the secondary flow stream function.

Additionally, the longitudinal slope factors $\iota$ show good agreement: for the square cross-section the analytical and the numerical values are 7.11 and 7.13, respectively, for the shallow cross-section these values are 3.39 and 3.44.

## 4.2. Comparison with other numerical results

Various investigators apply numerical methods to study axisymmetric incompressible laminar curved flow for intermediate or even high Dean numbers.

The system of differential equations and boundary conditions solved by CHENG AND AKIYAMA (1970) is essentially the same as the system solved at present, although the divergence terms are neglected (i.e. $\frac{1}{r}$ is set equal to 1 instead of $\frac{1}{1+\varepsilon\xi}$), which limits applications to relatively large radii of curvature. In general, the discretization of the equations is second order, but fourth order schemes are employed for the secondary velocity components in the advection terms and for the vertical derivative of the stream function equation.

*) DE VRIEND accounts for the divergence of the coordinate system in lower order terms of the expansions than the other authors.

The main flow equation and the stream function are solved simultaneously by the same iterative procedure as applied in the present work, using successive overrelaxation to solve the individual equations in an iteration step.
Figures 5 a-d show a comparison of the main and the secondary velocity components resulting from Cheng and Akiyama's work and from the present model for d/B = 0.5, with the Dean number as a parameter. In figure 5e the streamlines of the secondary flow are compared for De = 18.4 and figure 6 represents the relative magnitude of the longitudinal slope factor $\iota$ with respect to its value $\iota_0$ in an equivalent straight channel or pipe. All results show a good agreement.
JOSEPH, SMITH AND ADLER (1975) developed a procedure to solve time-dependent axisymmetric laminar flow problems. This procedure was also applied to steady state computations, time being an iteration parameter then. The differential equations and boundary conditions describing this steady state flow are equivalent to (3.23)-(3.29). The solution procedure, however, is quite different from the present one. The main velocity equation is solved explicitly in time with a Dufort-Frankel approximation of the second derivatives in the viscosity terms (ROACHE, 1973). The secondary velocity components and the pressure are determined from discretizations (with Dufort-Frankel approximations) of the momentum equations in radial and vertical direction and the equation of continuity. These are rewritten into explicit expressions for the secondary velocity components and a finite difference equation for the pressure which is solved using successive overrelaxation. This iterative procedure turns out to be convergent up to higher Dean numbers than the present method, but both suffer from weakly damped oscillations in time at higher Dean numbers.
One of the most striking results from Joseph, Smith and Adler's work is the occurence of a flow pattern with two counterrotating helices instead of one (in pipe terms: four rather than two) at higher Dean numbers. In a square pipe the transition from the usual low Dean number flow pattern to this higher Dean number pattern is found to occur quite abruptly at De = 50, which is confirmed experimentally.

Similar counterrotating helices have been observed during various experiments on turbulent flow in curved channels (B.C. YEN, 1965; RAO, 1975; CHOUDHARY AND NARASIMHAN, 1977; DE VRIEND AND KOCH, 1977). As the second helix stays close to the outer wall even in shallow channels, it will presumably be of minor importance for the development of a mathematical model of turbulent flow in river bends *). Nevertheless it provides a possibility to test the present axisymmetric laminar flow model at higher Dean numbers.

In figure 7 the main flow isovels and the streamlines of the secondary flow resulting from the present model are compared with those resulting from Joseph, Smith and Adler's model for a square pipe and Dean numbers close to 50. In both models the transition between the two flow patterns occurs at De $\cong$ 50. The positions of the main flow isovels and the secondary flow streamlines are in rather good agreement, especially when taking into account that for Dean numbers in the region about 50 a small deviation of the Dean number will give rise to considerable changes of the flow pattern.

As far as the magnitude of the stream function (i.e. the intensity of the secondary flow) is concerned, however, the two models differ: the values computed at present are about 20% higher. On making the comparison between the two models at a lower Dean number (De = 20.3, see figure 8), the same difference occurs whereas the positions of the main flow isovels and the secondary flow streamlines are in good agreement. By lack of experimental information on the secondary flow intensity and considering that in the same Dean number region the present secondary flow intensity agrees well with the intensity found by Cheng and Akiyama (see figure 5 c-e), the cause of this difference will not further be examined.

---

*) RAO (1975) suggests this second helix to be important to bank erosion and consequently to the entire configuration of a natural water course.

Finally, the transverse pressure drop at the surface is compared with the values for a square pipe computed by JOSEPH, SMITH AND ADLER (1975) and with the 1.92 power law resulting from circular pipe computations by AUSTIN AND SEADER (1973). Figure 9 shows a good agreement between the present results (exponent 1.91) and those from the two other models (Joseph, Smith and Adler: exponent 1.87). The transverse pressure drop is seen to be about a factor 1.3 higher in case of a rectangular cross-section.

The system of equations solved by CHENG, LIN AND OU (1976) agrees with the present one, except for the stream function equation, which is replaced by the vorticity transport equation (cf. equation 3.36) and the Poisson-type relation between stream function and vorticity (cf. equation 3.37). Although complications arise from the boundary conditions of $\omega$ at the fixed walls (see also: ROACHE, 1972), solution procedures solving these two second order equations appear to be superior to corresponding procedures solving the fourth order stream function equation. The system is discretized using second order finite difference schemes, even when deriving the secondary velocity components from the stream function, thus discarding artificial viscosity effects in the longitudinal momentum equation (see Appendix I). Both splitting the stream function equation and discarding artificial viscosity lead to convergence of the iteration procedure up to much higher Dean numbers than can be reached by the present method (in a square pipe Dean numbers as large as 250 could be reached, whereas the present method fails at De > 60).
The method was used to determine the axisymmetric velocity field in rectangular channels of various aspect ratios (d/B = 0.25, 0.50, 1.0, 2.5). The results show the same features as those discussed before, viz. an outward skewing of the horizontal distribution and a flattening of the vertical distribution of the main velocity as De increases (see also figure 10), longitudinal

slope factors increasing with De (see figure 6) and the formation of a counterrotating secondary circulation near the outerwall in the upper half of the vertical. Contrary to the present results and those obtained by JOSEPH, SMITH and ADLER (1975), in a square pipe the transition to the double secondary flow pattern occurs at a Dean number which is definitely higher than 53. Moreover, for De = 53 the secondary flow intensity is about 30% higher than the intensity found from the present model (whereas the intensity found by Joseph, Smith and Adler is about 20% smaller than the present one!) These differences are most likely to be caused by artificial viscosity effects reducing the effective Dean number.

An important conclusion to be drawn from this work is that the counterrotating secondary circulation can also occur in shallow channels, where, at least at the Dean numbers considered, the second helix stays close to the outer wall.

### 4.3. Comparison with measurements

In contradiction to circular pipes, little experimental data on incompressible flow through coiled rectangular pipes have been published: only MORI, UCHIDA AND UKON (1971) presented the main velocity distributions measured in air flow through a square pipe of 0.02 m side length with a radius of curvature of 0.267 m ($d/R_c = 0.0357$), at Dean numbers ranging from 10 to 900, i.e. both in the laminar and in the turbulent flow region. According to Mori, Uchida and Ukon's paper, the presented results concern the main velocity normalized by the mean velocity in longitudinal direction. On closer examination of these results, however, the overall mean value of the normalized velocity turns out to be less than unity[*]). It does not become evident from the paper how the mean longitudinal velocity was computed, but it seems obvious that something is wrong at this point.

---

[*]) Assuming $u(\xi,\zeta) = u(\xi,0) \cdot u(0,\zeta)/u(0,0)$, the mean values are about 0.8 for all Dean numbers.

Althoug this inconsistency is to spoil the quantitative comparison between computed and measured results, a numerical simulation of the experiment was carried out in order to get an indication on whether the computed results show the right tendencies for varying Dean numbers. As the computation did not converge at Dean numbers higher than 60, however, not all flow situations could be simulated. Therefore figure 10 represents only main velocity distributions for De = 9.9, 18.0 and 38.2.
As was to be expected, the quantitative agreement between measured data and computational results is not very good.
But in addition, the shapes of the equivalent measured and computed velocity distributions do not agree very well either.
Although the measured data show the same tendencies as the computed results (for increasing Dean numbers a shifting of the velocity maximum to the outer wall and a flattening of the vertical distribution were observed), the shapes of the measured distributions suggest the Dean number to be lower than indicated.
As the computed distributions found by CHENG, LIN AND OU (1976) agree well with the present ones (see figure 10), the cause of these differences is not likely to lie in the mathematical model, but rather in an error in the mean velocity, to which the Dean number is proportional.

## 4.4. Utility of the model

From the foregoing comparisons with other work it is conluded that the present mathematical model gives a rather good description of incompressible axisymmetric curved flow at low and intermediate Dean numbers (De < 60).
It must be assessed now whether this Dean number range is wide enough to make the model suited for the present purposes: analysing the velocity redistribution mechanism and developing a simplified computation method for the flow in river bends.
In laminar curved flow the Dean number indicates the importance of secondary flow advection relative to molecular diffusion of momentum. Likewise, in turbulent curved flow, where a qualitavely similar secondary flow occurs, the Dean number should indicate

the importance of secondary flow advection with respect to turbulent diffusion of momentum. Therefore the Dean number should be based on some equivalent turbulent viscosity rather than on molecular viscosity. A rough indication of turbulent viscosity (ENGELUND, 1974) is given by

$$\nu_T = \frac{1}{13} \frac{\sqrt{g}}{C} Vd \tag{4.1}$$

in which C denotes Chezy's constant. Then the turbulent Dean number can be evaluated as

$$De_T = 13 \frac{C}{\sqrt{g}} \sqrt{\frac{d}{R_c}} \tag{4.2}$$

In practice $C/\sqrt{g}$ will range from 10 to 20 and in natural rivers the ratio radius of curvature to channel width ranges from 2 to 3 (LEOPOLD, WOLMAN AND MILLER, 1964). For d/B = 0.5, the mathematical model is convergent up to De ≃ 60, but as d/B decreases, this critical Dean number increases. Taking 60 as a lower limit, the model is applicable when considering natural channels of a depth to width ratio up to 0.1, which is thought to be sufficient. In various flume experiments however, much higher Dean numbers are found, so that the mathematical model is not likely to give even a qualitative representation of the observed phenomana. Therefore a selection of flume data to moderate Dean numbers will be made.

## 5. Shallow channel computations

In order to study the influence of the Dean number the curvature ratio ε and the channel aspect ratio B/d on axisymmetric laminar flow in curved shallow channels, a series of shallow channel computations was carried out using the mathematical model described in the foregoing sections. Table 1 gives a survey of these computations.

| | | ε | | | |
|---|---|---|---|---|---|
| | | $10^{-4}$ | $10^{-2}$ | 0.04 | 0.16 |
| B/d | 2 | 25 | - | - | - |
| | 5 | 25 | - | - | - |
| | 10 | 25 | 25 | 0/6.25/12.5 25/37.5/50 | 25 |
| | 15 | 25 | - | - | - |

Table 1. Dean numbers for shallow channel computations

### 5.1. Influence of the Dean number

In the mathematical model the Dean number indicates the relative importance of the advection terms in the longitudinal momentum equation (3.49) and in the stream function equation (3.51). If these advection terms are dropped, the solutions of u and $\psi$ become identical to the zero Dean number solutions. Since the velocity distribution, both in a shallow channel and in a square pipe (see for instance figure 5), is strongly influenced by the Dean number, advection must play a promiment part in curved flow. Most of the phenomena observed when varying the Dean number can be explained from the main velocity redistribution due to the advective influence of the secondary flow. A description of this redistribution and its consequences will be given in the present

section, a more thorough analysis of the main velocity redistribution will be made in chapter 6.

a. Main velocity distribution.

One of the most important effects of advection in curved flow is the transverse redistribution of the main velocity. For De = 0, the vertical distribution of u is practically parabolic and the maximum lies at the surface near the inner wall (figures 11 a-b). When De increases, however, the maximum of the main velocity moves towards the outer wall and from the surface to a lower point, the vertical distribution of u becoming flatter in the upper half and steeper in the lower half of the vertical. All these phenomena qualitatively agree with those computed for square pipes (see chapter 4). Comparing figures 5 a-b and 11a-b, however, the influence of the Dean number appears to be stronger in a square pipe, especially when the vertical distribution of u is concerned: the same degree of deformation *) of the main velocity distribution is reached at a lower Dean number than in a shallow channel.

The main velocity redistribution due to advection is important for the prediction of the bed configuration in alluvial river bends, as it gives rise to a redistribution of the longitudinal shear stress at the fixed boundaries of the flow. This shear stress is proportional to the main velocity gradient at the boundary. Figure 11c shows that in the outer wall region this gradient decreases with the Dean number, whereas in the inner wall region it remains almost constant. Consequently, the longitudinal slope factor $\lambda$, which is correlated to the boundary shear

---

*) Measured, for instance, by the reduction of the main velocity at the surface with respect to the value if the vertical distribution would have been parabolic with the same depth-averaged value.

stress *), increases with the Dean number, as is shown in figure 12. This explains what is generally called the "curve resistance".

b. Secondary flow

The influence of the Dean number on the secondary flow is shown in figure 13. The redistribution of the main velocity influences the stream function through the source term $\frac{\partial}{\partial \zeta}(u^2)$ in the stream function equation (3.51). For increasing De this source term tends to decrease in the upper half of the vertical, where it may even become negative, and to increase the lower half. Consequently, its maximum shifts downwards (for De = 0 the maximum for $\xi = 0$ occurs at $\zeta = -0.58$, for De = 50 it occurs at $\zeta = -0.77$), i.e. towards the bottom, where its effect on $\psi$ decreases since both $\psi$ and $\frac{\partial \psi}{\partial \zeta}$ are prescribed to be zero at the bottom. In addition, the vertical mean value of the source term, which is equal to $u^2(\zeta=0)$, decreases for increasing De. As a consequence of this behaviour of the source term, the maximum of the stream function $\hat{\psi}$ tends to decrease as De increases and the centre of circulation, i.e. the point where $\hat{\psi}$ occurs, moves downwards (see figures 13 a-b). At higher Dean numbers the maximum of the source term in the outer wall region moves faster down than in the inner wall region (for De = 25 and 50, the maxima for $\xi = -4$ occur at $\zeta = 0.72$ and $\zeta = 0.76$, respectively, whereas for $\xi = 4$ they are found at $\zeta = -0.76$ and $\zeta = -0.84$). Consequently, at higher Dean numbers the reduction of the stream function near the outer wall is relatively stronger than near the inner wall. This explains why for increasing De the centre of circulation first moves towards the outer wall (under the influence of the redistribution) and above a certain value of De back inward again (see also figures 13d-e).

---

*) By integrating equation (3.35) multiplied by $r^2$ over the cross-section, $\frac{B\iota}{d}$ can be shown to be equal to the integral over the fixed boundaries of the main velocity gradient weighted by $r^2$.

As compared with the results for a square pipe, the reduction of $\hat{\psi}$ in the shallow channel is rather weak in the Dean number range considered (figure 13c). In square pipes the quantity $\hat{\psi}De$, which can be considered as an indication of the secondary flow intensity as long as $\varepsilon$ is constant, decreases at Dean numbers higher than about 20. The shallow channel data available*) suggest the Dean number at which $\hat{\psi}De$ is maximal to be considerably higher (between 30 and 40) and the value of the maximum to be about twice as large as in a square pipe.

Presumably, the shift of the maximum of $\hat{\psi}De$ to higher Dean numbers must be attributed to the aforementioned stronger influence of the Dean number on the main velocity distribution in a square pipe. The smaller values of $\hat{\psi}De$ found in a square pipe can be explained from the stronger influence of the sidewalls. Considering the main velocity distribution in a square pipe, the sidewall boundary layers cover a much larger part of the cross-section than in a shallow channel (cf. figures 5a and 11a). Consequently, the overall mean value of the source term in the stream function equations is smaller. Moreover, even if this source term would have had the same overall mean value, the smaller distance between the lateral boundaries would have led to smaller values of $\hat{\psi}$ in a square pipe.

Comparing the location of the centre of circulation in a shallow channel (figures 13 d-e ) with that in a square pipe in the same Dean number range (figure 5 c-d ), a qualitatively similar behaviour is observed. As a consequence of the stronger influence of the Dean number, however, the vertical displacement of the centre of circulation is larger in a square pipe than in a shallow channel at the same Dean number. For the same reason, the shifting back inwards starts at a lower Dean number in a square pipe. As in a shallow channel the influence of the sidewalls is much smaller, there is much more room for lateral displacements of the centre of circulation. Accordingly, these displacements are much larger than in a square pipe.

---

*) The high expenses of the shallow channel computations limited the number of runs that could be made

Finally it should be noted that figures 5 c-d, 13c and 13 d-e suggest the centre of circulation lies closest to the outer wall when the highest value of $\Psi De$ occurs, i.e. when the highest secondary flow intensity is reached.

c. Transverse pressure distribution.

Figure 14 shows the influence of De on the transverse pressure distribution. Since only the distribution of $p$ is important and not its absolute value, $p$ was set equal to zero in the inner top corner ($\zeta = 0$, $\xi = -5$). At low Dean numbers, when the maximum of the main velocity lies near the inner wall, the radial distribution of $p$ is concave, but as De increases and the maximum of u shifts towards the outer wall, a convex distribution is found. For all Dean numbers considered the vertical pressure distribution hardly changes: $p$ is almost constant throughout the vertical. From figure 14a it appears that the difference between the values of $p/\varepsilon Re$ at the outer and at the inner wall hardly depends on De. According to the definition

$$p = \frac{Re}{\rho V^2} (p + \rho g z) \tag{3.22}$$

this implies that the transverse pressure drop is closely proportional to $De^2$, which is confirmed by figure 14c, where an exponent of 1.96 is found. This figure also shows the transverse pressure drop in the channel considered to be about 5 times as large as in a square pipe (see also figure 9). Apparently, the transverse pressure gradients are almost the same in both cases.

From these results it can be concluded that, at least in shallow channels for the range of Dean numbers considered, ($De \leq 50$) the transverse pressure distribution is hardly influenced by the secondary flow. The only important source term in the pressure equation (3.43) is the main velocity term $\frac{\varepsilon Re}{r} \frac{\partial}{\partial \xi} (u^2)$.

d. Total energy distribution.

Finally, the total energy normalized by

$$e = \frac{Re}{\rho V^2}\left(p + \rho g z + \frac{1}{2}\rho v_{tot}^2\right) = p + Re\,\frac{u^2 + \varepsilon^2(v^2 + w^2)}{2} \qquad (5.1)$$

is given in figure 15. From this figure and the transverse distribution of $p$ given in figure 14 it becomes evident that the term with $u^2$ plays a prominent part in $e$. Consequently, the energy maximum shifts towards the outer wall as De increases and the vertical distribution tends to be flatter in the upper half and steeper in the lower half of the cross-section.

## 5.2. Influence of the curvature ratio

In axisymmetric curved flow two important effects influence the main velocity distribution in an opposite sense:

- the "potential flow" effect, represented by the factor $\frac{1}{r}$ in the pressure gradient term of the longitudinal momentum equation
- the effect of secondary flow advection

At low Dean numbers, the potential flow effect is predominant: outside the sidewall boundary layers the mean velocity is inversely proportional to r, as in free vortex flow (cf. low Dean number solution by DE VRIEND, 1973). When De increases, however, the influence of advection increases and the radial distribution of the main velocity gradually changes into a profile with its maximum near the outer wall instead of the inner wall (see figure 11a).

The factor $\frac{1}{r}$ varies from the inner to the outer wall. Consequently, the influence of the potential flow effect gets stronger when the bend becomes sharper, or in the present case,where d/B is kept constant: when the curvature ratio increases (see figures 16a and 16d).

According to figures 16b, c and e, the influence of $\varepsilon$ on the vertical distribution of u is more complicated. In the channel axis a slight flattening of the profile can be observed in case

of a very sharp bend [x]). In the sidewall regions, however, the influence of $\varepsilon$ is much stronger. Near the inner wall the effect of advection is drastically intensified when $\varepsilon$ increases, whereas near the outer wall the effect weakens.

From figures 16f and 16i it becomes evident that the stream function (and hence its radial and vertical derivatives) hardly depends on $\varepsilon$ near the inner wall and decreases for increasing $\varepsilon$ near the outer wall. The secondary velocity components, however, are proportional to $\frac{1}{r}$ times the derivatives of the stream function (definition 3.30), so as $\varepsilon$ increases they increase near the inner wall and decrease even stronger than the stream function near the outer wall. Consequently, the local effect of advection is intensified near the inner wall and weakened near the outer wall. From the slight increase of the advective influence on the main velocity profile in the channel axis (figure 16b) it becomes clear that the intensification near the inner wall is stronger than the weakening near the outer wall.

Figures 16f and 16i show that for increasing $\varepsilon$ the maximum of the stream function decreases and shifts towards the inner wall. This accords with the behaviour of the source term in the stream function equation: its vertical mean value $u^2(\zeta = 0)$ shows an overall decrease with the maximum shifting towards the inner wall (see also figure 16a). In the inner wall region, however, the maximum of the source term shifts to a lower point of the vertical as $\varepsilon$ increases. Thus the local increase of the vertical mean value of the source term is compensated, such that in this region $\psi$ hardly depends on $\varepsilon$.

According to figures 16g - h and 16j, the role of advection in the vertical distribution of $\psi$ is the same as in the main velocity distribution: intensification of the influence near

---

[x]) $\varepsilon = 0.16$ represents a very sharp bend here, the radius of curvature of the inner wall being as small as $0.2\ R_c$.

the inner wall and weakening near the outer wall. Consequently, as $\varepsilon$ increases the centre of circulation for a vertical moves down in the inner wall region and around the channel axis and it goes up in the outer wall region.

As regards the influence of the curvature ratio, the shallow channel results seem to differ from those for a square pipe, where, for instance, over a wide range of $\varepsilon$ hardly any effect on $\hat{\psi}$ was observed (figure 13c). It should be noted, however, that in case of a shallow channel a certain value of $\varepsilon$ represents a much sharper bend than in case of a square pipe, since the normalized radius of curvature of the inner wall is given by

$$r_{inner} = 1 - \frac{B\varepsilon}{2d} \qquad (5.2)$$

So in terms of $r_{inner}$, the shallow channel computations represented in figure 13c range from 0.9995 to 0.2 and the square pipe computations from 0.99995 to 0.95. This implies that the shallow channels cover a wide range of bend sharpnesses, but the square pipe computations all deal with gentle bends.

## 5.3. Influence of the channel aspect ratio

Figure 17 shows the influence of the channel aspect ratio B/d on the transverse distributions of the main velocity and the stream function of the secondary flow.

According to figure 17a, the location of the main velocity maximum shifts to higher values of the relative radial coordinate $\frac{2d\xi}{B}$ as B/d increases, but the value of the maximum is approximately constant. When plotting the depth-averaged main velocity distributions near the inner and near the outer wall on the same radial scale (figures 17c - d) the curves near the inner wall depend on B/d, but the curves near the outer wall practically coincide for all values of

B/d considered. Apparently, at the present Dean number the main velocity maximum moves outwards until it is stopped by the viscous forces near the outer sidewall. The vertical distribution of u in the channel axis (figure 17b) is strongly influenced by the channel aspect ratio, from a typical low Dean number profile in shallow channels (B/d = 10,15) to a typical higher Dean number profile in a square pipe (B/d = 2). According to figure 17e, however, the vertical distribution of u near the outer wall depends on B/d to a much lower extent than the distributions near the inner wall and in the channel axis (figure 17b). The influence of B/d on the vertical distribution of u in the channel axis confirms the hypothesis made in section 5.1.: the influence of the Dean number on the vertical distribution of the main velocity decreases when the channel aspect ratio increases. The differences between the effects of advection near the two sidewalls can be explained from the local intensity of the secondary flow, especially of the vertical velocity component. Figures 17h - i show that near the inner wall the vertical velocity decreases considerably as B/d increases, whereas in the outer wall region this velocity component slightly increases. Consequently, the influence of advection shows stronger variations with B/d in the inner wall region than near the outer wall.

As it was already mentioned and explained in section 5.1., the overall intensity of the secondary flow is strongly influenced by the channel aspect ratio: the smaller B/d, the smaller $\hat{\Psi}$. As B/d increases, the centre of circulation shifts to higher values of the relative radial coordinate $\frac{2d\xi}{B}$, but the distance to the outer wall increases (for B/d = 2, 5, 10 and 15, $\hat{\Psi}$ occurs at B/2d-$\xi$ ≈ 0.85, 1.38, 1.75 and 1.88, respectively).

The vertical distribution of $\psi$ in the channel axis reflects the influence of advection on the main velocity distribution: a low Dean number profile in shallow channels and a higher Dean number profile in a square pipe (see figure 17g).

## 5.4. Summary

The conclusions to be drawn from the shallow channel computations can be summarized as follows.

1. When the geometry is kept constant and the Dean number is raised from zero on,
   - the maximum of the main velocity shifts from the inner to the outer wall and the horizontal distribution changes from skewed inward to skewed outward.
   - the vertical distribution of the main velocity grows steeper near the bottom and flatter in the upper parts of the cross-section, until at higher Dean numbers the main velocity even decreases near the surface.
   - the boundary shear stress remains almost constant near and at the inner wall, whereas it drastically increases near and at the outer wall.
   - the longitudinal slope factor increases considerably
   - the intensity of the secondary flow grows to a maximum and then decreases again
   - the centre of circulation of the secondary flow moves outwards as long as the secondary flow intensity increases, and subsequently moves inwards again
   - the centre of circulation moves down, such that the inward radial velocity tends to concentrate near the bottom
   - the vertical distribution of the pressure remains almost hydrostatic
   - the transverse pressure drop increases in proportion with $De^2$ at low Dean numbers and with $De^{1.96}$ as De becomes higher
   - the mean radial pressure gradient is almost the same as in a square pipe
   - the transverse pressure distribution is hardly influenced by the secondary flow.
   - the kinetic energy distribution is completely dominated by $u^2$.
2. When the cross-sectional shape and the Dean number are kept constant and the curvature ratio $\varepsilon$ is raised from very small values on,

- the influence on the "potential flow effect" on the horizontal distribution of the main velocity increases
- the influence of advection on the vertical distribution of the main velocity intensifies near the inner wall and weakens near the outer wall
- the magnitude of the secondary velocity vector increases near the inner wall and decreases near the outer wall
- the maximum of the stream function of the secondary flow decreases and shifts inwards
- through the main velocity the vertical distribution of the stream function is more influenced by advection near the inner wall than near the outer wall.

3. When the Dean number and the curvature ratio are kept constant and the channel aspect ratio B/d is raised from 2 on,
   - the main velocity maximum moves outwards, but such that the horizontal distribution of the main velocity near the outer wall hardly changes
   - the influence of advection on the vertical distribution of the main velocity decreases
   - the secondary flow intensity increases
   - the centre of circulation of the secondary flow moves outwards, but the distance to the outer wall increases
   - through the main velocity, the influence of the Dean number on the vertical distribution of the stream function of the secondary flow decreases
4. The redistribution of the main velocity under the influence of advection is the cause of most of the other phenomena, such as the increase of the boundary shear stress and the longitudinal slope factor, the increase at smaller De and the decrease at higher De of the secondary flow intensity and the shifting of the centre of circulation of the secondary flow.

## 6. Analysis of the main velocity redistribution

In chapter 5 it was shown that most of the phenomena observed in the results of the shallow channel computations could be explained from the redistribution of the main velocity. In order to gain a better understanding of the physical mechanisms underlying this redistribution, it will be attempted to analyse it mathematically and physically.
According to the longitudinal momentum equation for axisymmetric curved flow.

$$De^2 \{- \frac{1}{r} \frac{\partial \psi}{\partial \zeta} (\frac{\partial u}{\partial \xi} + \frac{\varepsilon}{r} u) + \frac{1}{r} \frac{\partial \psi}{\partial \xi} \frac{\partial u}{\partial \zeta} \} = \frac{\iota}{r} + \frac{\partial^2 u}{\partial \zeta^2} + \frac{\partial^2 u}{\partial \xi^2} + \frac{\varepsilon}{r} \frac{\partial u}{\partial \xi} - \frac{\varepsilon^2}{r^2} u \qquad (6.1)$$

and the equivalent equation for fully developed straight flow

$$0 = \iota_o + \frac{\partial^2 u}{\partial \zeta^2} + \frac{\partial^2 u}{\partial \xi^2} \qquad (6.2)$$

, there are three kinds of differences between the fully developed main velocity distributions in curved and straight channels, arising from

- advection by the secondary flow
- the factor $\frac{1}{r}$ in the pressure gradient term
- the extra diffusion terms due to the divergence of the coordinate system

, respectively. The last two sources together give rise to the "potential flow" effect mentioned in section 5.2.: outside the sidewall boundary layers the radial distribution of the main velocity tends to be the same as in a potential vortex, viz. proportional to $\frac{1}{r}$, as can easily be shown from equation (6.1) for De = 0:

$$0 = \frac{\iota}{r} + \frac{\partial^2 u}{\partial \zeta^2} + \frac{\partial^2 u}{\partial \xi^2} + \frac{\varepsilon}{r} \frac{\partial u}{\partial \xi} + \frac{\varepsilon^2}{r^2} u \qquad (6.3)$$

Outside the sidewall boundary layers the solution of this equation can be written as:

$$u = \frac{\iota}{2r} (1 - \zeta^2) \tag{6.4}$$

(see also the low Dean number solution by DE VRIEND, 1973). When De is raised from zero on, the influence of advection grows more and more important and the main velocity distribution is gradually "inverted" until the maximum occurs near the outer wall and at some distance below the surface (see section 5.1.). This velocity redistribution under the influence of advection will be subject to further analysis in the next parts of this section.

## 6.1. Influence of advection at low Dean numbers

At low Dean numbers the influence of advection can be considered as a perturbation of the zero Dean number solution (cf. DEAN (1928) and ADLER (1934) for circular pipes, ITŌ (1951), CUMING (1952) and DE VRIEND (1973, a,b)). Accordingly, the main velocity, the longitudinal slope factor and the stream function can be written as power series expansions of $De^2$:

$$u = \sum_{k=0}^{\infty} De^{2k} u_k \quad ; \quad \iota = \sum_{k=0}^{\infty} De^{2k} \iota_k \quad ; \quad \psi = \sum_{k=0}^{\infty} De^{2k} \psi_k \tag{6.5}$$

The first main velocity perturbation $u_1$ of the zero Dean number solution $u_0$ is solved from

$$-\frac{1}{r}\frac{\partial \psi_0}{\partial \zeta}\left(\frac{\partial u_0}{\partial \xi} + \frac{\varepsilon}{r} u_0\right) + \frac{1}{r}\frac{\partial \psi_0}{\partial \xi}\frac{\partial u_0}{\partial \zeta} = \frac{\iota_1}{r} + \frac{\partial^2 u_1}{\partial \zeta^2} + \frac{\partial^2 u_1}{\partial \xi^2} + \frac{\varepsilon}{r}\frac{\partial u_1}{\partial \xi} - \frac{\varepsilon^2}{r^2} u_1 \tag{6.6}$$

Defining

$$u_1 = \frac{\iota_1}{\iota_0} u_0 + u_1' \tag{6.7}$$

the influence of advection is isolated in $u_1'$, which can be solved from

$$-\frac{1}{r}\frac{\partial \psi_0}{\partial \zeta}\left(\frac{\partial u_0}{\partial \xi} + \frac{\varepsilon}{r} u_0\right) + \frac{1}{r}\frac{\partial \psi_0}{\partial \xi}\frac{\partial u_0}{\partial \zeta} = \frac{\partial^2 u_1'}{\partial \zeta^2} + \frac{\partial^2 u_1'}{\partial \xi^2} + \frac{\varepsilon}{r}\frac{\partial u_1'}{\partial \xi} - \frac{\varepsilon^2}{r^2} u_1' \tag{6.8}$$

As an illustration of how advection influences the main flow, equation (6.8) is solved neglecting the lateral diffusion terms and approximating $u_0$ and $\psi_0$ by

$$u_0 \simeq \bar{u}_0 \frac{3}{2} (1 - \zeta^2) \tag{6.9}$$

$$\psi_0 \simeq \bar{\psi}_0 \frac{24}{19} (\zeta^7 - 7\zeta^5 + 11\zeta^3 - 5\zeta) \tag{6.10}$$

The resulting expression for $u_1'$ reads:

$$u_1' = \frac{\bar{\psi}_0}{r} (\frac{d\bar{u}_0}{d\xi} + \frac{\varepsilon}{r} \bar{u}_0) f_1(\zeta) + \frac{\bar{u}_0}{r} \frac{d\bar{\psi}_0}{d\xi} f_2(\zeta) \tag{6.11}$$

where $f_1(\zeta)$ and $f_2(\zeta)$ are polynomials in $\zeta$ (cf. DE VRIEND, 1973).

From equation (6.7) and the integral condition of continuity (3.38) an expression for $\iota_1$ can be derived, such that the first order approximation of u reads

$$u \simeq u_0 + De^2 u_1 = u_0 \{ 1 - De^2 \frac{d}{B} \int_{-B/2d}^{B/2d} d\xi' \int_{-1}^{} u_1' d\zeta \} + De^2 u_1' \tag{6.12}$$

The depth-averaged value of $u_1'$, given by

$$\bar{u}_1' = - \frac{\bar{\psi}_0}{r} (\frac{d\bar{u}_0}{d\xi} + \frac{\varepsilon}{r} \bar{u}_0) \frac{6656}{7315} - \frac{1}{r} \frac{d\bar{\psi}_0}{d\xi} \bar{u}_0 \frac{3328}{7315} \tag{6.13}$$

, will be negative near the inner sidewall, where both $\frac{d\bar{u}_0}{d\xi} + \frac{\varepsilon}{r} \bar{u}_0$ and $\frac{d\bar{\psi}_0}{d\xi}$ are positive, and positive near the outer sidewall, where these quantities are negative. Outside the sidewall regions of a shallow channel the radial derivatives (and hence $u_1'$) are small with respect to the peaks occuring near the sidewalls. Therefore the modulus of the overall mean value of $u_1'$ can be expected to be considerably smaller than the maxima of $|u_1'|$. Hence it can be concluded from (6.12) that under the influence of advection by the secondary flow a reduction of $\bar{u}$ with respect to $\bar{u}_0$ occurs near the inner wall, whereas near the outer wall $\bar{u}$ increases with respect

to $\bar{u}_0$. This is the same tendency as observed in the shallow channel computations by the complete model (see figure 11), although the influence is more local here, i.e. confined to the sidewall regions*).

An important feature of the advective influence on the vertical distribution of the main velocity, viz. the flattening tendency, can also be explained from (6.11). Rewriting (6.12) as

$$u = \left[ \bar{u}_0 \left\{ 1 - De^2 \frac{d}{B} \int_{-B/2d}^{B/2d} d\xi \int_{-1}^{0} u_1' d\zeta \right\} + De^2 \bar{u}_1' \right] \frac{3}{2} (1 - \zeta^2) +$$

$$+ De^2 \left\{ \frac{\bar{\psi}_0}{r} \left( \frac{d\bar{u}_0}{d\xi} + \frac{\varepsilon}{r} \bar{u}_0 \right) f_1(\zeta) + \frac{\bar{u}_0}{r} \frac{d\bar{\psi}_0}{d\xi} f_2(\zeta) \right\} \qquad (6.14)$$

, the functions $f_1(\zeta)$ and $f_2(\zeta)$ (polynomials in $\zeta$) indicate how the vertical distribution of u is influenced by advection due to the radial and the vertical velocity, respectively. The two functions are represented graphically in figures 18a-b, showing that, as long as $\frac{d\bar{u}_0}{d\xi} + \frac{\varepsilon}{r} \bar{u}_0$ is positive, the radial velocity component gives rise to a flattening of the main velocity profile, whereas, but to a much lower extent, a positive vertical velocity leads to more oblique profiles of u.

A physical interpretation of these results can be given when considering the main flow isovels and the secondary flow streamlines of the zero Dean number solution near the inner wall, for instance. Figure 18c shows the streamlines of the secondary flow to intersect the main flow isovels such that the main velocity always increases when moving along a streamline. Apparently, the secondary flow in the inner wall region always conveys fluid from places with lower longitudinal momentum of the undisturbed flow to places with higher longitudinal momentum of the undisturbed flow. As a consequence, an overall decrease of the main velocity with respect to $u_0$ occurs near the inner wall.

---

*) Even if lateral diffusion is taken into account this local character remains for the greater part (DE VRIEND, 1973).

The local advective effect of the secondary flow is likely to increase with the local values of the secondary flow intensity, the gradient of the undisturbed main velocity field and the angle of intersection between the isovels and the streamlines, in that the effect will be the strongest when the streamlines are normal to the isovels. The mathematical verification of this hypothesis can be found from the expressions for the directions of the isovels and the streamlines with respect to the horizontal axis, denoted by $\alpha_i$ and $\alpha_s$, respectively:

$$\tan \alpha_i = - \frac{\partial u_0}{\partial \xi} / \frac{\partial u_0}{\partial \zeta} \text{ and } \tan \alpha_s = - \frac{\partial \psi_0}{\partial \xi} / \frac{\partial \psi_0}{\partial \zeta} = \frac{w_0}{v_0} \tag{6.15}$$

Using these expressions it can easily be derived that

$$v_0 \frac{\partial u_0}{\partial \xi} + w_0 \frac{\partial u_0}{\partial \zeta} = \sqrt{v_0^2 + w_0^2} \sqrt{\left(\frac{\partial u_0}{\partial \xi}\right)^2 + \left(\frac{\partial u_0}{\partial \zeta}\right)^2} \sin(\alpha_s - \alpha_i) \tag{6.16}$$

So discarding the effect of the divergence of the coordinate system represented by the term $\varepsilon \frac{u_0 v_0}{r}$ *), the advection terms in equation (6.1) are proportional to each of the aforementioned quantities if the sine of the angle of intersection is taken.

In figure 18c the streamlines appear to intersect the isovels at much larger angles in the higher parts of the represented region than in the lower parts of it, where the two sets of lines are almost parallel. The secondary flow intensity is also somewhat higher in the upper parts and, at least within a distance of about the depth of flow from the inner wall, the main velocity gradients are of the same order of magnitude throughout the vertical. Consequently, the advection terms will increase from the bottom to the surface and the main velocity profile will grow flatter in the upper part and steeper in the lower part of

---

*) If the divergence effect is taken into account, the same reasoning holds for lines of constant $ru_0$ instead of the isovels.

the vertical [1]), as is confirmed by equation (6.11) and figures 18a-b.

## 6.2. Separation of horizontal and vertical distribution of u

In low Dean number flow the perturbations of the main velocity distribution with respect to the zero Dean number distribution $u_0$ have a local character in that the perturbation in a point is strongly dependent on the advection terms (based on $u_0$) in the vicinity[2]) of that point, but is hardly influenced by the advection terms further away. As the Dean number increases, however, the lateral interaction grows stronger and the influence of advection is felt throughout the cross-section, even if it is very shallow. In a shallow channel the lateral interaction outside the sidewall boundary layers takes place on a much larger length scale than the vertical interaction. This suggests the radial and the vertical distribution of u can be treated separately when analysing the influence of advection. This would be rather favourable, not only because of the easier understanding of the redistribution phenomenon, but also as regarding the expenses of the computations necessary for the analysis. Moreover, it would provide a possibility to develop a simplified computation method. Therefore it will first be investigated whether a similarity solution of the shape

$$u(\xi,\zeta) = \bar{u}(\xi)\, f(\zeta) \qquad (6.17)$$

, $\bar{u}(\xi)$ denoting the mean value of u in a vertical $\xi$, gives an appropriate approximation of the transverse distribution of the main velocity.
If (6.17) were exactly true, the quantity $u/u|_{\xi=0}$ would be equal to $\bar{u}/\bar{u}|_{\xi=0}$, i.e. independent on $\zeta$. According to figure 19a, $u/u|_{\xi=0}$ hardly depends on $\zeta$, except near the outer wall at higher Dean numbers.

---

1) A constant value of the advection terms throughout the vertical would have yielded a parabolic perturbation of u, so that the shape of the main velocity profile is not affected.
2) Area with a characteristic dimension of the order O(d)

Similarly, the quantity $u/\bar{u}$ would be equal to $f(\zeta)$, i.e. independent on $\xi$, if (6.17) were exact. From figure 19b it appears that the vertical distributions of u show the same features throughout the cross-section, especially as far as the flattening at higher Dean numbers is concerned. Adopting (6.17) as an approximation of u and assuming $\psi$ can also be approximated by a similarity solution

$$\psi(\xi,\zeta) = \bar{\psi}(\xi)\, g(\zeta) \tag{6.18}$$

, the following depth-averaged equation can be derived from the longitudinal momentum equation (3.35):

$$\frac{De^2}{r^2} \frac{d}{d\xi} (r\bar{\psi}\bar{u}) \int_{-1}^{0} g \frac{df}{d\zeta} d\zeta = \frac{\iota}{r} + \frac{d^2\bar{u}}{d\xi^2} + \frac{\varepsilon}{r} \frac{d\bar{u}}{d\xi} - \frac{\varepsilon^2}{r^2} \bar{u} - \bar{u} \frac{df}{d\zeta} \Big|_{\zeta=-1} \tag{6.19}$$

If $\bar{\psi}$, $f$ and $g$ are known functions, equation (6.19) can be considered as a linear differential equation in $\bar{u}$ with $\iota$ as an additional unknown constant. In combination with the integral condition of continuity (3.38) and the boundary conditions.

$$\bar{u} = 0 \quad \text{at} \quad \xi = \pm \frac{B}{2d} \tag{6.20}$$

this equation can be solved for $\bar{u}$ and $\iota$. If for $\bar{\psi}$, $f$ and $g$ the results of the complete mathematical model are substituted, taking $f(\zeta) = (u/\bar{u})\big|_{\xi=0}$ and $g(\zeta) = (\psi/\bar{\psi})\big|_{\xi=0}$, the above depth-averaged computation yields the mean velocity distributions represented in figure 20a. Although at higher Dean numbers the peak in the outer wall region is too pronounced, the essential features of the mean velocity redistribution are well represented*).

*) The observed redistribution may not be attributed to the substitution of the bed shear stress factor $\frac{df}{d\zeta}\big|_{\zeta=-1}$ derived from the results of the complete model. Neglecting advection, the solution of the depth averaged equation lies close to the depth-averaged solution of the complete system for all Dean numbers considered (figure 20b).

From the similarity approximations (6.17) and (6.18) and the longitudinal momentum equation (3.35) the following mathematical system can be derived:

$$De^2 \{- \frac{\bar{\psi}}{r} (\frac{d\bar{u}}{d\xi} + \frac{\varepsilon}{r} \bar{u}) \frac{dg}{d\zeta} f' + \frac{\bar{u}}{r} \frac{d\bar{\psi}}{d\xi} g \frac{df'}{d\zeta}\} = \frac{1}{r} + \bar{u} \frac{d^2 f'}{d\zeta^2} + (\frac{d^2\bar{u}}{d\xi^2} + \frac{\varepsilon}{r} \frac{d\bar{u}}{d\xi} - \frac{\varepsilon^2}{r^2} \bar{u}) f' \qquad (6.21)$$

with the boundary conditions

$$f' = 0 \text{ at } \zeta = -1; \quad \frac{df'}{d\zeta} = 0 \quad \text{at} \quad \zeta = 0 \qquad (6.22)$$

and the definition

$$f(\zeta) = f'(\zeta)/\bar{f}' \qquad (6.23)$$

If $\bar{u}$, $\bar{\psi}$ and $g(\zeta)$ are known functions, equation (6.21) is a linear differential in $f'$. Substituting $\bar{u}$, $\bar{\psi}$ and $g(\zeta)$ as they were computed by the complete mathematical model, $f(\zeta)$ can be solved from the above system in any vertical of the cross-section. For $\xi = -B/2d+0.5$, $\xi = 0$ and $\xi = B/2d-0.5$ the results are given in figure 21a, from which the agreement with the relevant results of the complete model appears to be good in the chanel axis and somewhat worse near the sidewalls, at least at higher Dean numbers *). Presumably, the differences near the sidewalls must be attributed to approximations made in the lateral diffusion terms and in the radial advection terms of equation (6.21) by replacing the radial derivatives of u by $u/\bar{u}$ times the relevant derivative of $\bar{u}$. Thus the interaction between $u/\bar{u}$ in various verticals is neglected. Nevertheless, it can be concluded that the horizontal and the vertical distribution of u can be separated when analysing the advective main velocity redistribution.

---

*) See footnote on page 45 and figure 21b

## 6.3. Horizontal distribution of the main velocity

In addition to the longitudinal slope term, the following terms of groups of terms can be distinguished in the depth-averaged longitudinal momentum equation (6.19):

- the radial advection term $De^2 \frac{\bar{\psi}}{r} \left(\frac{d\bar{u}}{d\xi} + \frac{\varepsilon}{r} \bar{u}\right) \int_{-1}^{0} g \frac{df}{d\zeta} d\zeta$

- the vertical advection term $De^2 \frac{\bar{u}}{r} \frac{d\bar{\psi}}{d\xi} \int_{-1}^{0} g \frac{df}{d\zeta} d\zeta$

- the lateral diffusion terms $\frac{d^2\bar{u}}{d\xi^2} + \frac{1}{r} \frac{d\bar{u}}{d\xi} - \frac{\varepsilon^2}{r^2} \bar{u}$

- the bed shear stress term $- \bar{u} \frac{df}{d\zeta} \Big|_{\zeta=-1}$

The influence of each of these terms on the solution of (6.19) and so on the redistribution of $\bar{u}$ has been investigated. Figure 22a shows the mean velocity distributions resulting from equation (6.19) when omitting each of the above terms or groups of terms, respectively. If the radial advection terms are neglected, the peak in $\bar{u}$ occurring near the outer wall becomes wider and higher, which suggests the advective effect on $\bar{u}$ to increase. If the vertical advection terms are neglected, however, the advective influence on $\bar{u}$ almost vanishes: the maximum of $\bar{u}$ liest near the inner wall for all Dean numbers considered and the peak near the outer wall is absent. Only the inner wall layer becomes thicker and the outer wall layer becomes thinner as De decreases.
At all Dean numbers considered the influence of the lateral diffusion terms in the central region of the cross-section ($-4<\xi<4$) appears to be negligible. In the sidewall regions lateral diffusion is important in combination with the no-slip condition at the sidewalls in that it gives rise to boundary layers of

nonzero thickness and, especially near the outer wall, to a limitation of the main velocity peak at higher Dean numbers. The latter effect is readily shown by comparing the solutions of (6.19) with no-slip conditions and with zero tangential shear stress conditions at the sidewalls (figure 22b). Additionally, it becomes evident from this comparison that the main velocity distributions in the central region are essentially the same, even though they differ by a constant factor as a consequence of the differences near the sidewalls (the overall mean value of $\bar{u}$ is always equal to 1; cf. (3.48) and (3.49)). Hence it is concluded that the influence of lateral diffusion and the sidewall boundary conditions on the distribution of $\bar{u}$ is restricted to the sidewall regions.

As was to be expected in this shallow channel, neglecting the bed shear stress has a dramatic effect. For De=0 the distribution of $\bar{u}$ becomes parabolic rather than inversely proportional to r with sidewall boundary layers (figure 22a). As De increases a very strong influence of the secondary flow is observed, pushing the maximum of $\bar{u}$ towards the outer wall and giving rise to very pronounced peaks in $\bar{u}$ near the outer wall at higher Dean numbers. Outside the wall regions $\frac{d\bar{u}}{d\xi}$ is practically constant. Apparently, the bed shear stress restricts the sidewall boundary layers*), thus giving rise to flatter distributions of $\bar{u}$, and it damps the effect of secondary flow advection.

This damping phenomenon can be illustrated by the following example for the central region. Taking $\bar{\psi}$ as a constant, neglecting lateral diffusion and setting r=1 for simplicity, equation (6.19) reduces to

$$k_1 \frac{d\bar{u}}{d\xi} = 1 - k_2\bar{u} \qquad (6.24)$$

---

*) The parabolic profile obtained for De=0 and zero bed shear stress implies that the sidewall boundary layers are fully interacting.

where $k_1 = De^2 \bar{\psi} \int_{-1}^{0} g \frac{df}{d\zeta} d\zeta$ and $k_2 = \frac{df}{d\zeta}\Big|_{\zeta=-1}$. Since this is a first order differential equation, only one boundary condition can be imposed on $\bar{u}$, say

$$\bar{u} = \bar{u}_0 \quad \text{at} \quad \xi = \xi_0 \tag{6.25}$$

where $\xi_0$ indicates a point close to the inner wall boundary layer. Then the solution of (6.24) reads

$$\bar{u} = \frac{1}{k_2} + (\bar{u}_0 - \frac{1}{k_2}) e^{-\frac{k_2}{k_1}(\xi - \xi_0)} \tag{6.26}$$

As a consequence of secondary flow advection, $\bar{u}_0$ is likely to be smaller than $1/k_2$, so $\bar{u}$ will increase towards its asymptote $\bar{u} = 1/k_2$. Both $\bar{u}_0$ and the quantity $k_2/k_1$ will decrease for increasing De, so $\bar{u}$ will approach its asymptote more gradually then. This explains why the inner wall boundary layer becomes thicker at higher Dean numbers.
If the bed shear stress is neglected, however, so if $k_2/k_1 \to 0$,

$$\bar{u} = \bar{u}_0 + \frac{1}{k_1} (\xi - \xi_0) \tag{6.27}$$

So by lack of the damping effect of the bed shear stress, the mean velocity in the central region increases linearly with $\xi$ (cf. figure 22a).
Reconsidering the advective influence of the secondary flow, it can be shown from (6.19) that in the central region, where lateral diffusion is negligible, the effect of the vertical velocity component has a local character. Omitting the radial advection term and neglecting lateral diffusion, equation (6.19) reduces to

$$De^2 \frac{\bar{u}}{r} \frac{d\bar{\psi}}{d\xi} \int_{-1}^{0} g \frac{df}{d\zeta} d\zeta = \frac{1}{r} - \bar{u} \frac{df}{d\zeta}\Big|_{\zeta=-1} \tag{6.28}$$

in the central region. Equation (6.28) can be rewritten as an

explicit expression for $\bar{u}$, containing only local values of the other variables. Accordingly, there is no lateral interaction between the mean velocities in adjacent points.
On the other hand, the radial advection term does give rise to lateral interaction: the mean velocity in a point is influenced by the mean velocities further inwards (cf. (6.26) and (6.27)). It should be noted, however, that, at least in the central region, the mean velocity in a point is hardly influenced by the mean velocities further outwards. This is readily illustrated by figure 22c, representing solutions of (6.19) when neglecting lateral diffusion in the central region and vertical advection in one half of the cross-section. If the radial advection term is also neglected, the solution in the central region corresponds with (6.28). If the radial advection is taken into account, however, the mean velocity tends to the solution of (6.28), but the adaptation is retarded in outward direction (cf. (6.26)) and the discontinuity at $\xi=0$ resulting from (6.28) is felt only for $\xi>0$.
A mathematical explication of this exclusively outward influence of advection can be given by considering the following $\phi$-dependent version of (6.19) without lateral diffusion and with r=1 for simplicity:

$$a\,\bar{u}\,\frac{\partial \bar{u}}{\partial \phi'} + De^2 \bar{\psi} \int_{-1}^{\theta} g\,\frac{df}{d\zeta}\,d\zeta\,\frac{\partial \bar{u}}{\partial \xi} = \iota - \bar{u}\,\frac{df}{d\zeta}\Big|_{\zeta=-1} - De^2\,\frac{d\bar{\psi}}{d\xi}\int_{-1}^{0} g\,\frac{df}{d\zeta}\,d\zeta\,\bar{u} \qquad (6.29)$$

where a is a positive constant. The direction of the characteristics of this equation is given by

$$\frac{d\xi}{d\phi'} = De^2\,\frac{\bar{\psi}}{a\bar{u}}\int_{-1}^{0} g\,\frac{df}{d\zeta}\,d\zeta \qquad (6.30)$$

so the characteristics are directed outward throughout the cross-section, $\bar{\psi}$, a, $\bar{u}$ the integral being positive. Consequently, disturbances can only move outwards, so the mean velocity in a point can be influenced by the mean velocities further inwards, but not by those further ourwards. In other words: in the flow described by equation (6.29) all information is transported

outwards at a celerity of which the radial component has a magnitude

$$De^2 \bar{\psi} \int_{-1}^{0} g \frac{df}{d\zeta} d\zeta$$

As a conclusion from the mathematical analysis of the depth-averaged equation (6.19) the following concept of the physical mechanism of advective main velocity redistribution can be drawn up:

- through the same mechanism as described in section (6.1.) for low Dean number flow, near the inner wall the secondary flow, and especially its vertical component, gives rise to lower values of $\bar{u}$ than would be found without accounting for advection, whereas near the outer wall it causes higher values of $\bar{u}$.
- the reduction of $\bar{u}$ near the inner wall influences the mean velocity further outwards through the outward retardation effect of radial advection combined with the bed shear stress and local vertical advection; as compared with the distribution of $\bar{u}$ without the influence of radial advection, the region of noticeable increase of $\bar{u}$ near the outer wall and the magnitude of this increase are reduced by the same retardation effect.
- in regions where the vertical velocity is positive, the bed shear stress and the vertical advection act in the same sense in combination with radial advection: radial variation tendencies of $\bar{u}$ are damped; when w is negative, however, the two elements have opposite effects, the bed shear stress still damping, but vertical advection destabilizing now.
- the peak in $\bar{u}$ near the outer wall is damped by the effect of lateral diffusion together with the no-slip condition at the wall.

Another verification of this concept can be obtained by analysing (6.19) in case of slipping sidewalls (for $\bar{u}$ only). Then the mean velocity gradients near the sidewalls will be much smaller than in case of no-slip walls, so the local advective effect of the

radial velocity component will be much smaller there. Accordingly, the solution for w=0 is practically independent on De (figure 22b). On the other hand, the local effect of vertical advection will increase in the sidewall regions, the sidewall conditions being less limitative. Attempts to verify this increase by solving (6.19) for v=0 and slipping sidewalls, however, fail as a consequence of negative values of $\bar{u}$ *) occurring near the outer wall for De=25 and De=50 (figure 22b). At smaller values of De the differences between the solutions with and without radial advection are too small to draw conclusions from.

According to the aforementioned concept of the advective redistribution mechanism, the mean velocity distribution outside the sidewall regions ought to show the same features as in case of no-slip walls, $\bar{u}$ being reduced near the inner wall and the outward retardation effect remaining unchanged. Figure 22b shows that in the central region the solutions for slipping sidewalls and for no-slip walls do agree, except for a constant factor arising from the differences near the sidewalls.

## 6.4. Vertical distribution of the main velocity

In equation (6.19) for the vertical distribution of the main velocity the following terms or groups of terms can be distinguished in addition to the reduced longitudinal slope term $\frac{1}{r}$:

- the radial advection term $- De^2 \frac{\bar{\psi}}{r} \left(\frac{d\bar{u}}{d\xi} + \frac{\varepsilon}{r} \bar{u}\right) \frac{dg}{d\zeta} f'$

- the vertical advection term $De^2 \frac{\bar{u}}{r} \frac{d\bar{\psi}}{d\xi} g \frac{df'}{d\zeta}$

- the lateral diffusion terms $\left(\frac{d^2\bar{u}}{d\xi^2} + \frac{\varepsilon}{r} \frac{d\bar{u}}{d\xi} - \frac{\varepsilon^2}{r^2} \bar{u}\right) f'$

---

*) Due to negative values of the quantity $\frac{De^2}{r} \frac{d\bar{\psi}}{d\xi} \int_{-1}^{0} g \frac{df}{d\zeta} d\zeta + \left.\frac{df}{d\zeta}\right|_{\zeta=-1}$

- the vertical diffusion term $\bar{u}\,\frac{d^2f'}{d\zeta^2}$

The structure of the equation is quite similar to that of equation (6.19)*) in that it contains a second order diffusion term (here the vertical, in (6.19) the lateral diffusion term) a first order transport term (here the vertical, in (6.19) the radial advection term) and, in addition to the longitudinal slope term, two production terms (here the radial advection term and the lateral diffusion terms, in (6.19) the vertical advection term and the vertical diffusion or bed shear stress term). Consequently, the mechanism of advective main velocity redistribution in the vertical must be similar to the mechanism of advective mean velocity redistribution, although the relative importance of the various effects may be different.
As shown by figure 23, the effects of advection on the vertical distributions of u near the sidewalls are qualitatively the same as described for low Dean number flow. Near the inner wall radial advection gives rise to an increase of u in the lower parts of the vertical and a decrease in the upper parts, whereas vertical advection causes a decrease in the lower parts and an increase in the upper parts. Near the outer wall the reverse effects occur.
In the central region both lateral diffusion and vertical advection turn out to have little influence. Neglecting the radial advection, however, appears to have a considerable effect, the main velocity profile staying close to the low Dean number profile for all Dean numbers considered.
Regarding the predominant impartance of the radial advection term, the vertical distribution of the main velocity in the central region must physically be explained as follows. In the upper part of a

---

*) This is to be expected since both equations are derived in a similar way from the longitudinal momentum equation (3.35), the structure of which is independent of the direction of the co-ordinates in the transverse plane, at least if divergence effects are discarded. Full similarity with equation (6.19) is attained by integrating (6.21), multiplied by $r^2$, in radial direction:

$$De^2\,\frac{d}{d\zeta}\,(f'g)\int_{-B/2d}^{B/2d}\bar{u}r\,\frac{d\bar{\psi}}{d\xi}\,d\xi=\frac{B}{d}+\frac{d^2f'}{d\zeta^2}\int_{-B/2d}^{B/2d}r^2\bar{u}d\xi+f'\left(r^2\,\frac{d\bar{u}}{d\xi}\right)\Big|_{-B/2d}^{B/2d} \qquad (6.31)$$

vertical the momentum of the fluid advected by the (outward) secondary flow is smaller than when advection would not affect the vertical distribution of the main velocity, as the mean velocity increases in outward direction and the vertical distribution of u is flatter than without advection. For the same reasons the momentum of the fluid advected in the lower part of the vertical is higher than without advection. Consequently, radial advection causes u to decrease in the upper part of the vertical and to increase in the lower part.

## 6.5. High Dean number flow

Although it may be of no direct interest to the problem of flow in river bends, some attention will be paid here to the flow at higher and very high Dean numbers, the former to explain the generation of a second spiral near the outer wall, the latter as a limit case of the intermediate Dean number flow described in the foregoing sections. The present model yielding no reliable solution for Dean numbers higher than about 60, the analysis of the high Dean number flow will be based on what is known from experimental and theoretical work reported in the literature (CHENG, LIN AND OU, 1976; MORI, UCHIDA AND UKON, 1971; SMITH, 1976).

As was reported in the literature (JOSEPH, SMITH AND ADLER, 1975) and confirmed by the present computations, in square pipes the regular secondary flow pattern, consisting of two counterrotating vortices, abruptly changes into a four vortex pattern if the Dean number becomes larger than about 50. The occurrence at higher Dean numbers of two counterrotating vortices near the centre of the outer wall was also reported by CHENG AND AKIYAMA (1970) and by CHENG, LIN AND OU (1976), the latter showing a second vortex to occur at sufficiently high Dean numbers in shallow channels, as well.
In terms of "open" channels, this breaking up can be explained as follows. If the Dean number is sufficiently large, secondary flow advection will give rise to negative vertical derivatives

of the main velocity in the upper part of the cross-section. Consequently, the source term in the stream function equation, $\frac{\partial}{\partial \zeta}(u^2)$, becomes negative there. If these negative values grow sufficiently strong, the stream function itself becomes negative in the upper part of the cross-section, so a second secondary circulation develops, with a sense of rotation opposite to the regular secondary flow. Near the inner wall and in the central region, where the mean velocity increases in outward direction, such a second circulation, when existing, would destroy itself, since its advective effect would cause the vertical derivatives of the main velocity in the upper part of the cross-section to become positive. In the outwall region, however, where the mean velocity sharply decreases in outward direction, the second circulation intensifies itself through its advective effect on the main flow, the main velocity near the surface being further reduced and the vertical derivatives of u growing more negative there. This also explains the abruptness of the transition from the regular secondary flow pattern with a single vortex to the double vortex pattern: as soon as a second vortex develops near the outer wall develops, it intensifies itself as far as viscous diffusion permits. In essence, the physical mechanism giving rise to the double vortex pattern in shallow channels is the same as the mechanism causing the instability for small disturbances of laminar flow in a narrow curved channel formed by two concentric plates (DEAN, 1928).

When the Dean number is further increased, the main velocity gradients and the secondary flow concentrate in rather thin layers along the fixed walls. Outside these layers an inviscid core develops, in which a small outward secondary flow occurs. Both this secondary flow and the main velocity in the core are constant in a vertical (MORI, UCHIDA AND UKON, 1971; SMITH, 9176). In the inviscid core the longitudinal momentum equation reduces to

$$De^2 \frac{\tilde{\psi}}{r}\left(\frac{du}{d\xi} + \frac{\varepsilon}{r} u\right) = \frac{1}{r} \tag{6.32}$$

in which $\tilde{\psi}$ is independent of $\zeta$. The solution reads

$$u = \frac{\iota}{De^2} \frac{1}{r} \int^{\xi} \frac{r}{\tilde{\psi}} \, d\xi + \frac{c}{r} \tag{6.33}$$

where c is a constant of integration to be determined by matching the core solution with the solution in the wall layers. Setting the vertical velocity in the core equal to zero, it can be shown from the equation of continuity that $\tilde{\psi}$ must be a constant, so that according to (6.33) the main velocity in the core consists of two parts, one increasing linearly with r and the other one inversely proportional to r. This core flow can be considered as the high Dean number limit of the mean velocity distribution at intermediate Dean numbers, with the damping effect of vertical diffusion (bed shear stress) and vertical advection reduced to zero in the core.
Essentially the same concept, with an inviscid core enclosed by a three dimensional boundary layer along the fixed walls, was adopted by MURAMOTO (1965) in order to describe fully developed flow in curved open channels. Assuming $\frac{\iota}{r}$ to be a constant rather than $\iota$, the mean velocity distribution he found in the core consisted of a part increasing with $r^2$ and a part inversely proportional to r. The experimental verification of this theory showed a rather good agreement in the downstream part of a $180^o$ bend.

## 6.6. Summary

As regarding the mathematical model, the analysis of the longitudinal momentum equation leads to the following conclusions:

1. Two opposite effects cause the main velocity distribution in axisymmetric curved flow to deviate from the distribution in the equivalent straight channel flow, viz.
   - the potential flow effect, represented in the equation by the factor $\frac{1}{r}$ in the pressure gradient term and the extra diffusion terms due to the divergence of the coordinate system, and making the velocity distribution oblique towards the inner sidewall

- the advective influence of the secondary flow, making the velocity distribution skewed towards the outer wall and causing the velocity maximum to occur below the surface at sufficiently high Dean numbers.

2. The relative importance of these two effects is indicated by the Dean number (or rather the square of it): if De is small, the potential flow effect is predominant, if De is large, the effect of advection is the most important one.
3. At low Dean numbers the effect of advection can be computed as a perturbation of the zero Dean number solution; it is of a local kind then and in comparison with the zero Dean number solution it reduces the mean velocity near the inner wall and gives rise to a flatter vertical distribution of u there, whereas near the outer wall and, to a much lower extent, in the central region it augments the mean velocity and gives rise to a more oblique vertical distribution.
4. At low and intermediate Dean numbers (in the present examples: De < about 50), a similarity solution provides a good approximation of the main velocity. Supposing a similarity solution to hold for the stream function of the secondary flow, as well, the mean velocity and $u/\bar{u}$ can be analysed separately.
5. Supposing the stream function of the secondary flow and the vertical distribution of the main velocity to be known, the mean velocity can be solved from the depth-averaged longitudinal momentum equation. When analysing this equation it appears that:
   - the vertical advection term forms the main cause of the decrease of $\bar{u}$ near the inner wall and the increase near the outer wall
   - the influence of the vertical advection term is of a local kind, especially in the central region
   - the radial advection term alone is of minor importance to the redistribution of $\bar{u}$
   - the radial advection term gives rise to an important lateral interaction in that in a point the mean velocity is influenced by $\bar{u}$ further inwards; as a consequence, the region

influenced by the reduction of $\bar{u}$ near the inner wall is extended until it covers the greater part of the cross-section (De > about 10) and the region influenced by the increase of $\bar{u}$ near the outer wall is compressed against the outer wall

- the influence of the lateral diffusion terms and the sidewall boundary conditions is restricted to the regions close to the sidewalls
- the bed shear stress has a damping effect, thus reducing the mean velocities and causing a retardation in the effect of the radial advection term.

6. Supposing the stream function of the secondary flow and the mean velocity to be known, the vertical distribution of the main velocity can be solved from an equation derived from the longitudinal momentum equation. Analysing this equation shows that:
   - near the inner wall, where the vertical velocity is positive, the vertical advection term causes a decrease of $u/\bar{u}$ in the lower parts of a vertical and an increase in the higher parts; near the outer wall, where w is negative, the effect is reverse
   - the radial advection term gives rise to an increase of $u/\bar{u}$ in the lower parts of a vertical near the inner wall (where the radial derivative of $\bar{u}$ is positive), and a decrease in the upper parts; near the outer wall, where $\frac{d\bar{u}}{d\xi}$ is negative, the reverse occurs
   - in the central region the influence of the vertical advection term is small, but the radial advection term is quite important; it gives rise to similar deviations from the low Dean number profile of $u/\bar{u}$ as near the inner wall
   - the influence of lateral diffusion and the sidewall boundary conditions is small
7. At very high Dean numbers an inviscid core develops, in which the main velocity consists of two components, one proportional and one inversely proportional to r and both independent to $\zeta$. This core flow represents the high Dean number limit of the mean velocity distribution.

8. When De is raised up to values of about 60 and higher, the stream function of the secondary flow tends to become negative in the upper part of the cross-section; near the inner wall and in the central region this tendency reduces itself through the advective influence of the secondary flow on the vertical distribution of the main flow, but near the outer wall it amplifies itself through the same mechanism as far as viscous diffusion permits. As a consequence, for De ≃ 60 a sudden transition occurs from a secondary flow pattern with a single vortex to a pattern with an additional counterrotating vortex near the surface close to the outer wall.

The physical interpretation of the advective redistribution of the main velocity can be summarized as follows

1. In regions where the longitudinal momentum increases along the streamlines of the secondary flow, i.e. near the inner wall and, if the Dean number is not too small, in the upper part of the central region, the main velocity tends to decrease as a result of advection; near the outer wall and, if De is large enough, in the lower part of the central region, where the secondary flow moves in a direction of decreasing longitudinal momentum, the main velocity tends to increase due to advection. Due to these inertial effects, the mean velocity is reduced near the inner wall and increased near the outer wall and in the central region the vertical distribution of the main velocity grows steeper near the bed and flatter higher up in the vertical if De is raised from zero on.
2. The advective effect of the secondary flow is stronger in the upper half of the vertical than in the lower half. Consequently, there is a net effect of advection when averaging over the depth of flow. The advective influence of the vertical velocity component gets a local character then, but the net influence of the radial velocity keeps its inertial features: in combination with the bed shear stress, which acts as a damping mechanism, it has an outward retardation effect on

the mean velocity. Through this retardation mechanism the local reduction of $\bar{u}$ near the inner wall (mainly caused by vertical advection) influences the mean velocities in the greater part of the cross-section if De is large enough, whereas the local peak in $\bar{u}$ near the outer wall (also due to vertical advection) is compressed against the wall, where it is partly damped by viscous forces.

## 7. Simplified computations

Since the solution of the full steady state Navier Stokes equations for axisymmetric flow takes a lot of computer time, especially for the shallow channel computations (one iteration on a 10 x 10 grid took about 20 s on an IBM 370/158), it is worthwhile to look for possibilities of simplification before attempting to solve developing curved flow problems or turbulent flow problems.

### 7.1. The advection terms in the stream function equation

As became evident from the foregoing paragraphs, the advection terms in the longitudinal momentum equation may definitely not be neglected unless the Dean number is very small. In the stream function equation, however, the importance of the advection terms has not yet been investigated. Neglecting these terms would greatly reduce the computation work per iteration step, as the coefficient matrix of the discretized stream function equation then becomes independent of the intermediate results of the iteration, so that it needs to be inverted only once rather than in each iteration step.
Figure 24 gives an impression of the influence of this secondary flow inertia on the flow in a shallow channel. Even though the Dean number is rather high, this influence appears to be negligible as far as the main velocity distribution is concerned, whereas considerable deviations in the secondary flow pattern are found only close to the outer wall.

### 7.2. Importance of the sidewall regions

In a mathematical model of the flow and the bed configuration in a curved alluvial river a detailed prediction of the flow near the banks is not likely to be of primary importance, unless the deformation of the river channel pattern (meandering) is studied. Nonetheless, simplifications of the mathematical model

in the sidewall regions must be carried out with caution, as was shown in the foregoing paragraphs, where the solution of $\bar{u}$ near the inner wall, for instance, appeared to influence the mean velocity in almost the entire cross-section. On the other hand, in the central region the distribution of $\bar{u}$ for slipping sidewalls appeared to differ only slightly from the distribution in case of no-slip walls (figure 22b), which suggest some simplification of the longitudinal momentum equation might be possible near the sidewalls.
As in the central region the influence of lateral diffusion is negligible (figure 22a), an obvious simplification in the sidewall regions would be to neglect lateral diffusion in the longitudinal momentum equation. If possible at all, however, this simplification will certainly not be allowed in combination with the no-slip condition at the sidewalls. Regarding the slight influence of changing the no-slip conditions into full slip conditions (figure 22b), it must be possible to find adequate boundary conditions when lateral diffusion is neglected, but even then the advantage of this simplification will be small: it does not alter the iterative solution procedure nor does it make the solution simpler, although the order of this equation is reduced in radial direction. Moreover, this reduction of the equation to first order in radial direction raised the question where lateral boundary conditions should be imposed when only one condition of this type can be used. Therefore, neglecting lateral diffusion in the longitudinal momentum equation is not very suitable for simplification.
Another advantageous simplification in the stream function equation would be to neglect all radial derivatives of $\psi$, thus reducing the equation to the ordinary differential equation

$$\frac{\partial^4 \psi}{\partial \zeta^4} = \frac{\partial}{\partial \zeta} (u^2) \qquad (7.1)$$

Together with the boundary conditions at the bottom and at the surface, this equation yields:

$$\psi = \int_{-1}^{\zeta} d\zeta \int_{-1}^{\zeta} d\zeta \int_{-1}^{\zeta} u^2 d\zeta - (1 + \frac{3}{2}\zeta - \frac{1}{2}\zeta^3) \int_{-1}^{0} d\zeta \int_{-1}^{\zeta} d\zeta \int_{-1}^{\zeta} u^2 d\zeta +$$

$$- \frac{1}{4}\zeta(1 + \zeta)^2 \int_{-1}^{0} u^2 d\zeta \qquad (7.2)$$

which is easy to evaluate numerically. If u satisfies the no-slip condition ($u = 0$) at the sidewalls, $\psi$ can readily be shown to satisfy both the condition of impermeability ($\psi = 0$) and the no-slip condition ($\frac{\partial \psi}{\partial \xi} = 0$) at the sidewalls.
In the central region this simiplification seems to be allowed, but near the sidewalls this is not quite evident. Therefore (7.2) has been evaluated for a given distribution of u and compared with the stream function resulting from the complete system. According to figure 25, representing the results for De = 50, important deviations from the solution of the complete equation occur near the outer wall, both in the mean value of $\psi$ and in the vertical distribution.
When attempting to solve the complete system of equations with the stream function equation truncated to (7.1), this truncation appears to induce divergence of the iterative solution procedure for Dean numbers at which the system with the full stream function equation has a convergent solution.
Simplifications of the stream function equation that are less drastic than those leading to (7.1) are hardly profitable, the resulting equation always being a partial differential equation the solution of which is not essentially simpler than when only secondary flow inertia is neglected.

In summary, even for shallow channels a substantial simplification of the differential equations without important influence on the results can only be attained by omitting the advection terms from the stream function equation. All other terms, both in the longitudinal momentum equation and in the stream function equation, must be retained, or dropping them yields no essential simplification of the mathematical system.

## 7.3. Successive approximation of the solution

Since the system of differential equations and boundary conditions can hardly be simplified by neglecting terms, other possibilities of simplification must be examined in the method of solution.

In the literature on flow in river bends perturbation methods are often used for successive approximation of the solution of the governing differential equations. Starting from a basic solution, which is mostly the equivalent straight channel flow, or in terms of the present work the low Dean number limit, perturbations of this solution are determined for small values of a geometric parameter (the ratio of the depth of flow or the hydraulic radius of the cross-section and the radius of curvature of the channel axis). Thus each dependent variable in the solution of the mathematical system is approximated by a perturbation series (i.e. a power series of the small parameter), the subsequent terms of which are determined successively, making use of the foregoing terms that are already known.

Table 2 gives a survey of various applications of this perturbation technique to the flow in river bends (see also paragraph 4.1).

| Author | flow regime | degree of development | validity | number of nonzero term | |
|---|---|---|---|---|---|
| | | | | main flow | secondary fl |
| BOUSSINESQ (1868) | L | A | C | 1 | 1 |
| ANANYAN (1965) | L/T | A | CS | 2 | 1 |
| ROZOVISKII (1961) | L/T | A | C/S | 1/2 | 1 |
| DE VRIEND (1973a,b) | L | A | CS/C/S | 2 | 1 |
| DE VRIEND (1976, 1977) | T | D | C | 2 | 1 |

(L = laminar; T = turbulent; A = axisymmetric; D = developing; C = central region; S = sidewall region; CS = entire cross-section)

Table 2. Survey of applications of perturbation methods.

As was mentioned already in paragraph 4.1, the laminar flow solution for the full cross-section obtained by DE VRIEND (1973a,b) as a perturbation series of the depth to radius of curvature ratio can be rewritten as a perturbation series of the Dean number, the basic solution being the low Dean number limit of the solution of the full steady state Navier-Stokes equations. If the cross-section is shallow, the same holds good for the separate laminar flow solutions in the central region and near the sidewalls that were obtained by several authors mentioned in table 2. Hence it would be interesting to find out to what extent (i.e. what Dean number) these perturbation methods are applicable to the present problem or how they could lead to simplified solution methods. In order to get an idea of the applicability of the straigtforward low Dean number perturbation axisymmetric laminar flow in a shallow curved channel with a given and invariable secondary flow is considered. Then the only equation to be solved reads

$$De^2\{-\frac{1}{r}\frac{\partial\psi}{\partial\zeta}(\frac{\partial u'}{\partial\xi}+\frac{\varepsilon}{r}u')+\frac{1}{r}\frac{\partial\psi}{\partial\xi}\frac{\partial u'}{\partial\zeta}\}=\frac{1}{r}+\frac{\partial^2 u'}{\partial\zeta^2}+\frac{\partial^2 u'}{\partial\xi^2}+\frac{\varepsilon}{r}\frac{\partial u'}{\partial\xi}-\frac{\varepsilon^2}{r^2}u' \qquad (7.3)$$

where $u' = u/\iota$. The longitudinal slope factor $\iota$ can be determined from the integral condition of continuity as described in paragraph 3.4.

The straightforward low Dean number perturbation method implies that the unknown quantity u' is expanded in a power series of $De^2$:

$$u' = \sum_{k=0}^{\infty} De^{2k}\, u'_k \qquad (7.4)$$

which is substituted into (7.3). Then this equation can be rewritten into the form

$$\sum_{k=0}^{\infty} De^{2k}\, Eq_k = 0 \qquad (7.5)$$

in which the expressions $Eq_k$ can contain $u'_i (i = 0, 1, \ldots, k)$.

As (7.5) must hold for a continuous range of De, each of the expression $Eq_k$ must be equal to zero, which yields a series of equations

$$Eq_k = 0 \tag{7.6}$$

For k = 0, this equation reads

$$\frac{\partial^2 u'_0}{\partial \zeta^2} + \frac{\partial^2 u'_0}{\partial \xi^2} + \frac{\varepsilon}{r}\frac{\partial u'_0}{\partial \xi} - \frac{\varepsilon^2}{r^2} u'_0 + \frac{1}{r} = 0 \tag{7.7}$$

With the appropriate boundary conditions $u'_0$ can be solved from this equation. For k > 0, equation (7.6) can be written as

$$\frac{\partial^2 u'_k}{\partial \zeta^2} + \frac{\partial^2 u'_k}{\partial \xi^2} + \frac{\varepsilon}{r}\frac{\partial u'_k}{\partial \xi} - \frac{\varepsilon^2}{r^2} u'_k = -\frac{1}{r}\frac{\partial \psi}{\partial \xi}\left(\frac{\partial u'_{k-1}}{\partial \xi} + \frac{\varepsilon}{r} u'_{k-1}\right) + \frac{1}{r}\frac{\partial \psi}{\partial \xi}\frac{\partial u'_{k-1}}{\partial \zeta} \tag{7.8}$$

from which, for successively increasing k, $u'_k$ can be solved. Substituting the results into (7.4) yields successive approximations of u'.

As an example, this computation was carried out for a shallow channel ($d/B = 0.1$; $d/R_c = 0.04$), taking the solution of the stream function equation with the source term based on $u_0$ (instead of u) as the stream function of the imposed secondary flow. Figure 26 shows the results for gradually increasing Dean numbers; the series expansion (7.4) turns out to be divergent for Dean numbers higher than 10. This implies that low Dean number perturbations are not applicable as a solution technique for the present problem.

In spite of this negative conclusion as to the applicability of low Dean number perturbation methods, some attention has to be paid to an even more restrictive perturbation method. The turbulent flow version of this method is most widely used in the literature on flow in shallow river bends (ROZOVSKII, 1961; YEN, 1965; ENGELUND, 1974; DE VRIEND, 1976 & 1977), especially when simplification of the differential equation by neglecting smaller terms is considered as a perturbation cut off after the first non-zero term in every power series. In addition to a

Reynolds number limitation*) that is seldomly mentioned explicitly, the influence of the sidewalls (banks) is assumed to be restricted to a region close to these walls (banks), such that in shallow channels a central region exists where the horizontal derivatives of the velocity components are much smaller than the vertical ones. Accordingly, the radial derivatives in the central region are normalized by $R_c$ rather than by d, which yields the normalized longitudinal momentum equation

$$\varepsilon^2 Re^2 \{- \frac{1}{r} \frac{\partial \psi}{\partial \zeta} (\frac{\partial u}{\partial r} + \frac{u}{r}) + \frac{1}{r} \frac{\partial \psi}{\partial r} \frac{\partial u}{\partial \zeta}\} = \frac{\iota}{r} + \frac{\partial^2 u}{\partial \zeta^2} + \varepsilon^2 (\frac{\partial^2 u}{\partial r^2} + \frac{1}{r} \frac{\partial u}{\partial r} - \frac{u}{r^2}) \tag{7.9}$$

and the integral condition of continuity

$$\int_{1-B/2R_c}^{1+B/2R_c} dr \int_{-1}^{0} u d\zeta = B/R_c \tag{7.10}$$

When secondary flow inertia is neglected, the normalized stream function equation becomes

$$\frac{\partial}{\partial \zeta} (u^2) = \frac{\partial^4 \psi}{\partial \zeta^4} + 2\varepsilon^2 (\frac{\partial^4 \psi}{\partial r^2 \partial \xi^2} - \frac{1}{r} \frac{\partial^3 \psi}{\partial r \partial \zeta^2}) + \varepsilon^4 (\frac{\partial^4 \psi}{\partial r^4} - \frac{2}{r} \frac{\partial^3 \psi}{\partial r^3} + \frac{3}{r^2} \frac{\partial^2 \psi}{\partial r^2} - \frac{3}{r^3} \frac{\partial \psi}{\partial r}) \tag{7.11}$$

The solution of this system is approximated successively, with $\varepsilon^2$ as a perturbation parameter and supposing $Re^2$ to be $O(\varepsilon^o)$. Considering the first non-zero terms in the expansions of u, ι and ψ

*) In turbulent flow this limitation concerns the Reynolds number based on a representative turbulence viscosity rather than on molecular viscosity.

$$u_0 = \frac{\iota_0}{r}\frac{1-\zeta^2}{2} \; ; \; \iota_0 = 3\frac{B}{R_c}\left(\ln\frac{1+B/2R_c}{1-B/2R_c}\right)^{-1} \; ; \; \psi_0 = \frac{\iota_0^2}{r^2}\frac{1}{840}(\zeta^7 - 7\zeta^5 + 11\zeta^3 - 5\zeta) \qquad (7.12)$$

, which agree with the solutions of the velocity components given by BOUSSINESQ (1868), the distributions of the main velocity and the stream function in the central region appear to agree well with the low Dean number limit of the solution in the whole cross-section, especially when the exact value of $\iota$ is substituted for $\iota_o$ (figure 27).

It should be noted that the solutions (7.12) do not satisfy the boundary conditions at the sidewalls: all terms in (7.9) and (7.11) containing radial derivatives are at least an order $\varepsilon^2$ smaller than the leading terms, so that they drop out of the zero order approximation of these equations. In the higher order equations from which $u_k$ and $\psi_k$ $(k > 1)$ are solved, only radial derivatives of lower order perturbations $u_1$ and $\psi_1$ $(1 < k)$ occur, which are known quantities in that stage. Hence the sidewall boundary conditions for u and $\psi$ are not satisfied in any order of approximation. This is consistent with the aforementioned assumption that the sidewalls do not influence the flow in the central region. In order to satisfy the boundary conditions at the sidewalls a local solution for the regions near these walls must be determined (ROZOVSKII, 1961; DE VRIEND, 1973a,b)

In order to have an impression of the convergence and the applicability of the successive approximation method for the central region, the above method was used to solve (7.9) and (7.10) with the stream function of the secondary flow fixed at

$$\psi = \frac{1}{r^2}\frac{\iota_0^2}{840}(\zeta^7 - 7\zeta^5 + 11\zeta^3 - 5\zeta) \qquad (7.13)$$

For a shallow channel ($d/B = 0.1$; $\varepsilon = 0.04$) and Dean numbers up to 10, the perturbation was carried out on computer until 11 non-zero terms in the series expansion of u were obtained.

Figure 28a, showing the values of $\bar{u}'$ at the inner wall, in the channel axis and at the outer wall as functions of the order of approximation k, gives an impression of the intermediate results during the iteration. Apparently, convergence is poorest at the inner wall, where even at De = 7.5 the mean velocity finally "explodes". In addition, this figure and figure 28b show the velocity tends to grow more oblique as De increases, the maximum staying at the inner wall rather than shifting outwards.
This must be attributed, of course, to the absence of the sidewall influence (cf. paragraph 6.3). In the central region the vertical velocity and the radial derivative of the main velocity are negative, so that secondary flow advection gives rise to a more oblique mean velocity distribution. This in turn yields more negative vertical velocities and radial derivatives of the main velocity, etc.
Hence it must be concluded that successive approximations for the central region with $\varepsilon$ as a perturbation parameter are only applicable at very low Dean numbers, but are essentially wrong as soon as secondary flow advection becomes important. This conclusion stands when local solutions near the sidewalls are included (ROZOVSKII, 1961; DE VRIEND, 1973a,b). The solution in the central region is fully determined in itself, so it can not be influenced by these local solutions.

## 7.4. Depth-averaged equations derived by successive approximations

Although successive approximation of the solution with $\varepsilon$ or De as a perturbation parameter fails as a solution method at the Dean numbers of interest, the method can be used to derive approximations of the depth-averaged equations (cf. for turbulent flow: DE VRIEND, 1976). According to figures 11a and b, for instance, the influence of the Dean number on the vertical distribution of the main velocity becomes important at considerably higher values of De than the influence on the radial distribution.

Hence a low Dean number perturbation method is likely to work well for the vertical distribution of u at higher Dean numbers than for the radial distribution. According to paragraph 6.2, the low Dean number limit of u can be approximated by

$$u_0(\xi,\zeta) = \bar{u}_0(\xi)\, f_0(\zeta) \tag{6.17}$$

Substituting this into the zero Dean number longitudinal momentum equation 7.7, $\bar{u}_0$ and $f_0$ can be solved. Far from the sidewalls lateral diffusion is negligible, so $f_0$ follows from

$$\frac{d^2 f_0'}{d\zeta^2} = -1 \quad \text{with } f_0'|_{\zeta=-1} = 0; \quad \frac{df_0'}{d\zeta}|_{\zeta=0} = 0 \; ; \; f_0 = f_0'/\overline{f_0'} \tag{7.14}$$

with the solution

$$f_0 = \frac{3}{2}(1-\zeta^2) \tag{7.15}$$

(cf. equations 6.4 and 7.12). Making use of this information, equation (7.7) can be averaged over the depth of flow to yield

$$0 = \frac{\iota_0}{r} + \frac{d^2\bar{u}_0}{d\xi^2} + \frac{\varepsilon}{r}\frac{d\bar{u}_0}{d\xi} - \frac{\varepsilon^2}{r^2}\bar{u}_0 - 3\bar{u}_0 \tag{7.16}$$

Similarly, the low Dean number limit of the stream function is approximated by

$$\psi_0(\xi,\zeta) = \bar{\psi}_0(\xi)\, g_0(\zeta) \tag{6.18}$$

which leads to

$$g_0(\zeta) = \frac{24}{19}(\zeta^7 - 7\zeta^5 + 11\zeta^3 - 5\zeta) \tag{7.17}$$

(cf. equation 7.12) and the depth-averaged stream function equation

$$u_0^2|_{\zeta=0} = \frac{d^4\bar{\psi}_0}{d\xi^4} - 2\frac{\varepsilon}{r}\frac{d^3\bar{\psi}_0}{d\xi^3} + (3\frac{\varepsilon^2}{r^2} - \frac{240}{19})\frac{d^2\bar{\psi}_0}{d\xi^2} - (3\frac{\varepsilon^3}{r^3} - \frac{240}{19}\frac{\varepsilon}{r})\frac{d\bar{\psi}_0}{d\xi} + \frac{5040}{19}\bar{\psi}_0$$

(7.18)

According to (7.8), the first perturbation of the main velocity, $u_1$, follows from

$$\frac{\partial^2 u_1}{\partial\zeta^2} + \frac{\partial^2 u_1}{\partial\xi^2} + \frac{\varepsilon}{r}\frac{\partial u_1}{\partial\xi} - \frac{\varepsilon^2}{r^2}u_1 = -\frac{\imath_1}{r} - \frac{1}{r}\frac{\partial\psi_0}{\partial\zeta}(\frac{\partial u_0}{\partial\xi} + \frac{\varepsilon}{r}u_0) + \frac{1}{r}\frac{\partial\psi_0}{\partial\xi}\frac{\partial u_0}{\partial\zeta}$$

(7.19)

Suppose $u_1$ can be approximated by

$$u_1(\xi,\zeta) = \bar{u}_{1,0}(\xi)\, f_0(\zeta) + \bar{u}_{1,1}(\xi)\, f_{1,1}(\zeta) + \bar{u}_{1,2}(\xi)\, f_{1,2}(\zeta) \qquad (7.20)$$

such that the first component represents the influence of the longitudinal slope term, the second component the influence of the radial advection term and the third one the influence of the vertical advection term. Substitution of (7.20) into (7.19) yields an equation from which $f_{1,1}$ and $f_{1,2}$ can be solved. In the central region, where lateral diffusion is negligible, this leads to

$$\frac{d^2 f'_{1,1}}{d\zeta^2} = -f_0\frac{dg_0}{d\zeta} \text{ with } f'_{1,1}|_{\zeta=-1} = 0;\ \frac{df'_{1,1}}{d\zeta}|_{\zeta=0} = 0;\ f_{1,1} = f'_{1,1}/\overline{f'_{1,1}} \qquad (7.20)$$

$$\frac{d^2 f'_{1,2}}{d\zeta^2} = g_0\frac{df_0}{d\zeta} \quad \text{with } f_{1,2}|_{\zeta=-1} = 0;\ \frac{df'_{1,2}}{d\zeta}|_{\zeta=0} = 0;\ f_{1,2} = f'_{1,2}/f'_{1,2} \qquad (7.21)$$

the solutions of which are polynomials in $\zeta$. Making use of these solutions, the depth-averaged version of (7.19) becomes

$$\frac{d^2\bar{u}_{1,0}}{d\xi^2} + \frac{\varepsilon}{r}\frac{d\bar{u}_{1,0}}{d\xi} - \frac{\varepsilon^2}{r^2}\bar{u}_{1,0} - 3\bar{u}_{1,0} = -\frac{\imath_1}{r} \qquad (7.23a)$$

$$\frac{d^2\bar{u}_{1,1}}{d\xi^2} + \frac{\varepsilon}{r}\frac{d\bar{u}_{1,1}}{d\xi} - \frac{\varepsilon^2}{r^2}\bar{u}_{1,1} - \frac{77}{52}\bar{u}_{1,1} = \frac{128}{95}\frac{\bar{\psi}_0}{r}(\frac{d\bar{u}_0}{d\xi} + \frac{\varepsilon}{r}\bar{u}_0) \qquad (7.23b)$$

$$\frac{d^2\bar{u}_{1,1}}{d\xi^2} + \frac{\varepsilon}{r}\frac{d\bar{u}_{1,2}}{d\xi} - \frac{\varepsilon^2}{r^2}\bar{u}_{1,2} - \frac{77}{26}\bar{u}_{1,2} = \frac{128}{95}\frac{\bar{u}_0}{r}\frac{d\bar{\psi}_0}{d\xi} \tag{7.23c}$$

When $\bar{u}_0 + \varepsilon\bar{u}_1$ and $\iota_0 + \varepsilon\iota_1$ are considered as approximations $O(De^4)$ of $\bar{u}$ and $\iota$, respectively, $De^2$ times equations (7.23) added to equation (7.16) yields

$$\frac{d^2\bar{u}}{d\xi^2} + \frac{\varepsilon}{r}\frac{d\bar{u}}{d\xi} - (\frac{\varepsilon^2}{r^2} + 3)\bar{u} = -\frac{\iota}{r} + De^2\left[-\frac{79}{52}\bar{u}_{1,1} - \frac{1}{26}\bar{u}_{1,2} + \frac{128}{95}\{\frac{\bar{\psi}}{r}(\frac{d\bar{u}}{d\xi} + \frac{\varepsilon}{r}\bar{u}) + \right.$$

$$\left. + \frac{\bar{u}}{r}\frac{d\bar{\psi}}{d\xi}\}\right] \tag{7.24}$$

in which the quantities $\bar{u}_{1,1}$ and $\bar{u}_{1,2}$ are solved from

$$\frac{d^2\bar{u}_{1,1}}{d\xi^2} + \frac{\varepsilon}{r}\frac{d\bar{u}_{1,1}}{d\xi} - \frac{\varepsilon^2}{r^2}\bar{u}_{1,1} - \frac{77}{52}\bar{u}_{1,1} = \frac{128}{95}\frac{\bar{\psi}}{r}(\frac{d\bar{u}}{d\xi} + \frac{\varepsilon}{r}\bar{u}) \tag{7.25}$$

$$\frac{d^2\bar{u}_{1,2}}{d\xi^2} + \frac{\varepsilon}{r}\frac{d\bar{u}_{1,2}}{d\xi} - \frac{\varepsilon^2}{r^2}\bar{u}_{1,2} - \frac{77}{26}\bar{u}_{1,2} = \frac{128}{95}\frac{\bar{u}}{r}\frac{d\bar{\psi}}{d\xi} \tag{7.26}$$

The stream function $\bar{\psi}$ is approximated by the solution of

$$\frac{d^4\bar{\psi}}{d\xi^4} - 2\frac{\varepsilon}{r}\frac{d^3\bar{\psi}}{d\xi^3} + (3\frac{\varepsilon^2}{r^2} - \frac{240}{19})\frac{d^2\bar{\psi}}{d\xi^2} - (3\frac{\varepsilon^3}{r^3} - \frac{240}{19}\frac{\varepsilon}{r})\frac{d\bar{\psi}}{d\xi} = \bar{u}^2 f^2|_{\zeta=0} \tag{7.27}$$

With the appropriate boundary conditions, equations (7.24) through (7.27) can be solved iteratively, starting from the zero Dean number solution, for instance. As an example, this computation was carried out for the same shallow channel as in the foregoing ($d/B = 0.1$; $\varepsilon = 0.04$), using the zero order approximation of the secondary flow. Convergence is far better than for the complete low Dean number perturbation method described in paragraph 7.3 (even for De = 50 the procedure converges now), but as De increases the agreement with the equivalent solution of the complete system soon becomes rather poor (see figure 29). If in equations (7.25) and (7.26) the lateral diffusion terms are neglected, they reduce to explicit expressions for $\bar{u}_{1,1}$ and $\bar{u}_{1,2}$

in terms of $\bar{u}$ and $\bar{\psi}$:

$$\bar{u}_{1,1} = -\frac{52}{77}\frac{128}{95}\frac{\bar{\psi}}{r}\left(\frac{d\bar{u}}{d\xi} + \frac{\varepsilon}{r}\bar{u}\right) \quad \text{and} \quad \bar{u}_{1,2} = -\frac{26}{77}\frac{128}{95}\frac{\bar{u}}{r}\frac{d\bar{\psi}}{d\xi} \tag{7.28}$$

When substituted into equation (7.24), this yields

$$\frac{d^2\bar{u}}{d\xi^2} + \frac{\varepsilon}{r}\frac{d\bar{u}}{d\xi} - \frac{\varepsilon^2}{r^2}\bar{u} = -\frac{1}{r} + De^2\frac{78}{77}\frac{128}{95}\left\{2\frac{\bar{\psi}}{r}\left(\frac{d\bar{u}}{d\xi} + \frac{\varepsilon}{r}\bar{u}\right) + \frac{\bar{u}}{r}\frac{d\bar{\psi}}{d\xi}\right\} \tag{7.29}$$

In contrast with the system (7.24) through (7.27), of which the iterative solution procedure can be considered as a semi-implicit solution method for the longitudinal momentum equation (when solving this equation part of the advection terms is incorporated in the solving operator and part in the known source terms $\bar{u}_{1,1}$ and $\bar{u}_{1,2}$), equation (7.29) can be solved implicitly*). So if, as in the foregoing example, the secondary flow is fixed at its zero order approximation, no convergence problems are encountered in the solution of the longitudinal momentum equation. The mean velocity distribution found this way for the same shallow channel as before appears to agree better with the solution of the complete system than the results from (7.24) through (7.26) (see figure 29), but if the Dean number gets higher than 20, considerable differences occur here, as well. Convergence grows poorer when the secondary flow is correlated to the actual mean velocity instead of being kept fixed. According to figure 30, the procedure with the implicit solution of the longitudinal momentum equation converges at higher Dean numbers than the procedure with the semi-implicit solution ($De \leq 17.5$ vs. $De \leq 10$).

From the comparison between the four examples discussed in this paragraph it appears that implicit solution of the longitudinal momentum equation improves the convergence of the iterative procedure that solves this equation and the stream function equation simultaneously.

---

*) The combination of equations (7.27) and (7.29) still has to be solved iteratively, of course.

Still the smallness of the critical Dean numbers and the considerable deviations from the solution of the complete system as soon as advection grows important lead to the conclusion that the simplified solution methods discussed here must be rejected for the flow in shallow river bends.

## 7.5. Similarity solution

A logical continuation of the foregoing is to maintain the similarity hypothesis, which has appeared to be rather good, even for De > 15, but drop the low Dean number approximations of the vertical distributions of u and $\psi$. Instead, these distributions can be solved from differential equations to be derived from the longitudinal momentum equation and the stream function equation (cf. paragraph 6.2, equations (6.21) through (6.23)). Neglecting lateral diffusion, the longitudinal momentum equation yields

$$\frac{d^2f'}{d\zeta^2} - De^2\left(\frac{1}{r}\frac{d\bar{\psi}}{d\xi}\right)_{\xi=\xi_0} g\frac{df'}{d\zeta} + De^2\left(\frac{\bar{\psi}}{r\bar{u}}\frac{d\bar{u}}{d\xi} + \frac{\varepsilon}{r^2}\bar{\psi}\right)_{\xi=\xi_0}\frac{dg}{d\zeta} f' = -1 \qquad (7.30)$$

with $f'|_{\zeta=-1} = 0$; $\frac{df'}{d\zeta}|_{\zeta=0} = 0$; $f = f'/\overline{f'}$

Taking $\xi_0 = 0$, $f$ can be solved from this system when $\bar{u}|_{\xi=0}$, $\frac{d\bar{u}}{d\xi}|_{\xi=0}$ $\bar{\psi}|_{\xi=0}$ and $\frac{d\bar{\psi}}{d\xi}|_{\xi=0}$ are known.

If lateral diffusion and advection are neglected in the stream function equation, it yields

$$\frac{d^4g'}{d\zeta^4} = \frac{d}{d\zeta}(f^2) \qquad (7.31)$$

with $g'|_{\zeta=-1}=0$; $g'|_{\zeta=0}=0$; $\frac{dg'}{d\zeta}|_{\zeta=-1}=0$; $\frac{d^2g'}{d\zeta^2}|_{\zeta=0}=0$; $g = g'/\overline{g'}$

When $g$ is known, $f$ can be solved from this system. Consequently, (7.30) and (7.31) can be used in an iterative solution procedure in combination with the depth-averaged equations for the mean velocity and the stream function (see also paragraph 6.2)

$$\frac{d^2\bar{u}'}{d\xi^2} + \left(\frac{\varepsilon}{r} - De^2 g \overline{\frac{df}{d\zeta}} \frac{\bar{\psi}}{r}\right)\frac{d\bar{u}'}{d\xi} - \left\{\frac{\varepsilon^2}{r^2} + \frac{df}{d\zeta}\Big|_{\zeta=-1} + De^2 g \overline{\frac{df}{d\zeta}} \left(\frac{1}{r}\frac{d\bar{\psi}}{d\xi} + \frac{\varepsilon}{r^2}\bar{\psi}\right)\right\}\bar{u}' = -\frac{1}{r}$$

(7.32)

$$\text{with } \bar{u}'\Big|_{\xi=\pm\frac{B}{2d}} = 0 \quad \text{and} \quad \bar{u} = \bar{u}'B/\left(d\int_{-B/2d}^{B/2d} \bar{u}'d\xi\right)$$

$$\frac{d^4\bar{\psi}}{d\xi^4} - 2\frac{\varepsilon}{r}\frac{d^3\bar{\psi}}{d\xi^3} + \left(3\frac{\varepsilon^2}{r^2} + 2\frac{dg}{d\zeta}\Big|_{\zeta=0}\right)\frac{d^2\bar{\psi}}{d\xi^2} - \frac{\varepsilon}{r}\left(3\frac{\varepsilon^2}{r^2} + 2\frac{dg}{d\zeta}\Big|_{\zeta=0}\right)\frac{d\bar{\psi}}{d\xi} +$$

$$+ \left(\frac{d^3g}{d\zeta^3}\Big|_{\zeta=0} - \frac{d^3g}{d\zeta^3}\Big|_{\zeta=-1}\right)\bar{\psi} = \bar{u}^2 f^2\Big|_{\zeta=0} \qquad (7.33)$$

$$\text{with } \bar{\psi}\Big|_{\xi=\pm\frac{B}{2d}} = 0; \quad \frac{d\bar{\psi}}{d\xi}\Big|_{\xi=\pm\frac{B}{2d}} = 0$$

As was shown in paragraph 6.2, equation (7.32) yields satisfactory results for $\bar{u}$, even if the Dean number is not small, when $\bar{\psi}$, $g$ and $f$ are introduced as known functions derived from the solution of the complete system. The same holds for the results of $f$ when $\bar{u}$, $\bar{\psi}$ and $g$ are introduced as known functions into (7.30). An iterative procedure consisting of (7.30) through (7.33), however, has not been investigated yet. Therefore, this procedure was applied to the same shallow channel example as before ($d/B = 0.1$; $\varepsilon = 0.04$). As figure 31 shows, convergence is hardly reduced, even though the system consists of more equations with more sources of disturbances. On the contrary,

introducing a simple damping rule, viz. (3.53) with $\alpha = 2$, leads to fast convergence up to much hihger Dean numbers (De = 37.5) than the foregoing methods.
The mean velocity distribution (figure 31b) agrees well with the corresponding result of the complete system, except for the outer wall region. The same holds for the horizontal distribution of the stream function (figure 31d). In the channel axis, the vertical distributions of the main velocity (figure 31c) and the stream function (figure 31e) fairly agree with those found from the complete system. Near the outer wall and, as far as the main velocity is concerned, also near the inner wall deviations from the solution of the complete system are found.
The only deviations from the solution of the complete system that may spoil the applicability of the similarity method are those near the outer wall, especially in the main velocity distribution. If the peak in the mean velocity there grows much too high, the mean velocity in the other parts of the cross-section, and hence the bed shear stress there, will be reduced considerably. So the mean velocity distribution in the outer wall region must be predicted rather well, even if it is of no direct interest for the present purpose. In the present example (figure 31b) this prediction is good enough, as the reduction of the mean velocity away from the outer wall is rather small for all Dean numbers considered. Hence it is concluded that the similarity system (7.30) through (7.33) is suited as a simplified solution method for axisymmetric laminar flow in shallow channels.
Finally, it should be noted that, although the similarity system provides a satisfactory approximation of the velocities in axisymmetric flow, it may give rise to errors when applied to developing curved flow. There the vertical velocity distributions are influenced by longitudinal accelerations of the main flow (DE VRIEND, 1976 & 1977), which will vary in a cross-section. Hence it may be necessary to determine the vertical velocity distributions in more than one vertical (quasi-similarity approximation).

## 7.6. Summary

The conclusions to be drawn as to the possibility of neglecting terms in the differential equations and as to the applicability of simplified computation methods can be summarized as follows.

1. The influence of the advection terms in the stream function equation is negligible as far as the main velocity distribution is concerned. Considerable deviations from the stream function solved from the complete system occur only near the outer wall.
2. Lateral diffusion could be neglected in the central region, but not close to the sidewalls. There lateral diffusion terms must be retained, both in the longitudinal momentum equation and in the stream function equation, in order to satisfy the sidewall boundary conditions (main velocity) or to avoid serious errors in the solution (secondary flow).
3. Successive approximation of the solution with the Dean number as a perturbation parameter can only be applied at very low Dean numbers.
4. Perturbation methods making use of the curvature ratio $\varepsilon$ as a perturbation parameter implicitly include an additional Reynolds number limitation.
5. Solution methods in which the influence of the sidewalls on the flow in the central region is neglected are only applicable to rectangular channels if the Dean number is very small. Even if local solutions for the sidewall regions are incorporated, these methods are essentially wrong as soon as advection grows important.
6. In shallow channels the influence of advection on the vertical distribution of the main velocity is smaller than on the horizontal one. As a consequence, depth-averaged equations derived from the complete system using successive approximations are applicable at higher Dean numbers than the successive approximations themselves. Nevertheless, simplified solution

methods based on these depth-averaged equations are only applicable at rather low Dean numbers, which makes them unsuited for the prediction of flow in river bends.

7. A mathematical model based on the similarity approximation of the main velocity and the stream function of the secondary flow yields rather good predictions of axi-symmetric laminar flow at sufficiently high Dean numbers. Only in the outer wall region considerable deviations from the equivalent solution of the complete system occur at higher Dean numbers, but these deviations are not so large that they influence the velocities further inwards in an unallowable way.

# 8. Conclusions

## 8.1. General

1. Although perhaps not as good as other numerical models at the point of convergence, the present model provides a good approximation of axisymmetric laminar flow in curved ducts up to Dean numbers of about 60.

2. A (turbulent) Dean number range from 0 through 60 is sufficient to describe the flow in curved alluvial rivers. For the simulation of flume experiments, however, a limitation to experiments with sufficiently low Dean numbers may be necessary.

## 8.2. Main velocity redistribution

1. Opposite effects cause the main velocity distribution in a curved flow to deviate from the distribution in the equivalent straight flow, viz. the potential flow effect, drawing the main velocity maximum inwards, and the advective effect of the secondary flow, pushing the maximum outwards. At small Dean numbers the potential flow effect predominates, at high Dean numbers the advective effect is the most important one.

2. Starting from the velocity field that would occur if the advective influence of the secondary flow were absent, the mechanism of the advective redistribution of the main velocity can be explained as follows. In the parts of the velocity field where the longitudinal momentum increases along the streamlines of the secondary flow, this secondary flow conveys fluid of relatively low longitudinal momentum to points where the momentum of the undisturbed flow is relatively high, thus causing a reduction of the longitudinal momentum, i.e. of the main velocity there. Conversely, in

parts of the velocity field where the longitudinal momentum decreases along the secondary flow streamlines, advection gives rise to an increase of the main velocity. This velocity redistribution goes on until the influence of advection is counterbalanced by the influence of additional viscous stresses generated by the redistribution.

3. The advective effect of the vertical velocity component is of a local kind. It is only important near the sidewalls. Near the inner wall it gives rise to a reduction of the mean velocity and a more oblique vertical distribution of $u/\bar{u}$. Near the outer wall the effect is reverse.

4. The advective effect of the radial velocity component alone is hardly felt in the mean velocity distribution, but it strongly influences the vertical distribution of $u/\bar{u}$ in that it causes a reduction of this quantity in the upper part of the cross-section and an increase in the lower part.

5. In combination with vertical advection, the advective influence of the radial velocity component on the mean velocity is quite important. With the bed shear stress as a damping factor, radial advection forms an outward retardation mechanism in the mean velocity redistribution. Through this mechanism the influence of the local reduction of $\bar{u}$ near the inner wall (which is mainly due to vertical advection) is extended to the greater part of the cross-section, such that the mean velocity maximum is shifted outwards. The mean velocity peak caused by vertical advection near the outer wall is compressed against the wall, where it is damped by viscous forces.

6. The advective influence of the secondary flow on the main velocity gives rise to the following phenomena when the Dean number is increased from zero on and the channel geometry is kept constant:
   - the mean velocity maximum shifts outwards (see also 5)
   - the vertical distribution of $u/\bar{u}$ grows steeper near the bottom and flatter higher up in the vertical (cf. 4), such that at higher Dean numbers the maximum lies below the surface
   - the shear stress at the fixed boundaries remains constant near the inner wall and increases near the outer wall
   - the longitudinal slope factor increases
   - the intensity of the secondary flow, indicated by $\hat{\Psi}$, first increases and then decreases again.
   - at a certain, rather high Dean number (between 50 and 60 here), the single vortex secondary flow pattern suddenly changes into a double vortex pattern, as an additional counterrotating vortex, caused by the same mechanism as Dean's instability, develops near the surface close to the outer wall
   - the transverse pressure drop increases almost in proportion with $De^2$
   - the vertical distribution of the pressure remains almost hydrostatic
   - at very high Dean numbers (a few hundreds) the main velocity gradients due to viscosity and the secondary flow are concentrated in rather thin layers along the fixed boundaries; outside these boundary layers the flow becomes inviscid.

7. The most important effects of raising the curvature ratio $\varepsilon$ while keeping the Dean number and the channel aspect ratio constant are:

- the "potential flow effect" in the mean velocity distribution grows more important with respect to the advective influence of the secondary flow
- the magnitude of the vertical velocity component and the advective influence of the secondary flow on the vertical distribution of the main velocity are intensified near the inner wall and weakened near the outer wall.

8. When the Dean number and the curvature ratio are kept constant and the channel aspect ratio is raised,
   - the main velocity maximum moves outwards
   - the secondary flow intensity indicated by $\hat{\psi}$ grows, but the influence of advection on the vertical distribution of the main velocity decreases

## 8.3. Sensitivity analysis of the differential equations

1. The main conclusions to be drawn from a sensitivity analysis of the longitudinal momentum equation are
   - the vertical advection term is the main cause of the mean velocity reduction near the inner wall and the increase near the outer wall, but it hardly influences the main velocity distribution in the central region.
   - the radial advection terms alone are unimportant for the mean velocity, but they strongly influence the vertical distribution $u/\bar{u}$; in combination with the bed shear stress term and the vertical advection term, the radial advection terms give rise to an important lateral interaction in the main velocity distribution: the outwards retardation effect
   - the influence of the lateral diffusion terms and the sidewall boundary conditions is restricted to the mean velocity close to the sidewalls.

2. In the stream function equation
   - the advection terms are negligible, at least in shallow channels
   - the lateral diffusion terms are important close to the sidewalls.

## 8.4. Simplified computation methods

1. At intermediate Dean numbers the mathematical system can not be simplified essentially by neglecting terms, except for the advection terms in the stream function equation.

2. At low Dean numbers (De < 10) the system of differential equations can be solved using a perturbation method with the Dean number as a perturbation parameter.

3. Perturbation methods as often applied to the flow in curved shallow channels, making use of $\varepsilon$ as a perturbation parameter and neglecting the influence of the sidewalls, are applicable to rectangular channels if the Dean number is very small. Even if local solutions in the sidewall regions are included, these methods are essentially wrong as soon as advection grows important.

4. Simplified mathematical models consisting of depth-averaged equations derived from the complete system by successive low Dean number approximations can be applied at higher Dean numbers than the successive approximations themselves. Nevertheless, the range of applicability of these simplified models is too small to make them suited for the prediction of flow in river bends.

5. Both the main velocity and the stream function of the secondary flow can be approximated by similarity solutions. A mathematical model based on this similarity approximation works rather well at sufficiently high Dean numbers.

REFERENCES


1 ADLER, M., Strömung in gekrümmten Rohren, ZAMM, Band 14, Heft 5, Oktober 1934, p. 257

2 ANANYAN, A.K., Fluid flow in bend of conduits, (1957), Israel Program for Scientific Translations, Jerusalem, 1965

3 AUSTIN, L.R. and SEADER, J.D., Fully developed viscous flow in coiled circular pipes, AICHE Journal, 19, no. 1, January 1973, p. 85

4 BAYLIS, J.A., Experiments on laminar flow in curved channels of square section, J. Fluid Mech. 48, part 3, 1971, p. 417

5 BOUSSINESQ, J., Memoire sur l'influence de frottement dans les mouvements réguliers des fluides; XII - Essai sur le mouvement permanent d'un liquide dans un canal horizontal à axe circulaire, Journal de Mathématiques pures et appliquées, Deuxième série, Tome XIII, 1868, p. 413

6 CHENG, K.C. and AKIYAMA, M., Laminar forced convection heat transfer in curved rectangular channels, Int. J. Heat Mass Transfer, 13, 1970, p. 471

7 CHENG, K.C., LIN, R.-C. and OU, J.-W., Fully developed laminar flow in curved rectangular channels, Trans. ASME, Jnl. of Fluids Engineering, 98, series I, no. 1, March 1976, p. 41

8 CHOUDHARY, U.K. and NARASIMHAN, S., Flow in 180° open channel rigid boundary bends, Proceedings of the ASCE, Jnl. Hydr. Division, 103, no. HY6, June 1977, p. 651

9 CUMING, H.G., The secondary flow in curved pipes, Aeron. Res. Council, Reports and Memoranda no. 2880, London, February 1952

10 DEAN, W.R., Note on the motion of fluid in a curved pipe, Phil Mag., Ser. 7, 4, 1927, p. 208

11 DEAN, W.R., (a), The streamline motion of fluid in a curved pipe, Phil. Mag., Ser. 7, 5, 1928, p. 673

12 DEAN, W.R., Fluid motion in a curved channel, Proc. Royal Soc. London, series A, 121, no. 787, November 1928, p. 402

13 ENGELUND, F., Flow and bed topography in channel bends, Proceedings of the ASCE, Jnl. Hydr. Division, 100, no. HY 11, November 1974, p. 1631

14 GHIA, K.G. and SOKHEY, J.S., Laminar incompressible viscous flow in curved ducts of regular cross-section, Trans. ASME, Jnl. of Fluids Engineering, 99, series I, December 1977, p. 640

15 HUMPHREY, J.A.C., TAYLOR, A.M.K. and WHITELAW, J.H., Laminar flow in a square duct of strong curvature, J. Fluid Mech., 83, part 3, 1977, p. 509

16 ITŌ, H., Theory on laminar flows through curved pipes of elliptic and rectangular cross-section, The Reports of the Institute of High Speed Mechanics, Tohoku Univ., Sendai, Japan, 1, 1951, p.1

17 ITŌ, H., Laminar flow in curved pipes, The Reports of the Institute of High Speed Mechanics, Tohoku Univ., Sendai, Japan, 22, Report no. 224, 1970, p. 161 Also: ZAMM, 49, Heft 11, 1969, p. 653

18 JOSEPH, B., SMITH, E.P. and ADLER, R.J., Numerical treatment of laminar flow in helically coiled tubes of square cross-section; Part I - Stationary helically coiled tubes, AICHE Journal, 21, no. 5, September 1975, p. 965

19 LEOPOLD, L.B., WOLMAN, M.G. and MILLER, J.P., Fluvial processes in geomorphology, San Fransisco, 1964

20 LESCHZINER, M., Berechnungen mit tiefengemittelten zweidimensionalen Modellen, in: Numerische Berechnung turbulenter Strömungen in Forschung und Praxis, Hochschulkursus an der Universität Karlsruhe, April 1978, Vorlesung 12

21 LUDWIEG, H., Die ausgebildete Kanalströmung in einem rotierenden System, Ingenieur-Archiv, XIX, 1951, p. 296

22 McCONALOGUE, D.J. and SRVISTAVA, R.S., Motion of fluid in a curved tube, Proc. Roy. Soc., A, 307, 1968, p. 37

23 McGUIRK, J. Numerische Verfahren für dreidimensionale Strömungen, in: Numerische Berechnung turbulenter Strömungen in Forschung und Praxis, Hochschulkursus an der Universität Karlsruhe, April 1978, Vorlesung 9

24 McGuirk, J., Beispiele der Berechnung dreidimensionaler Strömungen ohne Ablösungsgebiet, in: Numerische Berechnung turbulenter Strömungen in Forschung und Praxis, Hochschulkursus an der Universität Karlsruhe, April 1978, Vorlesung 13

25 MORI, Y., UCHIDA, U. and UKON, T., Forced convective heat transfer in a curved channel with a square cross-section, Int. J. Heat Mass Transfer, 14, 1971, p. 1787

26 MURAMOTO, Y., Flow through curved open channels, Part I - On characteristics of upper layer in fully developed region, Bull.Dis.Prev.Res.Inst., 14, pt. 2, February 1965, p. 1

27 PATANKAR, S.V., PRATAP, V.S. and SPALDING, D.B., Prediction of turbulent flow in curved pipes, J. Fluid Mech., 62, part 3, 1974, p. 539

28 PATANKAR, S.V., PRATAP, V.S. and SPALDING, D.B., Prediction of turbulent flow in curved pipes, J. Fluid Mech. 67, part 3, 1975, p. 583

29 PATANKAR, S.V. and SPALDING, D.B. A calculation procedure for heat, mass and momentum transfer in three-dimensional parabolic flows, Int. J. Heat Mass Transfer, 15, 1972, p. 1787

30 PRATAP, V.S. and SPALDING, D.B., Numerical computations of the flow in curved ducts, Aeronautical Quarterly, 26, August 1975, p. 219

31 PRATAP, V.S. and SPALDING, D.B., Fluid flow and heat transfer in three-dimensional duct flows, Int. J. Heat Mass Transfer, 19, 1976, p. 1183

32 RAO, K.V., Secondary flow in a curved channel as revealed by a laser Doppler anemometer, Proceedings of the LDA Symposium, Copenhagen, 1975, p. 710

33 ROACHE, P.J., Computational Fluid Dynamics, Hermosa Publishers, Albuquerque (N.M.), 1972

34 RODI, W., Zusammenfassung und Ausblick auf weitere Entwickelungen, in: Numerische Berechnung turbulenter Strömungen in Forschung und Praxis, Hochschulkursus an der Universität Karlsruhe, April 1978, Vorlesung 15

35 ROZOVSKII, I.L., Flow of water in bends of open channels, (1957), Israel Program for Scientific Translations, Jerusalem, 1961

36 SMITH, F.T., Steady motion within a curved pipe, Proc. Roy., Soc. Lond., A, 347, 1976, p. 345

37 VRIEND, H.J. DE, (a), Theory of viscous flow in curved shallow channels, Communications on Hydraulics, Delft University of Technology, Dept. of Civil Engng., Report no. 72-1, 1973

38 VRIEND, H.J. DE (b), Theory of viscous flow in wide curved open channels, Proceedings of the International Symposium on River Mechanics, Bangkok, Thailand, January 1973, Paper A17

39 VRIEND, H.J. DE, A mathematical model of steady flow in curved shallow channels, Communications on Hydraulics, Delft University of Techn., Dept. of Civil Engng, Rept. no. 76-1, 1976

40 VRIEND, H.J. DE, A mathematical model of steady flow in curved shallow channels, J. Hydr. Research, 15, 1977, no.1, p. 37

41 VRIEND, H.J. DE and KOCH, F.G., Flow of water in a curved open channel with a fixed plane bed, Delft Hydraulics Laboratory/ Delft University of Technology, TOW-report R657-V/M1415 I October 1977

42 VRIEND, H.J. DE and KOCH, F.G., Flow of water in a curved open channel with a fixed uneven bed, Delft Hydraulics Laboratory/Delft University of Technology, TOW-report R657-VI/ M1415 II, to appear in 1978

43 WILKINSON, J.H. and REINSCH, C., Linear algebra (Chief Ed. F.L. Bauer), Springer Verlag, Berlin, 1971

44 YEN, B.C., Characteristics of subcritical flow in a meandering channel, Rept. Inst. Hydr. Res., Univ. of Iowa, Iowa City, 1965

# APPENDIX I

## Discretization of the equations

## Appendix I Discretization of the equations

### 1. Numerical accuracy

The numerical computations are carried out on a grid of N by M rectangular meshes of size $\Delta\zeta \times \Delta\xi$, where $\Delta\zeta = 1/N$ and $\Delta\xi = 1(Md)$, as shown in figure 2. A grid point $(\zeta, \xi)$ is referred to by the indices $(i,j)$, such that $\zeta = -1 + i\Delta\zeta$ and $\xi = -B/2d + j\Delta\xi$.
In principle, the discretization of the differential equations in the mathematical system to be solved is second order. If second order finite difference schemes would be employed to every individual term, however, higher order derivatives would occur both in the differential equations and in the truncation errors of the finite difference equations, which gives rise to numerical incaccuracies (artificial viscosity). On considering, for example, two of the viscosity terms in the stream function equation

$$\frac{\partial^4\psi}{\partial\xi^4} + 3\,\frac{\varepsilon^2}{r_j^2}\,\frac{\partial^2\psi}{\partial\xi^2} \tag{I.1}$$

the application of central finite difference schemes to each individual term would yield

$$\frac{\psi_{i,j+1} - 4\psi_{i,j+1} + 6\psi_{i,j} - 4\psi_{i,j-1} + \psi_{i,j-2}}{\Delta\xi^4} + 3\,\frac{\varepsilon^2}{r_j^2}\,\frac{\psi_{i,j+1} - 2\psi_{i,j} + \psi_{i,j-1}}{\Delta\xi^2} \tag{I.2}$$

Using Taylor series expansions about the point $(i,j)$, this can be shown to be equivalent to:

$$\left(1 + 3\,\frac{\varepsilon^2}{r_j^2}\,\frac{\Delta\xi^2}{12}\right)\frac{\partial^4\psi}{\partial\xi^4} + 3\,\frac{\varepsilon^2}{r_j^2}\,\frac{\partial^2\psi}{\partial\xi^2} + O\left(\Delta\xi^2\,\frac{\partial^6\psi}{\partial\xi^6}\right) \tag{I.3}$$

Thus in the leading viscosity term $\frac{\partial^4\psi}{\partial\xi^4}$ an artificial viscosity is introduced. The influence of this artificial viscosity will be

small if $\varepsilon^2\Delta\xi^2/4$ is sufficiently small with respect to unity, but such a requirement is rather hard to evaluate for some of the sources of artificial viscosity in the present system. Another way to avoid this effect is applying higher order finite difference schemes to the lower derivatives. Employing a five-point scheme for $\frac{\partial^2\psi}{\partial\xi^2}$ in (I.1), for instance,

$$\frac{\psi_{i,j+2} - 4\psi_{i,j+1} + 6\psi_{i,j} - 4\psi_{i,j-1} + \psi_{i,j-2}}{\Delta\xi^4} +$$

$$3\frac{\varepsilon^2}{r_j^2}\frac{-\psi_{i,j+2} + 16\psi_{i,j+1} - 30\psi_{i,j} + 16\psi_{i,j-1} - \psi_{i,j-2}}{12\Delta\xi^2} \qquad \text{(I.4)}$$

this discretized expression becomes equivalent to:

$$\frac{\partial^4\psi}{\partial\xi^4} + 3\frac{\varepsilon^2}{r_j^2}\frac{\partial^2\psi}{\partial\xi^2} + O(\Delta\xi^2\frac{\partial^6\psi}{\partial\xi^6}) \qquad \text{(I.5)}$$

In the present set of differential equations, various sources of artificial viscosity or similar inaccuracies may occur:

a. the secondary velocity components in the advection terms, both in the main flow equation (2.50) and in the stream function equation (2.52). Employing second order finite difference schemes to compute these components from the stream function would lead to third derivatives of this stream function in the truncation error, and hence to artificial viscosity, these derivatives being equivalent to second derivatives of the secondary velocity components.

b. the divergence terms with $\frac{\varepsilon^2}{r_2}$ and $\frac{\varepsilon^3}{r_3}$ in the stream function equation (2.52), both in the advection terms and in the viscosity terms. See also the example elaborated in this section.

c. the derivatives of $\psi^{(n)}$ in the advection terms of (2.52). In addition to the advection terms mentioned under b, the terms with $\frac{\varepsilon}{r}$ lead to fourth derivatives in the truncation error when discretizing them by a second order scheme.

d. the vertical derivative of $u^{(n)}$ in the source term of (2.52). Discretizing this derivative by a 3-point scheme would bring into the truncation error a third derivative of $u^{(n)}$, being equivalent to the fourth derivatives of $\psi^{(n)}$ (i.e. third derivatives of the secondary velocity components) in the viscosity terms of this equation.

All these sources could be avoided by employing fourth order schemes for the relevant terms. Doing so for the terms mentioned under c, however, would lead to a larger computational molecule and higher computer costs. Therefore it is worthwhile to investigate under which conditions the artificial viscosity arising from these terms is negligible. Elaborating the three-point finite difference representation of these terms and requiring the truncation error to be much smaller than the leading terms leads to:

$$\frac{\varepsilon}{r_j}\,\varepsilon Re|v_{i,j}|\,\frac{\Delta\zeta^2}{6} \ll 1 \quad ; \quad \frac{\varepsilon}{r_j}\,\varepsilon Re|v_{i,j}|\,\frac{\Delta\xi^2}{4} \ll 1$$

$$\frac{\varepsilon}{r_j}\,\varepsilon Re|w_{i,j}|\,\frac{\Delta\zeta^2}{6} \ll 1 \quad ; \quad \frac{\varepsilon}{r_j}\,\varepsilon Re|w_{i,j}|\,\frac{\Delta\xi^2}{6} \ll 1 \qquad \text{(I.6)}$$

Apart from the artificial viscosity and similar inaccuracies mentioned before, another type of numerical inaccuracy may occur in the present system: if the mesh size of the computational grid is too large with respect to the thickness of the boundary layers at the fixed walls, spatial oscillations (wiggles) will occur in the finite difference solution of u (ROACHE, 1972). Applying the one-dimensional analysis given by Roache to the present two-dimensional problem, wiggles will be suppressed when

$$\varepsilon Re|v_{i,j}|\frac{\Delta\xi}{2} < 1 \qquad \text{and} \qquad \varepsilon Re|w_{i,j}|\frac{\Delta\zeta}{2} < 1 \tag{I.7}$$

throughout the flow.
Combining (I.6) and (I.7) shows, that if

$$\frac{\varepsilon}{r_j}\Delta\xi \ll 1 \qquad \text{and} \qquad \frac{\varepsilon}{r_j}\Delta\zeta \ll 1 \tag{I.8}$$

the artificial viscosity due to the use of a second order finite scheme in terms of type c is negligible. Especially in not too sharp bends, condition (I.8) will be satisfied for reasonably large values of $\Delta\xi$ and $\Delta\zeta$, such as 0.1. Therefore, this type of artificial viscosity is neglected. It should be noted that if (I.8) holds good, the inaccuracies originated by second order schemes for the divergence terms mentioned under b are negligible too, their negligibility requiring:

$$\frac{\varepsilon^2}{r_j^2}\Delta\varepsilon^2 \ll 1 \tag{I.9}$$

## 2. Discretization of the main velocity equation

For $1 \le i \le N$, $1 \le j \le M-1$, equation (2.50) for u' is discretized as follows:

$$\frac{\varepsilon Re^2}{r_j}\left[-\frac{\delta\psi_{i,j}^{(n-1)}}{\delta\zeta}\left\{\frac{\delta u'^{(n)}_{i,j}}{\delta\xi}+\frac{\varepsilon}{r_j}u'^{(n)}_{i,j}\right\}+\frac{\delta\psi_{i,j}^{(n-1)}}{\delta\xi}\frac{\delta u'^{(n)}_{i,j}}{\delta\zeta}\right]=\frac{1}{r_j}+\nabla^2 u'^{(n)}_{i,j} \qquad (I.10)$$

where

$$r_j = 1 + (j - \frac{M}{2})\varepsilon\Delta\xi \qquad (I.11)$$

$$\frac{\delta\psi_{i,j}}{\delta\zeta} = \frac{120\psi_{i,j} + 36\psi_{i+1,j} + 8\psi_{i+2,j} - 3\psi_{i+3,j}}{144\Delta\zeta} \quad \text{for } i = 1 \qquad (I.12a)$$

$$= \frac{\psi_{i-2,j} - 8\psi_{i-1,j} + 8\psi_{i+1,j} - \psi_{i+2,j}}{12\Delta\zeta} \quad \text{for } 1 < i < N-1 \qquad (I.12b)$$

$$= \frac{\psi_{i-3,j} + 4\psi_{i-2,j} - 66\psi_{i-1,j} - 4\psi_{i,j}}{120\Delta\zeta} \quad \text{for } i = N-1 \qquad (I.12c)$$

$$= \frac{-4\psi_{i-3,j} + 27\psi_{i-2,j} - 108\psi_{i-1,j}}{66\Delta\zeta} \quad \text{for } i = N \qquad (I.12d)$$

$$\frac{\delta\psi_{i,j}}{\delta\xi} = \frac{120\psi_{i,j} + 36\psi_{i,j+1} + 8\psi_{i,j+2} - 3\psi_{i,j+3}}{144\Delta\xi} \quad \text{for } j = 1 \qquad (I.13a)$$

$$= \frac{\psi_{i,j-2} - 8\psi_{i,j-1} + 8\psi_{i,j+1} - \psi_{i,j+2}}{12\Delta\xi} \quad \text{for } 1 < j < M-1 \qquad (I.13b)$$

$$= \frac{3\psi_{i,j-3} - 8\psi_{i,j-2} - 36\psi_{i,j-1} - 120\psi_{i,j}}{144\Delta\xi} \quad \text{for } j = M-1 \qquad (I.13c)$$

$$\frac{\delta u'_{i,j}}{\delta\xi} = \frac{u'_{i,j+1} - u'_{i,j-1}}{2\Delta\xi} \qquad (I.14)$$

$$\frac{\delta u'_{i,j}}{\delta\zeta} = \frac{u'_{i+1,j} - u'_{i-1,j}}{2\Delta\xi} \qquad \text{for } 1 \le i \le N-1 \qquad \text{(I.15a)}$$

$$= 0 \qquad \text{for } i = N \qquad \text{(I.15b)}$$

$$\nabla^2 u'_{i,j} = \frac{u'_{i+1,j} - 2u'_{i,j} + u'_{i-1,j}}{\Delta\zeta^2} + \frac{u'_{i,j+1} - 2u'_{i,j} + u'_{i,j-1}}{\Delta\xi^2} +$$

$$+ \frac{\varepsilon}{r_j} \frac{u'_{i,j+1} - u'_{i,j-1}}{2\Delta\xi} - \frac{\varepsilon^2}{r_j^2} u'_{i,j} \qquad \text{for } 1 \le i \le N-1 \qquad \text{(I.16a)}$$

$$= \frac{-2u'_{i,j} + 2u'_{i-1,j}}{\Delta\zeta^2} + \frac{u'_{i,j+1} - 2u'_{i,j} + u'_{i,j-1}}{\Delta\xi^2} +$$

$$+ \frac{\varepsilon}{r_j} \frac{u'_{i,j+1} - u'_{i,j-1}}{2\Delta\zeta} - \frac{\varepsilon^2}{r_j^2} u'_{i,j} \qquad \text{for } i = N \qquad \text{(I.16b)}^*$$

3. Discretization of the stream function equation

For $1 \le i \le N-1$, $1 \le j \le M-1$, the stream function equation (2.52) is discretized by

$$\frac{\varepsilon Re^2}{r_j}\Big[-\frac{\delta\psi^{(n-1)}_{i,j}}{\delta\zeta}\Big\{\frac{\delta^3\psi^{(n)}_{i,j}}{\delta\xi\delta\zeta^2} + \frac{\delta^3\psi^{(n)}_{i,j}}{\delta\xi^3} - 2\frac{\varepsilon}{r_j}\frac{\delta^2\psi^{(n)}_{i,j}}{\delta\zeta^2} - 3\frac{\varepsilon}{r_j}\frac{\delta^2\psi^{(n)}_{i,j}}{\delta\xi^2} + 3\frac{\varepsilon^2}{r_j^2}\frac{\delta\psi^{(n)}_{i,j}}{\delta\xi}\Big\} +$$

$$+ \frac{\delta\psi^{(n-1)}_{i,j}}{\delta\xi}\Big\{\frac{\delta^3\psi^{(n)}_{i,j}}{\delta\zeta^3} + \frac{\delta^3\psi^{(n)}_{i,j}}{\delta\xi^2\delta\zeta} - \frac{\varepsilon}{r_j}\frac{\delta^2\psi^{(n)}_{i,j}}{\delta\xi\delta\zeta}\Big\}\Big] + 2\,u^{(n)}_{i,j}\frac{\delta u^{(n)}_{i,j}}{\delta\zeta} =$$

$$\frac{\delta^4\psi^{(n-1)}_{i,j}}{\delta\xi^4} + 2\frac{\delta^4\psi^{(n)}_{i,j}}{\delta\xi^2\delta\zeta^2} + \frac{\delta^4\psi^{(n)}_{i,j}}{\delta\zeta^4} - 2\frac{\varepsilon}{r_j}\Big\{\frac{\delta^3\psi^{(n)}_{i,j}}{\delta\xi^3} + \frac{\delta^3\psi^{(n)}_{i,j}}{\delta\xi\delta\zeta^2}\Big\} + \frac{\varepsilon^2}{r_j^2}\frac{\delta^2\psi^{(n)}_{i,j}}{\delta\xi^2} - 3\frac{\varepsilon^3}{r_j^3}\frac{\delta\psi^{(n)}_{i,j}}{\delta\xi} \qquad \text{(I.17)}$$

where in the advection terms

$$\frac{\delta^3\psi_{i,j}}{\delta\zeta^3} = \frac{-120\psi_{i,j} + 36\psi_{i+1,j} - 8\psi_{i+2,j} + 3\psi_{i+3,j}}{24\Delta\zeta^3} \qquad \text{for } i = 1 \qquad \text{(I.18a)}$$

$$= \frac{-\psi_{i-2,j} + 2\psi_{i-1,j} - 2\psi_{i+1,j} + \psi_{i+2,j}}{2\Delta\zeta^3} \qquad \text{for } 1<i<N-1 \qquad \text{(I.18b)}$$

---

* As $\left.\frac{\partial^3 u'}{\partial\zeta^3}\right|_{\zeta=0} = 0$, the first term is a second order approximation of $\left.\frac{\partial^2 u'}{\partial\zeta^2}\right|_{\zeta=0}$

$$= \frac{-\psi_{i-3,j} - 4\psi_{i-2,j} + 6\psi_{i-1,j} + 4\psi_{i,j}}{20\Delta\zeta^3} \quad \text{for } i = N-1 \qquad \text{(I.18c)}$$

$$\frac{\delta^3\psi_{i,j}}{\delta\xi\delta\zeta^2} = \frac{\psi_{i+1,j+1} - 2\psi_{i,j+1} + \psi_{i-1,j+1} - \psi_{i+1,j-1} + 2\psi_{i,j-1} - \psi_{i-1,j-1}}{2\Delta\xi\Delta\zeta^2} \qquad \text{(I.19)}$$

$$\frac{\delta^3\psi_{i,j}}{\delta\xi^2\delta\zeta} = \frac{\psi_{i+1,j+1} - 2\psi_{i+1,j} + \psi_{i+1,j-1} - \psi_{i-1,j+1} + 2\psi_{i-1,j} - \psi_{i-1,j-1}}{2\Delta\xi^2\Delta\zeta} \qquad \text{(I.20)}$$

$$\frac{\delta^3\psi_{i,j}}{\delta\xi^3} = \frac{-120\psi_{i,j} + 36\psi_{i,j+1} - 8\psi_{i,j+2} + 3\psi_{i,j+3}}{24\Delta\xi^3} \quad \text{for } j = 1 \qquad \text{(I.21a)}$$

$$= \frac{-\psi_{i,j-2} + 2\psi_{i,j-1} - 2\psi_{i,j+1} + \psi_{i,j+2}}{2\Delta\xi^3} \quad \text{for } 1<j<M-1 \qquad \text{(I.21b)}$$

$$= \frac{-3\psi_{i,j-3} + 8\psi_{i,j-2} - 36\psi_{i,j-1} + 120\psi_{i,j}}{24\Delta\xi^3} \quad \text{for } j = M-1 \qquad \text{(I.21c)}$$

$$\frac{\delta^2\psi_{i,j}}{\delta\zeta^2} = \frac{\psi_{i+1,j} - 2\psi_{i,j} + \psi_{i-1,j}}{\Delta\zeta^2} \qquad \text{(I.22)}$$

$$\frac{\delta^2\psi_{i,j}}{\delta\xi\delta\zeta} = \frac{\psi_{i+1,j+1} - \psi_{i-1,j+1} - \psi_{i+1,j-1} + \psi_{i-1,j-1}}{4\Delta\xi\Delta\zeta} \qquad \text{(I.23)}$$

$$\frac{\delta^2\psi_{i,j}}{\delta\xi^2} = \frac{\psi_{i,j+1} - 2\psi_{i,j} + \psi_{i,j-1}}{\Delta\xi^2} \qquad \text{(I.24)}$$

$$\frac{\delta\psi^{(n)}_{i,j}}{\delta\xi} = \frac{\psi^{(n)}_{i,j+1} - \psi^{(n)}_{i,j-1}}{2\Delta\xi} \qquad \text{(I.25)}$$

$\frac{\delta\psi^{(n-1)}_{i,j}}{\delta\xi}$ and $\frac{\delta\psi^{(n-1)}_{i,j}}{\delta\zeta}$ : see (I.13) and (I.12), respectively.

In the viscous terms the discretizations are

$$\frac{\delta^4\psi_{i,j}}{\delta\zeta^4} = \frac{192\psi_{i,j} - 108\psi_{i+1,j} + 32\psi_{i+2,j} - 3\psi_{i+3,j}}{12\Delta\zeta^4} \quad \text{for } i = 1 \qquad \text{(I.26a)}$$

$$= \frac{\psi_{i-2,j} - 4\psi_{i-1,j} + 6\psi_{i,j} - 4\psi_{i-1,j} + \psi_{i-2,j}}{\Delta\zeta^4} \quad \text{for } 1<i<N-1 \qquad \text{(I.26b)}$$

$$= \frac{64\psi_{i,j} - 54\psi_{i-1,j} + 16\psi_{i-2,j} - \psi_{i-3,j}}{10\Delta\zeta^4} \quad \text{for } i = N-1 \qquad \text{(I.26c)}$$

$$\frac{\delta^4\psi_{i,j}}{\delta\xi^2\delta\zeta^2} =$$

$$\frac{\psi_{i+1,j+1} - 2\psi_{i,j+1} - \psi_{i-1,j+1} - 2\psi_{i+1,j} + 4\psi_{i,j} - 2\psi_{i-1,j} + \psi_{i+1,j} - 2\psi_{i,j-1} + \psi_{i-1,j-}}{\Delta\xi^2\Delta\zeta^2}$$

(I. 27)

$$\frac{\delta^4\psi_{i,j}}{\delta\xi^4} = \frac{192\psi_{i,j} - 108\psi_{i,j+1} + 32\psi_{i,j+2} - 3\psi_{i,j+3}}{12\Delta\xi^4} \quad \text{for } j = 1 \qquad \text{(I.28a)}$$

$$= \frac{\psi_{i,j-2} - 4\psi_{i,j-1} + 6\psi_{i,j} - 4\psi_{i,j+1} + \psi_{i,j+2}}{\Delta\xi^4} \quad \text{for } 1<j<M-1 \qquad \text{(I.28b)}$$

$$= \frac{192\psi_{i,j} - 108\psi_{i,j-1} + 32\psi_{i,j-2} - 3\psi_{i,j-3}}{12\Delta\xi^4} \quad \text{for } j = M-1 \qquad \text{(I.28c)}$$

$\frac{\delta^3\psi_{i,j}}{\delta\xi^3}$ and $\frac{\delta^3\psi_{i,j}}{\delta\xi\delta\zeta^2}$ : see (I.21) and (I.19), respectively

$\frac{\delta^2\psi_{i,j}}{\delta\xi^2}$ and $\frac{\delta\psi_{i,j}}{\delta\xi}$ : see (I.24) and (I.25), respectively.

In the source term $\frac{\delta u^{(n)}_{i,j}}{\delta\zeta}$ is discretized by

$$\frac{\delta u_{i,j}}{\delta\zeta} = \frac{-10u_{i,j} + 18u_{i+1,j} - 6u_{i+2,j} + u_{i+3,j}}{12\Delta\zeta} \quad \text{for } i = 1 \tag{I.29a}$$

$$= \frac{u_{i-2,j} - 8u_{i-1,j} + 8u_{i+1,j} - u_{i+2,j}}{12\Delta\zeta} \quad \text{for } 1<i<N-1 \tag{I.29b}$$

$$= \frac{34u_{i+1,j} - 18u_{i,j} - 18u_{i-1,j} + 2u_{i-2,j}}{36\Delta\zeta} \quad \text{for } i = N-1 \tag{I.29c}$$

## 4. Discretization of the pressure equation

Equation (2.44) for the pressure $p$ can be rewritten as:

$$\frac{\partial^2 E}{\partial\xi^2} + \frac{\partial^2 E}{\partial\zeta^2} + \frac{\varepsilon}{r}\frac{\partial E}{\partial\xi} = \frac{\varepsilon^2 Re^2}{r^2}\Big[\frac{\partial\psi}{\partial\xi}\Big\{\frac{\partial^3\psi}{\partial\xi^3} + \frac{\partial^3\psi}{\partial\xi\partial\zeta^2} - \frac{\varepsilon}{r}\frac{\partial^2\psi}{\partial\xi^2} + \frac{\varepsilon^2}{r^2}\frac{\partial\psi}{\partial\xi}\Big\} +$$
$$+ \frac{\partial\psi}{\partial\zeta}\Big\{\frac{\partial^3\psi}{\partial\xi^2\partial\zeta} + \frac{\partial^3\psi}{\partial\zeta^3} - \frac{\varepsilon}{r}\frac{\partial^2\psi}{\partial\xi\partial\zeta}\Big\} +$$
$$+ \Big\{\frac{\partial^2\psi}{\partial\xi^2} + \frac{\partial^2\psi}{\partial\zeta^2} - \frac{\varepsilon}{r}\frac{\partial\psi}{\partial\xi}\Big\}^2\Big] + \frac{\varepsilon Re}{r}\,2u\,\frac{\partial u}{\partial\xi} \tag{I.30}$$

where

$$E = p + \varepsilon^2 Re\,\frac{v^2 + w^2}{2} \tag{I.31}$$

The relevant boundary conditions read

$$\frac{\partial E}{\partial\xi} = -\frac{\varepsilon}{r}\frac{\partial^3\psi}{\partial\zeta^3} \quad \text{at } \zeta = -1 \tag{I.32}$$

$$\frac{\partial E}{\partial\zeta} = 0 \quad \text{at } \zeta = 0 \tag{I.33}$$

$$\frac{\partial E}{\partial\zeta} = \frac{\varepsilon}{r}\frac{\partial^3\psi}{\partial\xi^3} - \frac{\varepsilon^2}{r^2}\frac{\partial^2\psi}{\partial\xi^2} \quad \text{at } \xi = \pm\frac{B}{2d} \tag{I.34}$$

Equation (I.31) is discretized for $1 \leq i \leq N$, $1 \leq j \leq M-1$, making use of the following finite difference approximations:

$$\frac{\partial^2 E}{\partial \xi^2} + \frac{\varepsilon}{r}\frac{\partial E}{\partial \xi} = \frac{E_{i,j+1} - 2E_{i,j} + E_{i,j-1}}{\Delta\xi^2} + \frac{\varepsilon}{r_j}\frac{E_{i,j+1} - E_{i,j-1}}{2\Delta\xi} \qquad \text{(I.35)}$$

$$\frac{\partial^2 E}{\partial \zeta^2} = \frac{E_{i+1,j} - 2E_{i,j} + E_{i-1,j}}{\Delta\zeta^2} \quad \text{for } 1 \leq i \leq N-1 \qquad \text{(I.36a)}$$

$$= \frac{2E_{i-1,j} - 2E_{i,j}}{\Delta\zeta^2} \quad \text{for } i = N-1 \qquad \text{(I.36b)}^{*}$$

$\frac{\partial \psi}{\partial \zeta}$ and $\frac{\partial \psi}{\partial \xi}$ : see (I.12) and (I.13), respectively

$\frac{\partial^3 \psi}{\partial \xi \partial \zeta^2} + \frac{\partial^3 \psi}{\partial \xi^3} - \frac{\varepsilon}{r}\frac{\partial^2 \psi}{\partial \xi^2} + \frac{\varepsilon^2}{r^2}\frac{\partial \psi}{\partial \xi}$ : see (I.19), (I.21), (I.24) and (I.25)

$\frac{\partial^3 \psi}{\partial \zeta^3} + \frac{\partial^3 \psi}{\partial \xi^2 \partial \zeta} - \frac{\varepsilon}{r}\frac{\partial^2 \psi}{\partial \xi \partial \zeta}$ : see (I.18), (I.20) and (I.23)

For accuracy reasons similar to those mentioned in section 1 of this Appendix, five point schemes are employed for the $\omega^2$-term and for $\frac{\partial u}{\partial \xi}$ in (I.30):

$$\frac{\partial^2 \psi}{\partial \xi^2} = \frac{-480\psi_{i,j} + 252\psi_{i,j+1} - 32\psi_{i,j+2} + 3\psi_{i,j+3}}{576\Delta\xi^2} \quad \text{for } j = 1 \qquad \text{(I.37a)}$$

$$= \frac{-\psi_{i,j-2} + 16\psi_{i,j-1} - 30\psi_{i,j} + 16\psi_{i,j+1} - \psi_{i,j+2}}{12\Delta\xi^2} \quad \text{for } i \leq j \leq M-1 \qquad \text{(I.37b)}$$

$$= \frac{-480\psi_{i,j} + 252\psi_{i,j-1} + 32\psi_{i,j-2} + 3\psi_{i,j-3}}{567\Delta\xi^2} \quad \text{for } j = M-1 \qquad \text{(I.37c)}$$

---

* As $\left.\frac{\partial^3 E}{\partial \zeta^3}\right|_{\zeta=0} = 0$, this is a second order approximation of $\left.\frac{\partial^2 E}{\partial \zeta^2}\right|_{\zeta=0}$

$$\frac{\partial^2\psi}{\partial\zeta^2} = \frac{-480\psi_{i,j} + 252\psi_{i+1,j} - 32\psi_{i+2,j} + 3\psi_{i+3,j}}{576\Delta\zeta^2} \quad \text{for } i = 1 \tag{I.38a}$$

$$= \frac{-\psi_{i-2,j} + 16\psi_{i-1,j} - 30\psi_{i,j} + 16\psi_{i+1,j} - \psi_{i+2,j}}{12\Delta\xi^2} \quad \text{for } 1 \leq i \leq N-1 \tag{I.38b}$$

$$= \frac{\psi_{i-3,j} - 16\psi_{i-2,j} + 174\psi_{i-1,j} - 304\psi_{i,j}}{120\Delta\xi^2} \quad \text{for } i = N-1 \tag{I.38c}$$

$$= 0 \quad \text{for } i = N \tag{I.38d}$$

Applying second order finite difference schemes to the derivatives of $\psi$ in the boundary conditions (I.32) and (I.34),

$$\frac{\partial^3\psi}{\partial\zeta^3}\bigg|_{\zeta=-1} = \frac{-15\psi_{i+1,j} + 6\psi_{i+2,j} - \psi_{i+3,j}}{\Delta\zeta^3} \tag{I.39}$$

$$\left(\frac{\partial^3\psi}{\partial\xi^3} - \frac{\varepsilon}{r}\frac{\partial^2\psi}{\partial\xi^2}\right)\bigg|_{\xi = -\frac{B}{2d}} = \frac{-15\psi_{i,j+1} + 6\psi_{i,j+2} - \psi_{i,j+3}}{\Delta\xi^3} + \\ - \frac{\varepsilon}{r_j}\frac{108\psi_{i,j+1} - 27\psi_{i,j+2} + 4\psi_{i,j+3}}{18\Delta\xi^2} \tag{I.40a}$$

$$\left(\frac{\partial^3\psi}{\partial\xi^3} - \frac{\varepsilon}{r}\frac{\partial^2\psi}{\partial\xi^2}\right)\bigg|_{\xi = +\frac{B}{2d}} = \frac{15\psi_{i,j-1} - 6\psi_{i,j-2} + \psi_{i,j-3}}{\Delta\xi^3} - \\ - \frac{\varepsilon}{r_j}\frac{108\psi_{i,j-1} - 27\psi_{i,j-2} + 4\psi_{i,j-3}}{18\Delta\xi^2} \tag{I.40b}$$

the values of E on the fixed boundaries can be determined by integrating (I.32) and (I.34) along these boundaries.

FIGURES

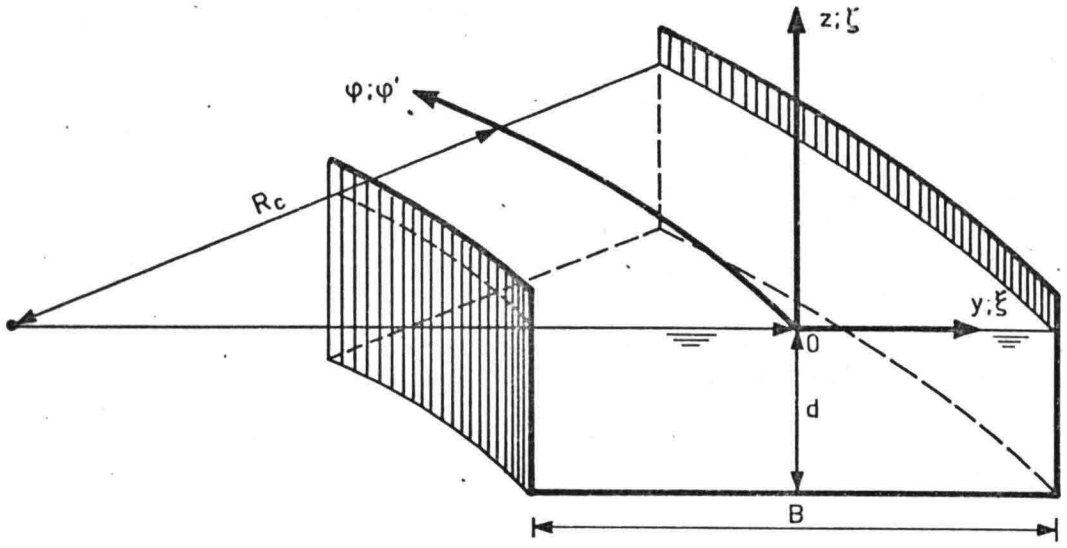


Figure 1. Definition sketch

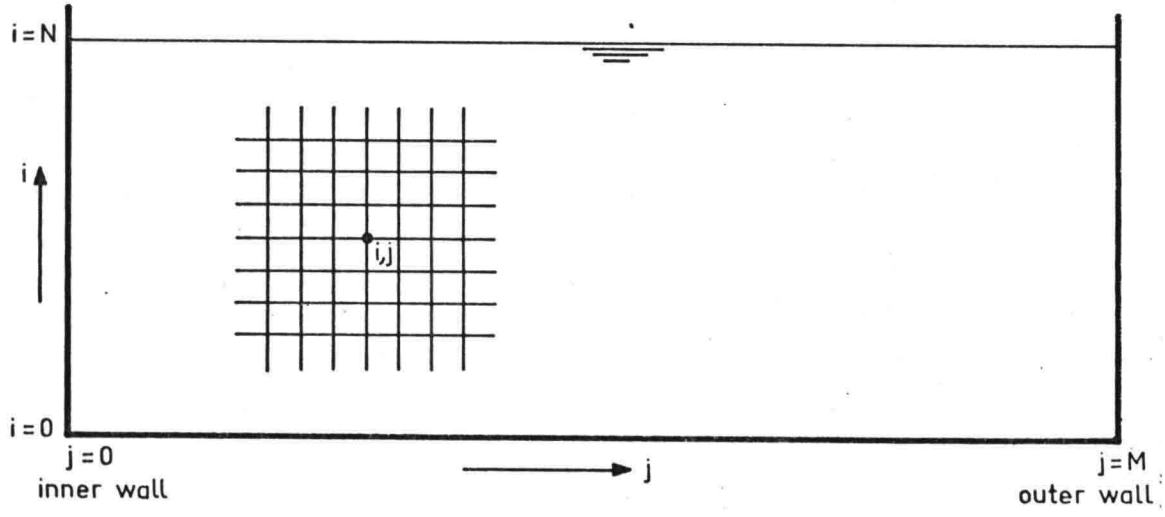


Figure 2. Computational grid

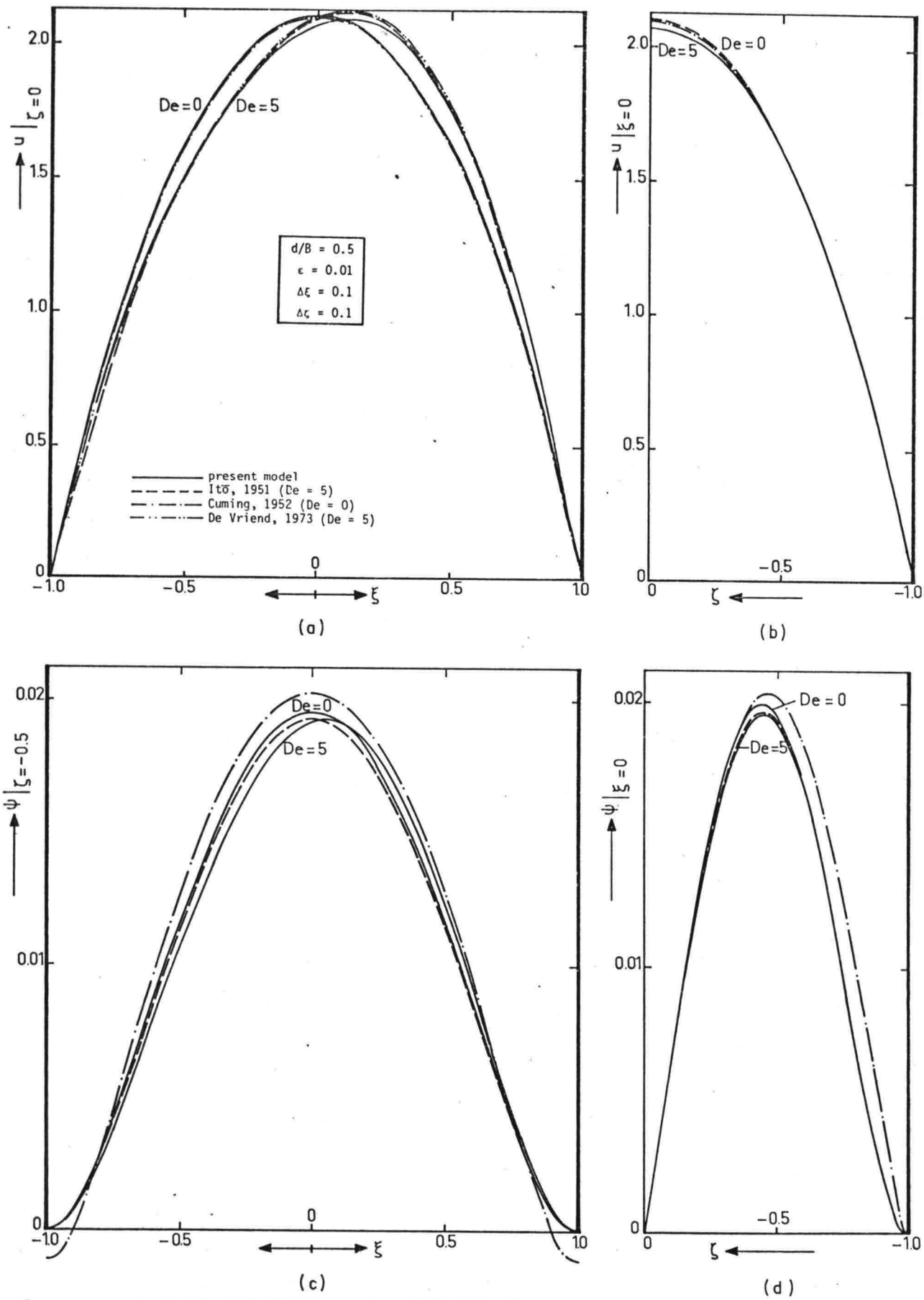


Figure 3. Comparison with analytical results for a square pipe at low Dean numbers
(a) Main velocity at the surface
(b) Main velocity in the centreline
(c) Stream function at half depth
(d) Stream function in the centreline

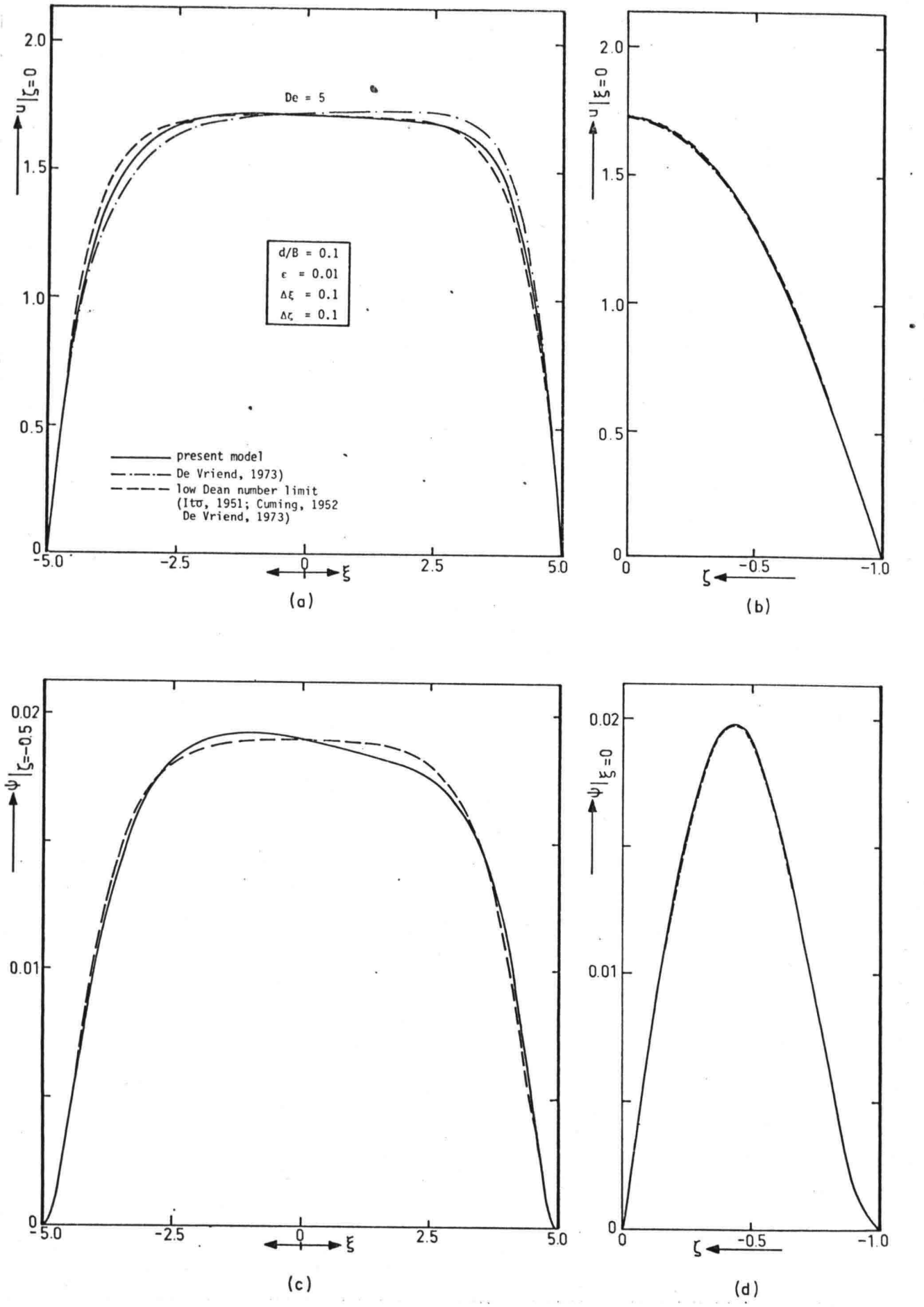


Figure 4. Comparison with analytical results for a shallow pipe at low Dean numbers
(a) Main velocity at the surface
(b) Main velocity in the centreline
(c) Stream function at half depth
(d) Stream function in the centreline

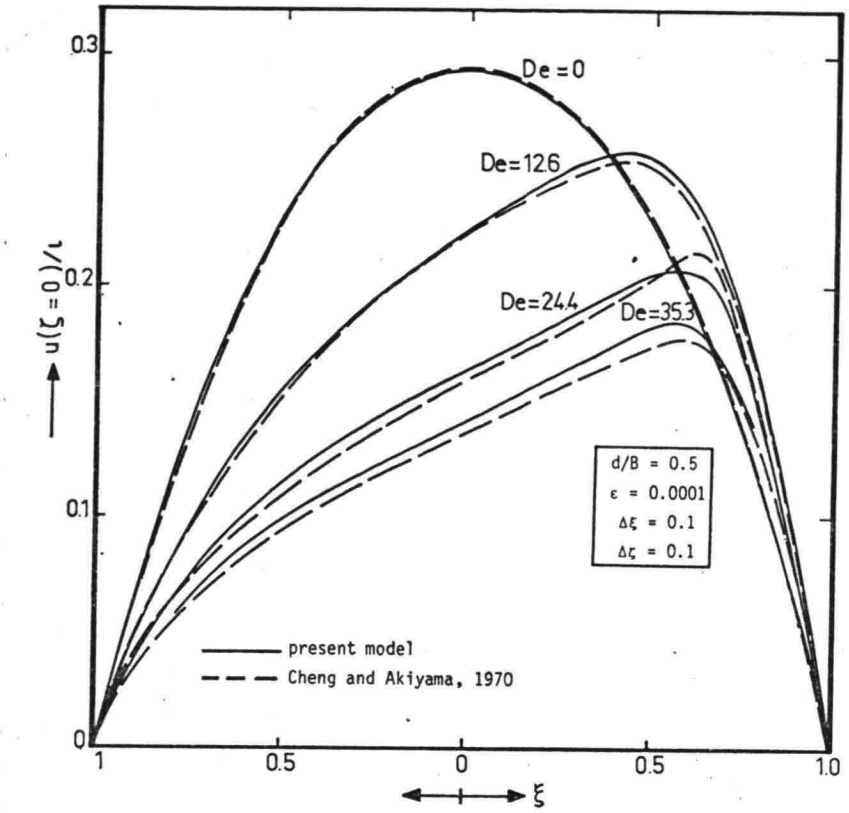


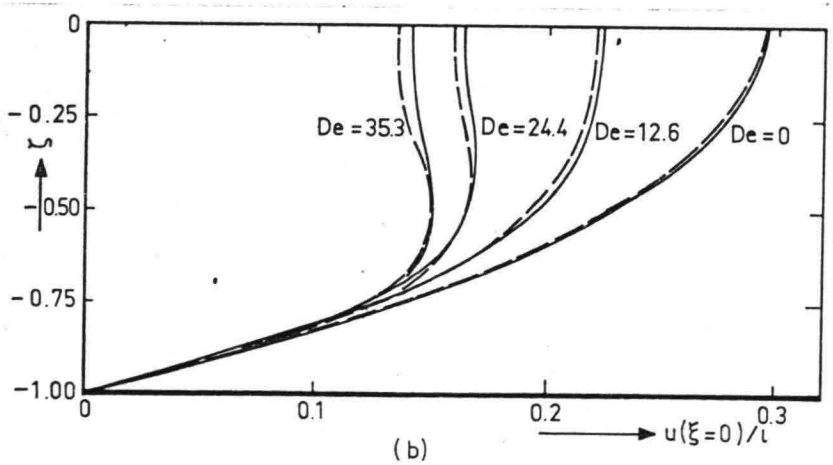


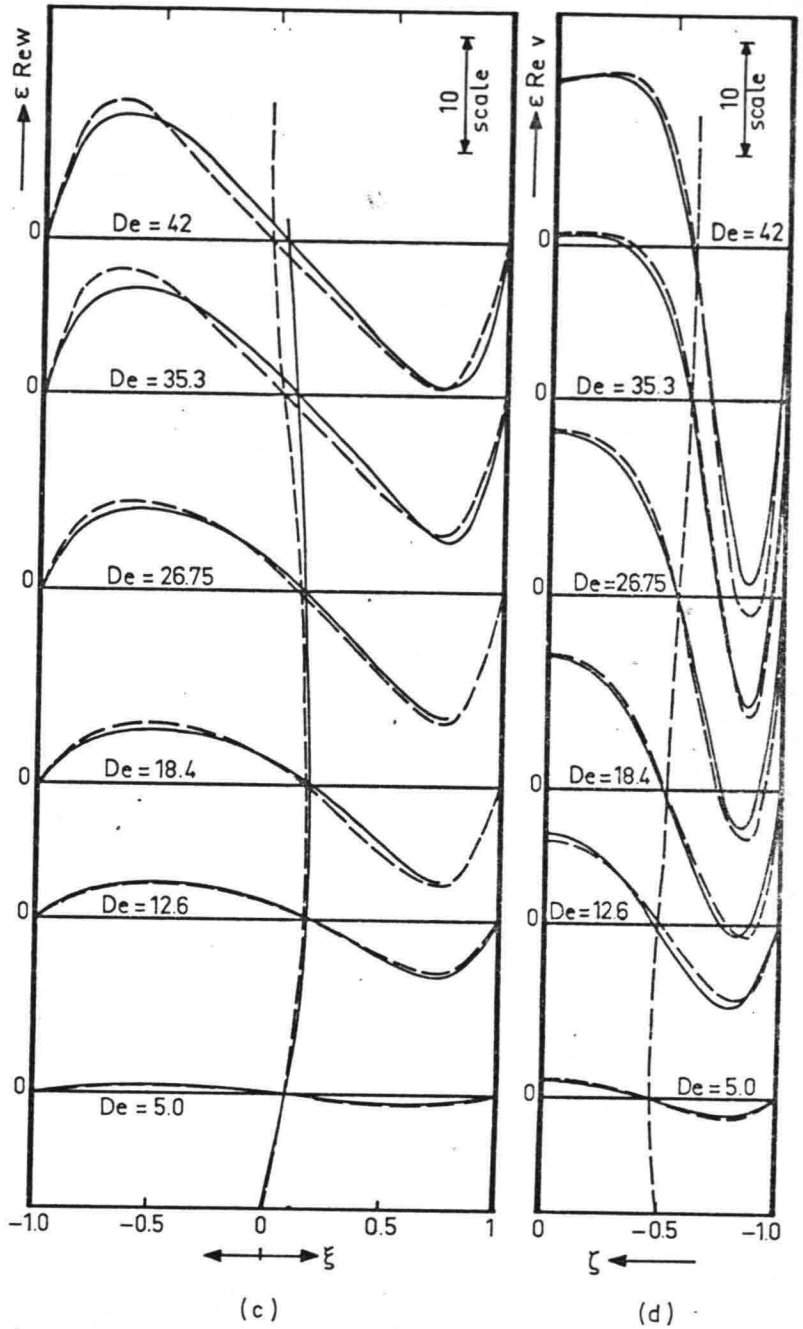


Figure 5. Comparison with Cheng and Akiyama's numerical results for a square pipe
(a) Main velocity at the surface (c) Vertical velocity through the centre of circulation
(b) Main velocity in the centreline (d) Radial velocity through the centre of circulation

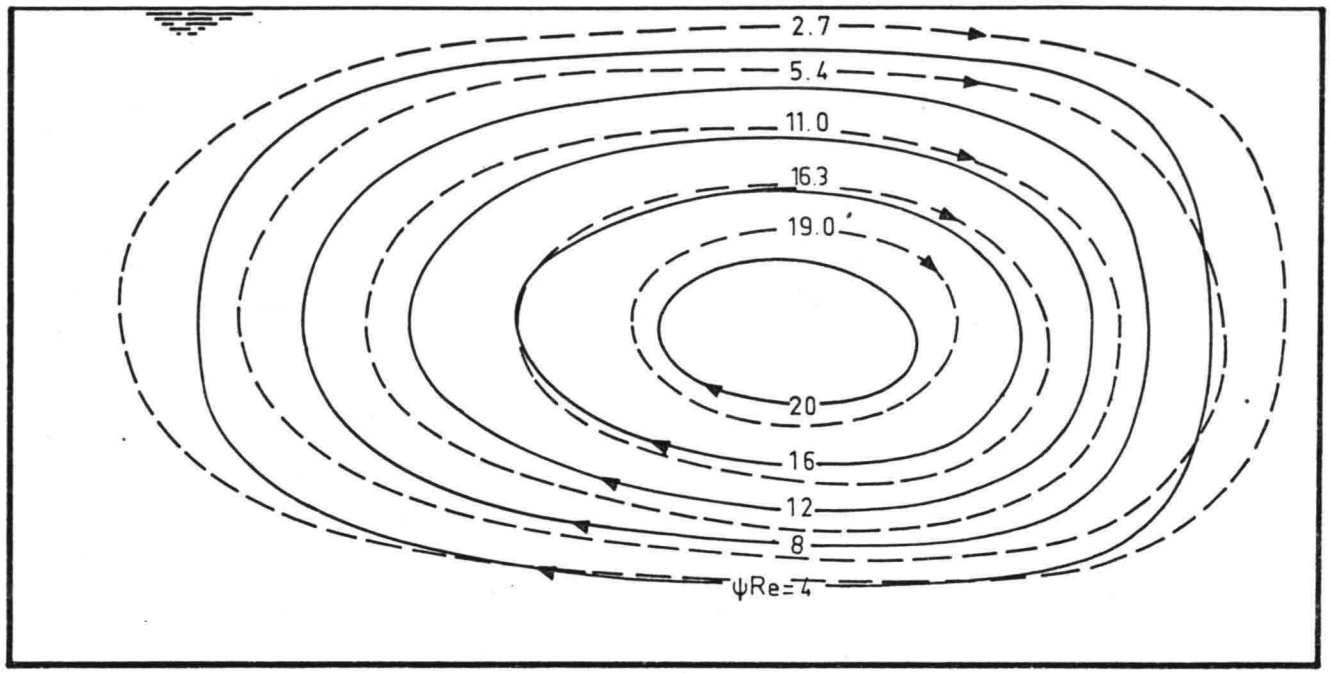


(e)

——— present model

— — — — Cheng and Akiyama, 1970

Figure 5. Comparison with Cheng and Akiyama's results for a square pipe
(e) Streamlines of the secondary flow for De=18.4

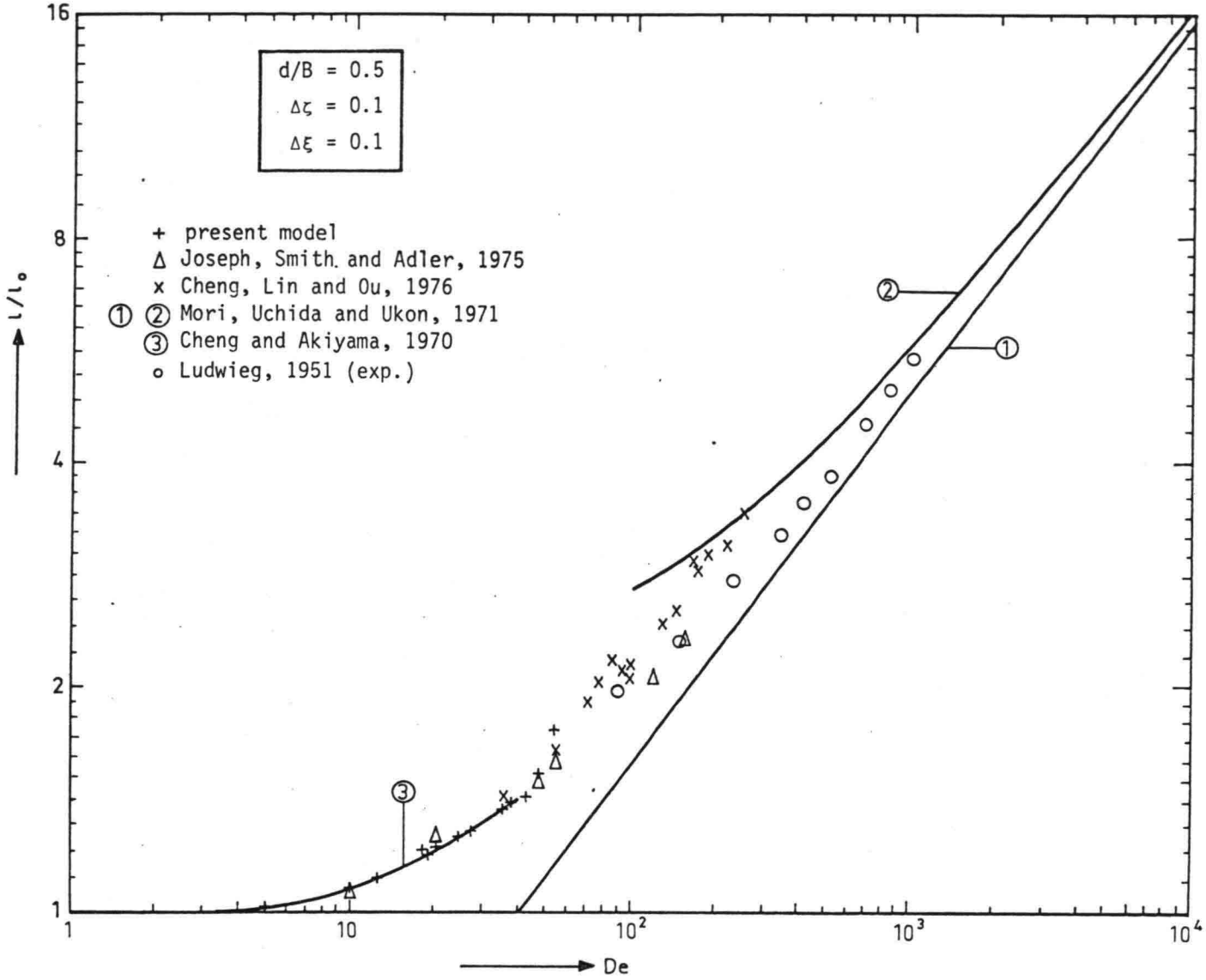


Figure 6. Longitudinal slope factor vs. Dean number for a square pipe

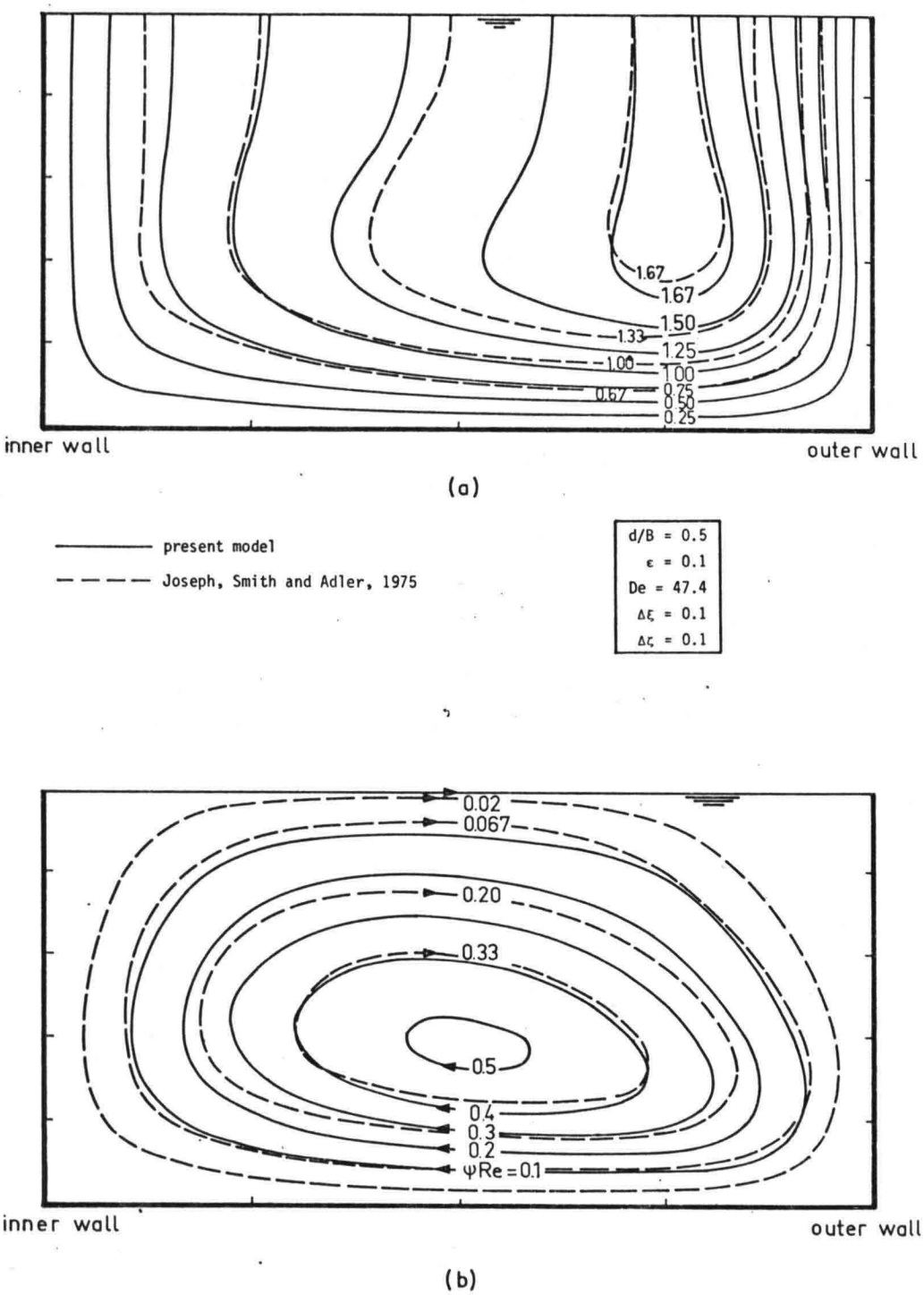


Figure 7. Transition to double helical flow pattern in a square pipe
(a) Main flow isovels for De = 47.4
(b) Streamlines of the secondary flow for De = 47.4

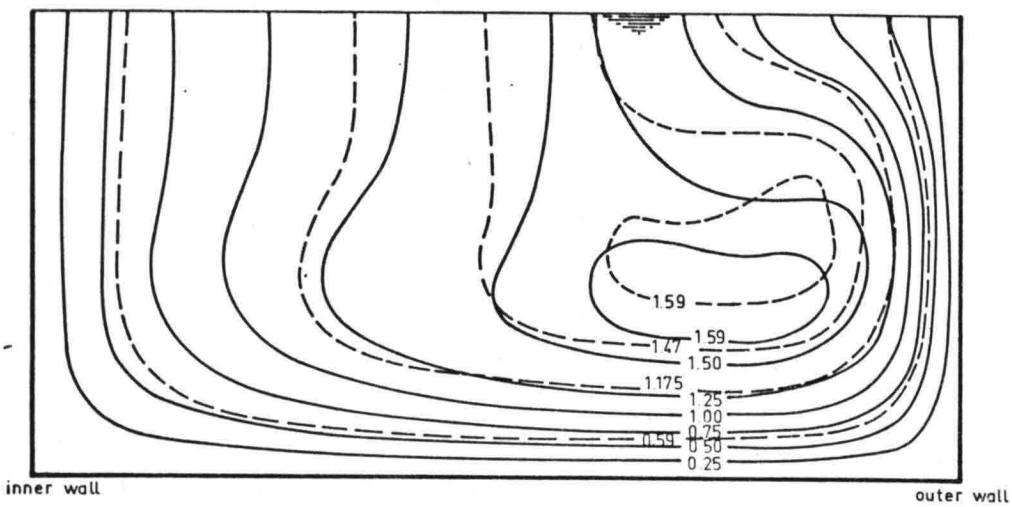


(c)

——— present model

— — — — Joseph, Smith and Adler, 1975

| |
|---|
| d/B = 0.5 |
| ε = 0.1 |
| De = 53.8 |
| Δξ = 0.1 |
| Δζ = 0.1 |

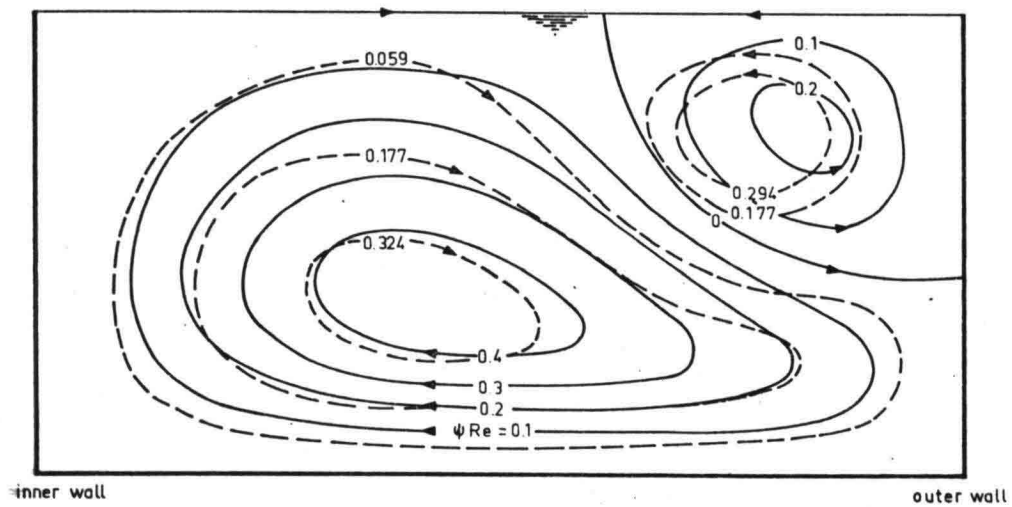


(d)

Figure 7. Transition to double helical flow pattern in a square pipe
(c) Main flow isovels for De=53.8
(d) Streamlines of the secondary flow for De=53.8

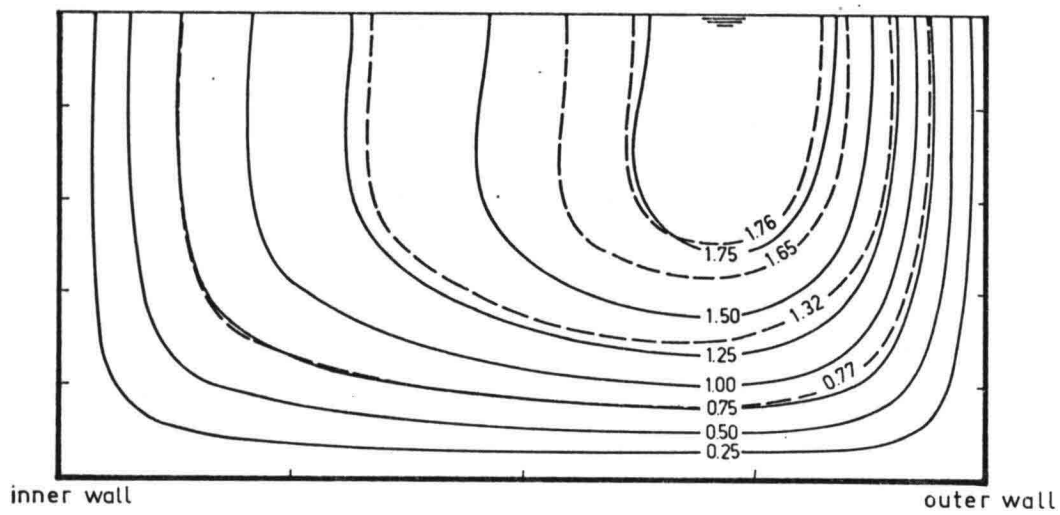


(a)

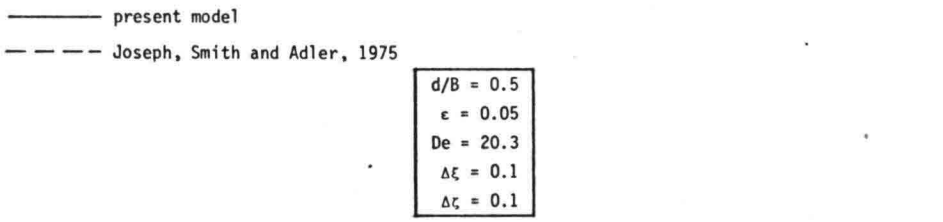


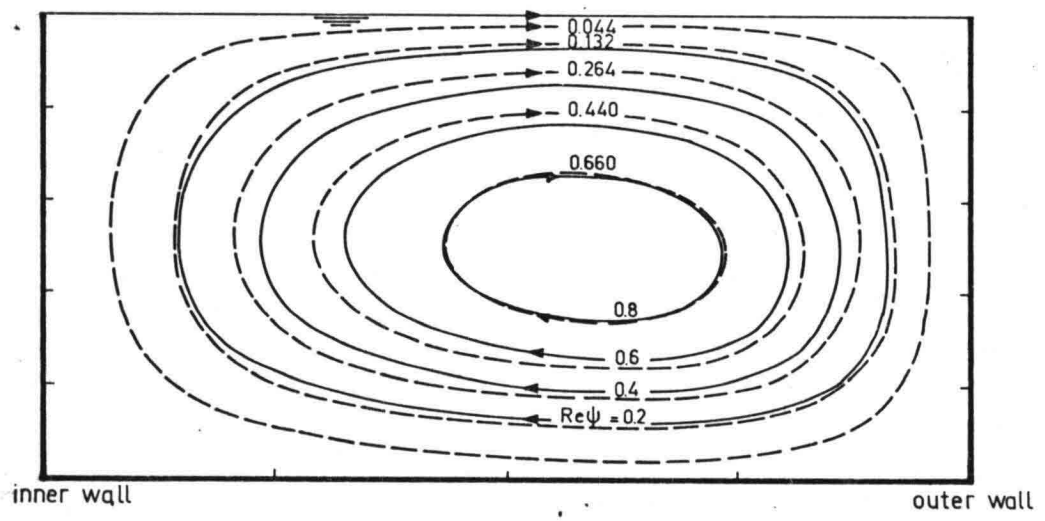


(b)

Figure 8. Comparison with Joseph, Smith and Adler's results for a square pipe at De=20.3
(a) Main flow isovels
(b) Streamlines of the secondary flow

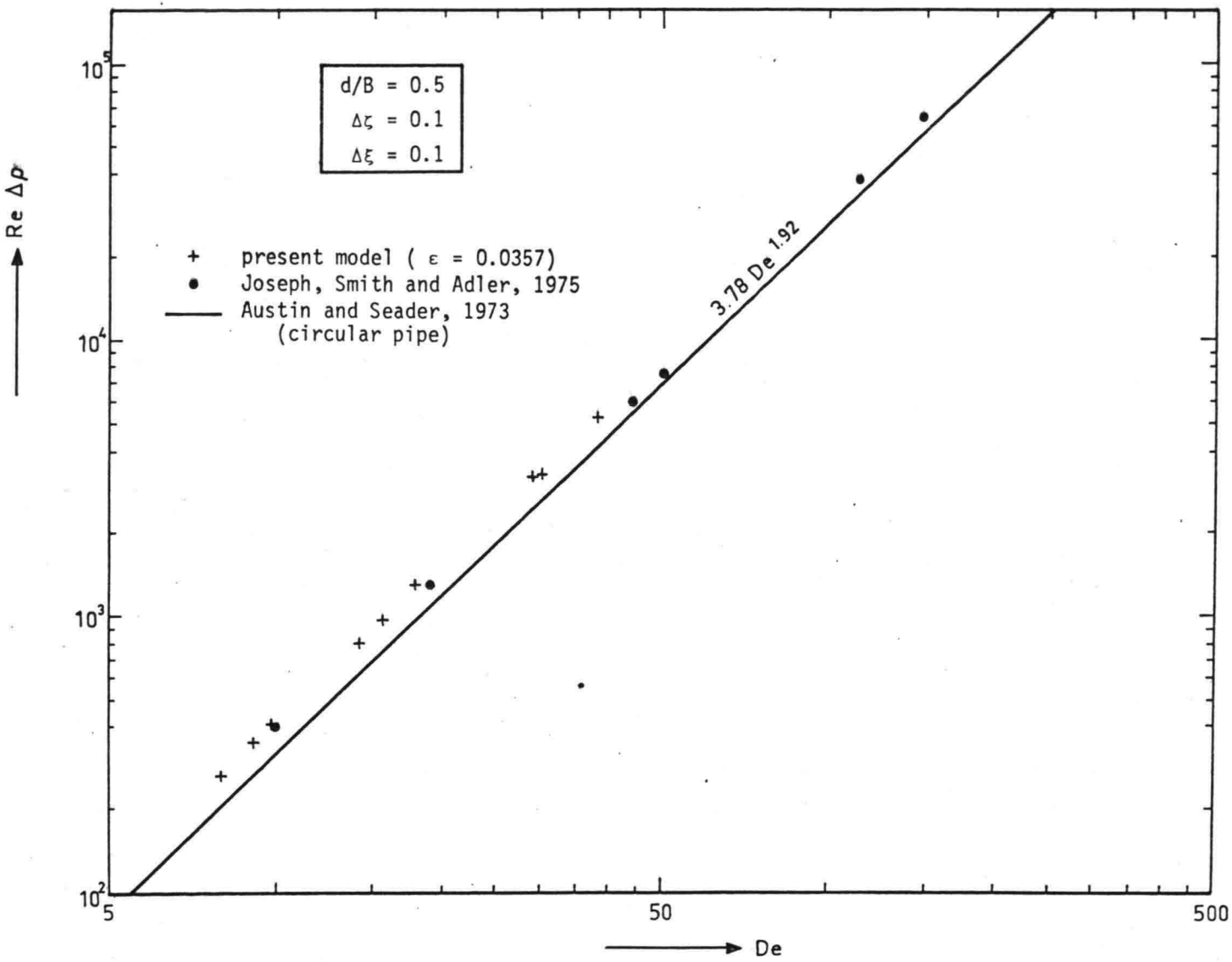


Figure 9. Transverse pressure drop at the surface compared with results for a square and a circular pipe

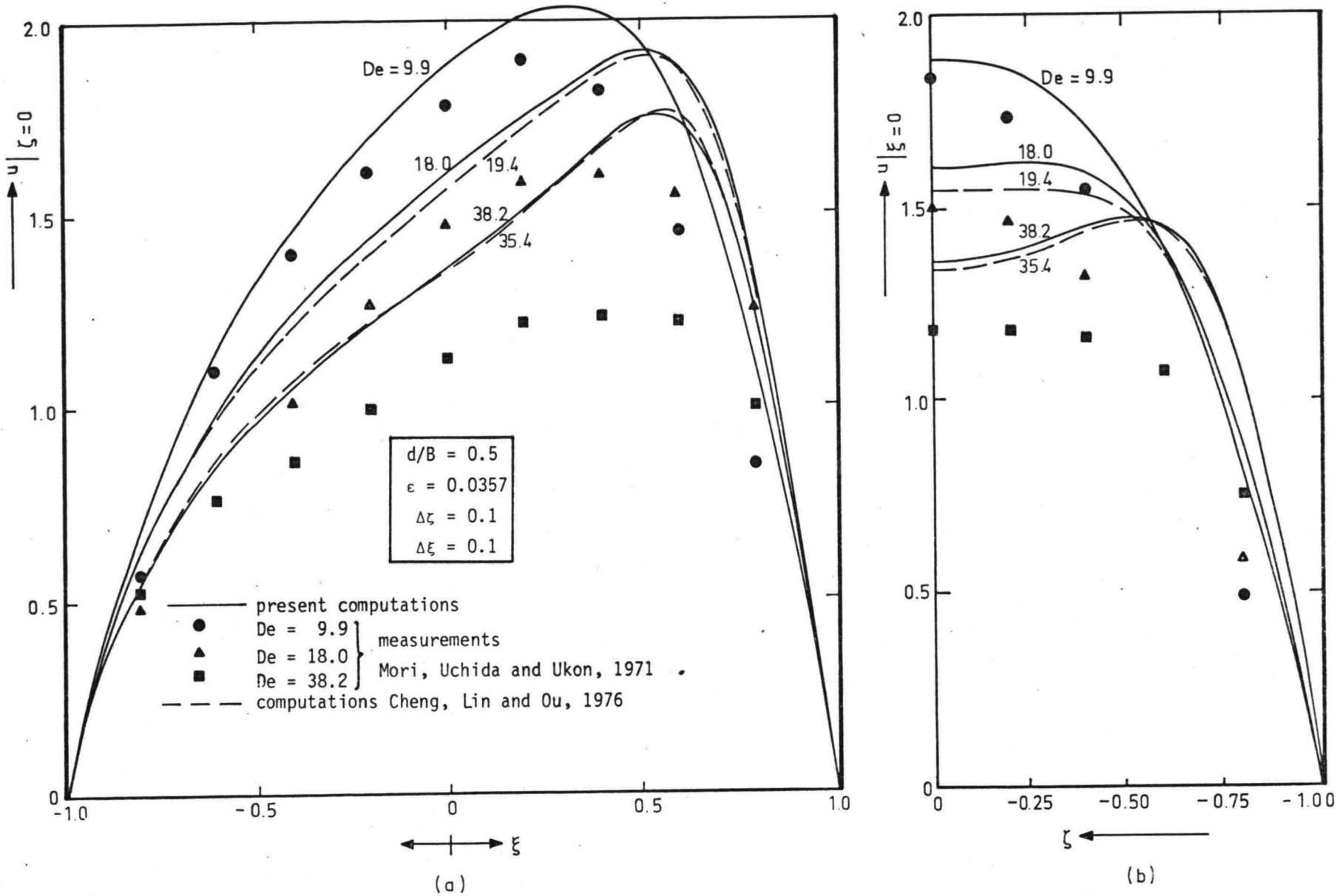


Figure 10. Comparison with Mori, Uchida and Ukon's measured data for a square pipe
(a) Main velocity at the surface
(b) Main velocity in the centreline

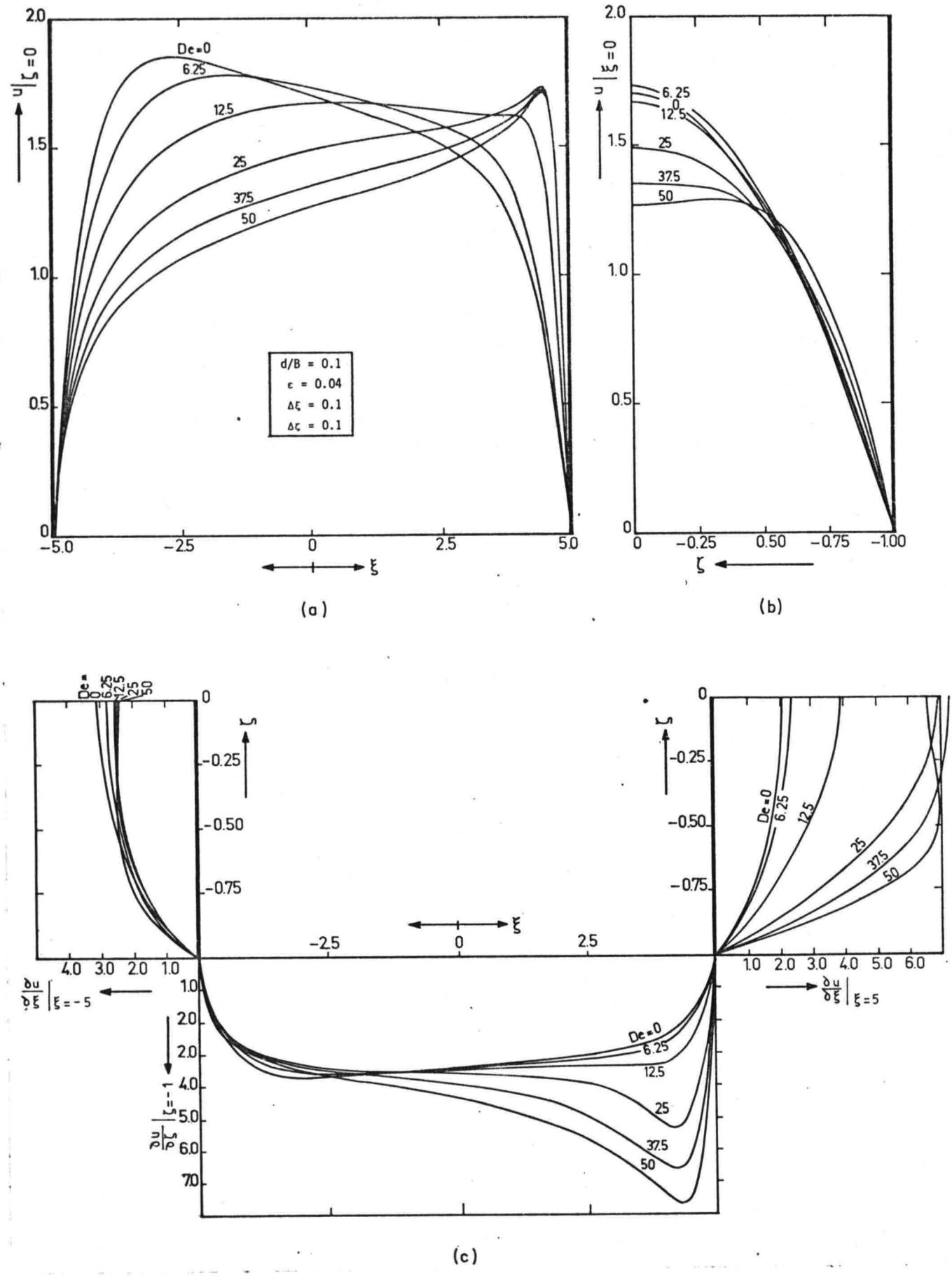


Figure 11. Influence of the Dean number on the main flow in a shallow channel
(a) Main velocity at the surface
(b) Main velocity in the centreline
(c) Main velocity gradients normal to the fixed boundaries

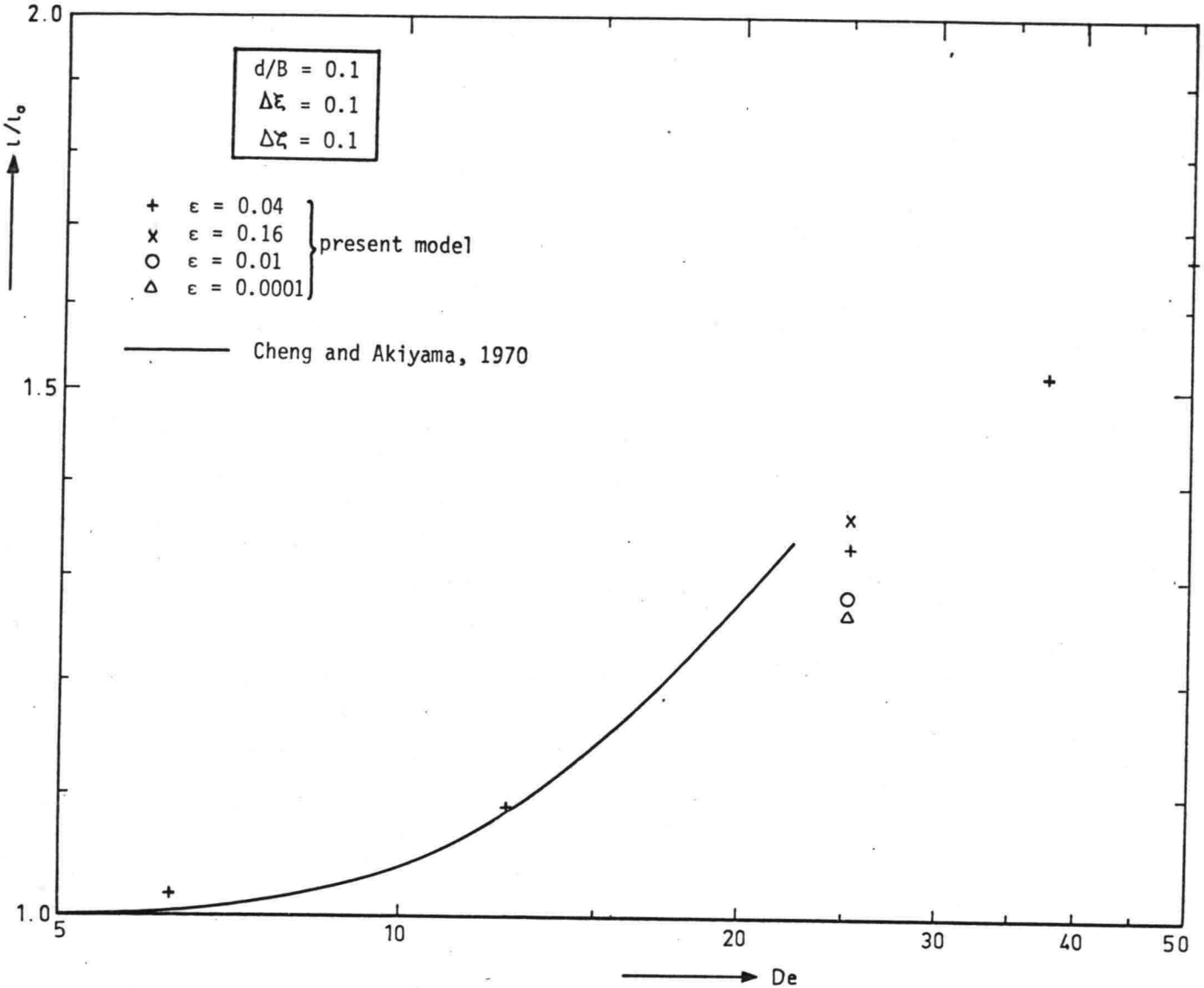


Figure 12. Influence of the Dean number on the longitudinal slope factor in a shallow channel

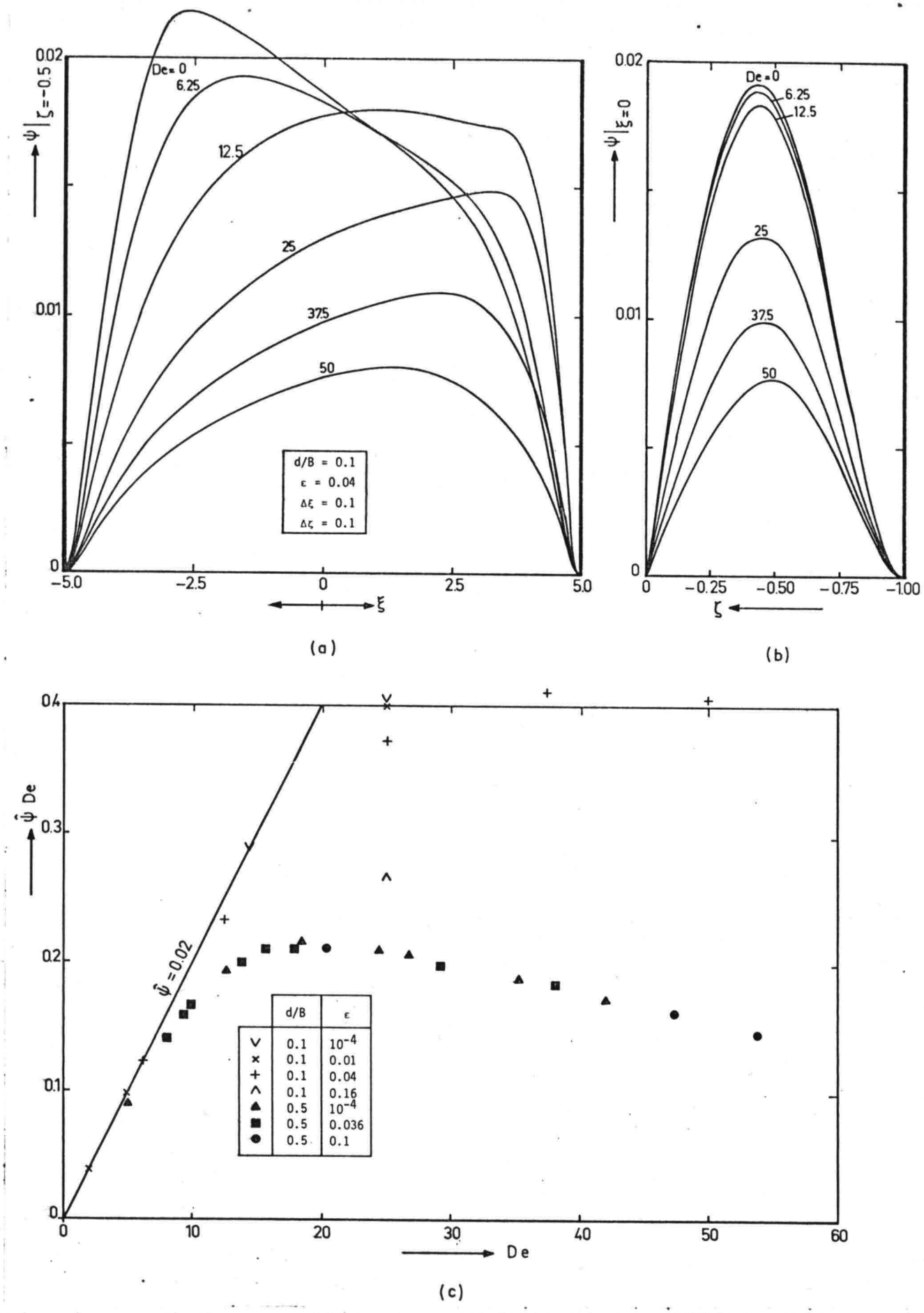


Figure 13. Influence of the Dean number on the secondary flow in a shallow channel
(a) Stream function at half depth
(b) Stream function in the centreline
(c) Maximum of the stream function compared with values for a square pipe

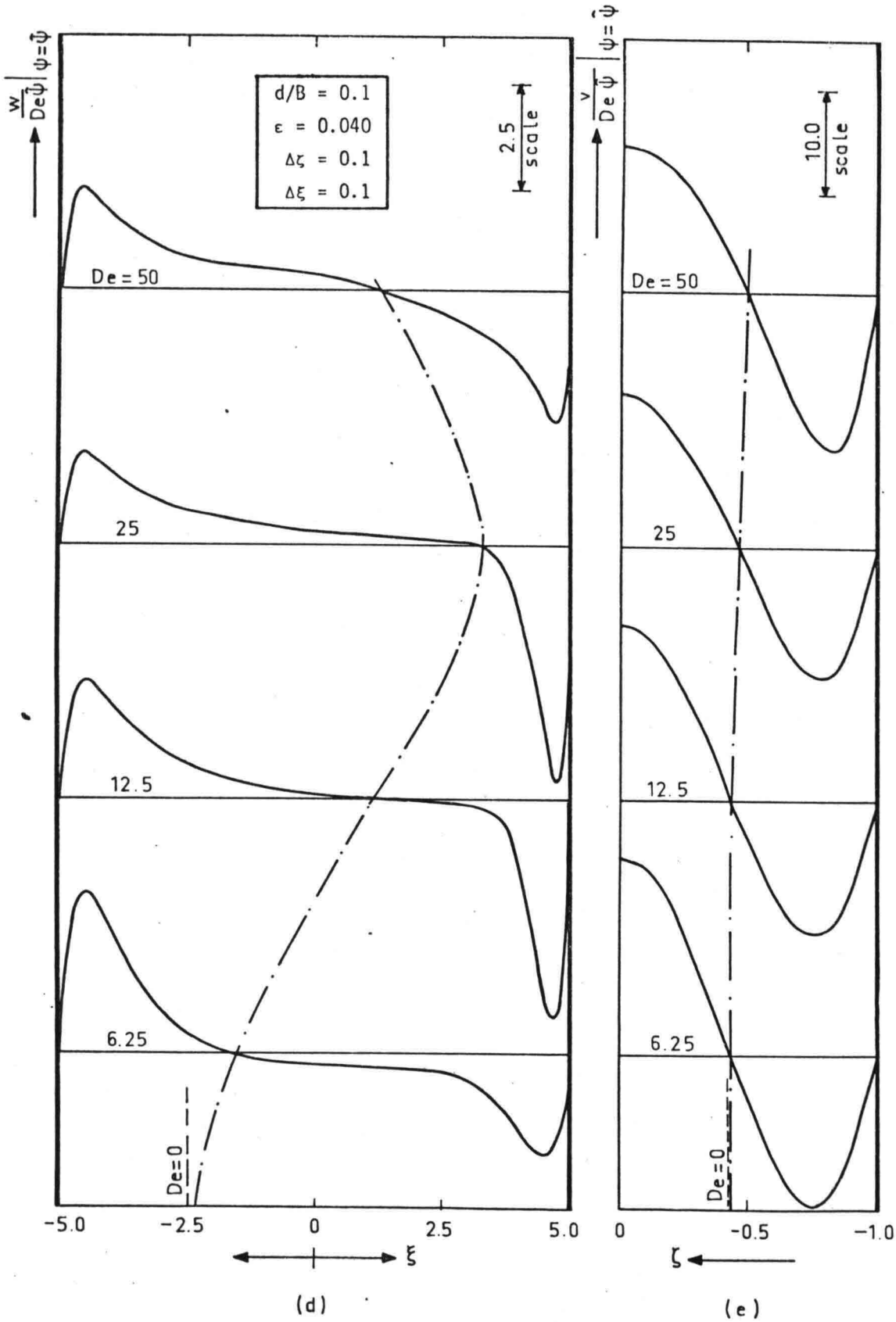


Figure 13. Influence of the Dean number on the secondary flow in a shallow channel
(d) Vertical velocity distribution
(e) Radial velocity distribution

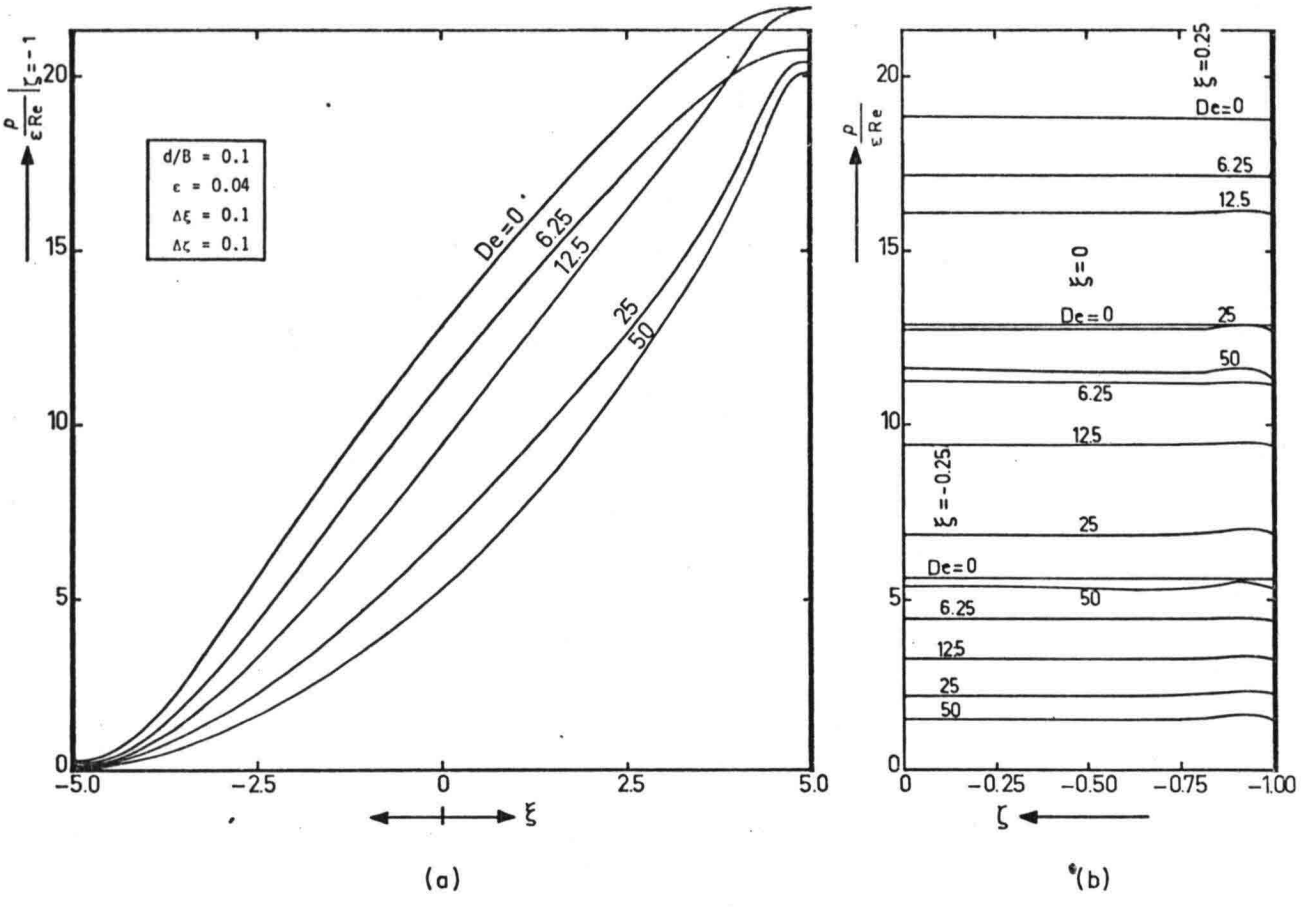


(a) (b)

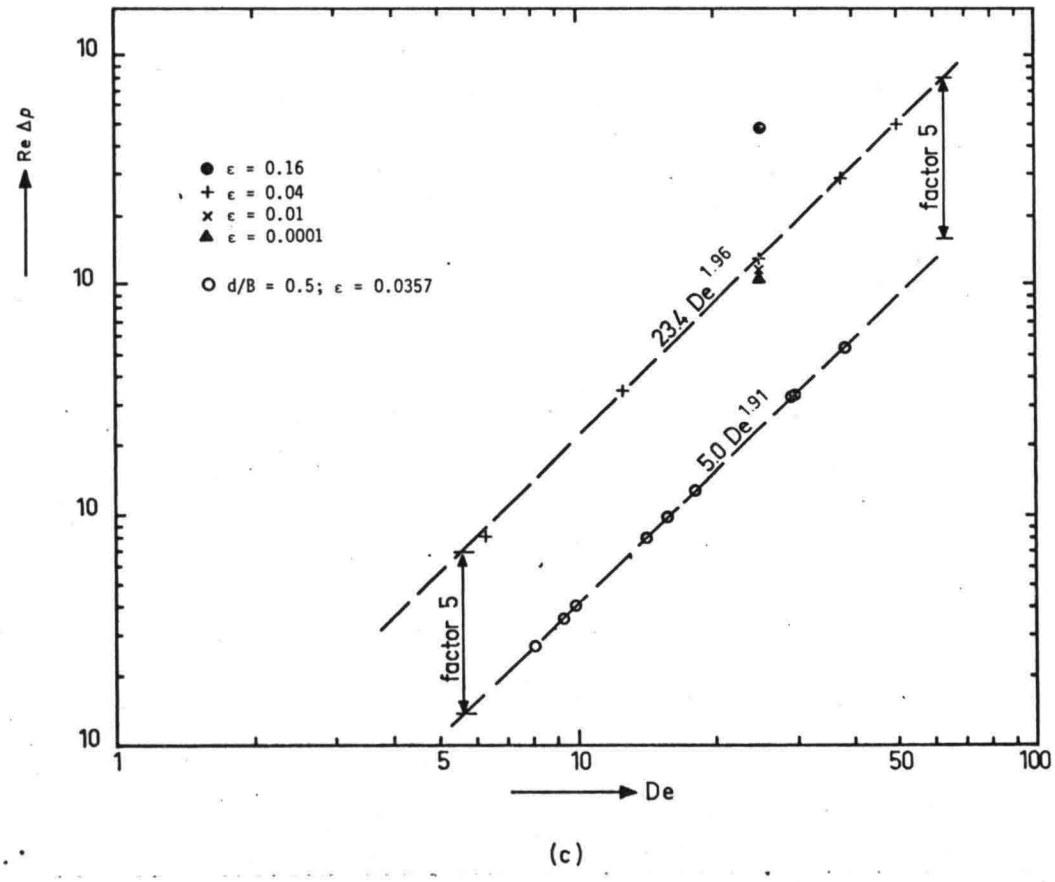


(c)

Figure 14. Influence of the Dean number on the transverse pressure distribution in a shallow channel
(a) Total pressure at the bottom
(b) Total pressure in the verticals $\xi=-2.5$, $\xi=0$ and $\xi=2.5$
(c) Transverse pressure drop

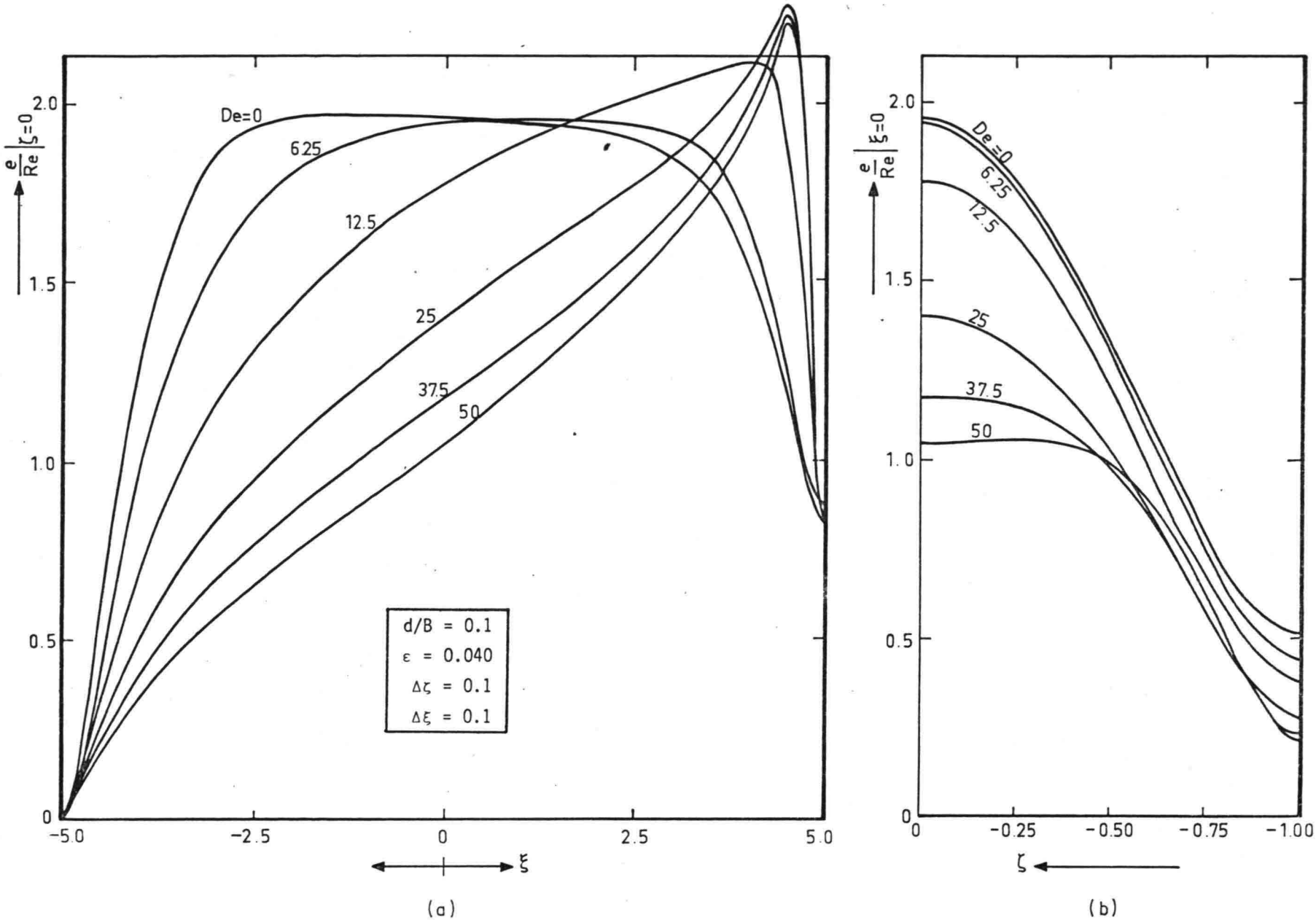


Figure 15. Influence of the Dean number on the total energy in a shallow channel
(a) Total energy at the surface
(b) Total energy in the centreline

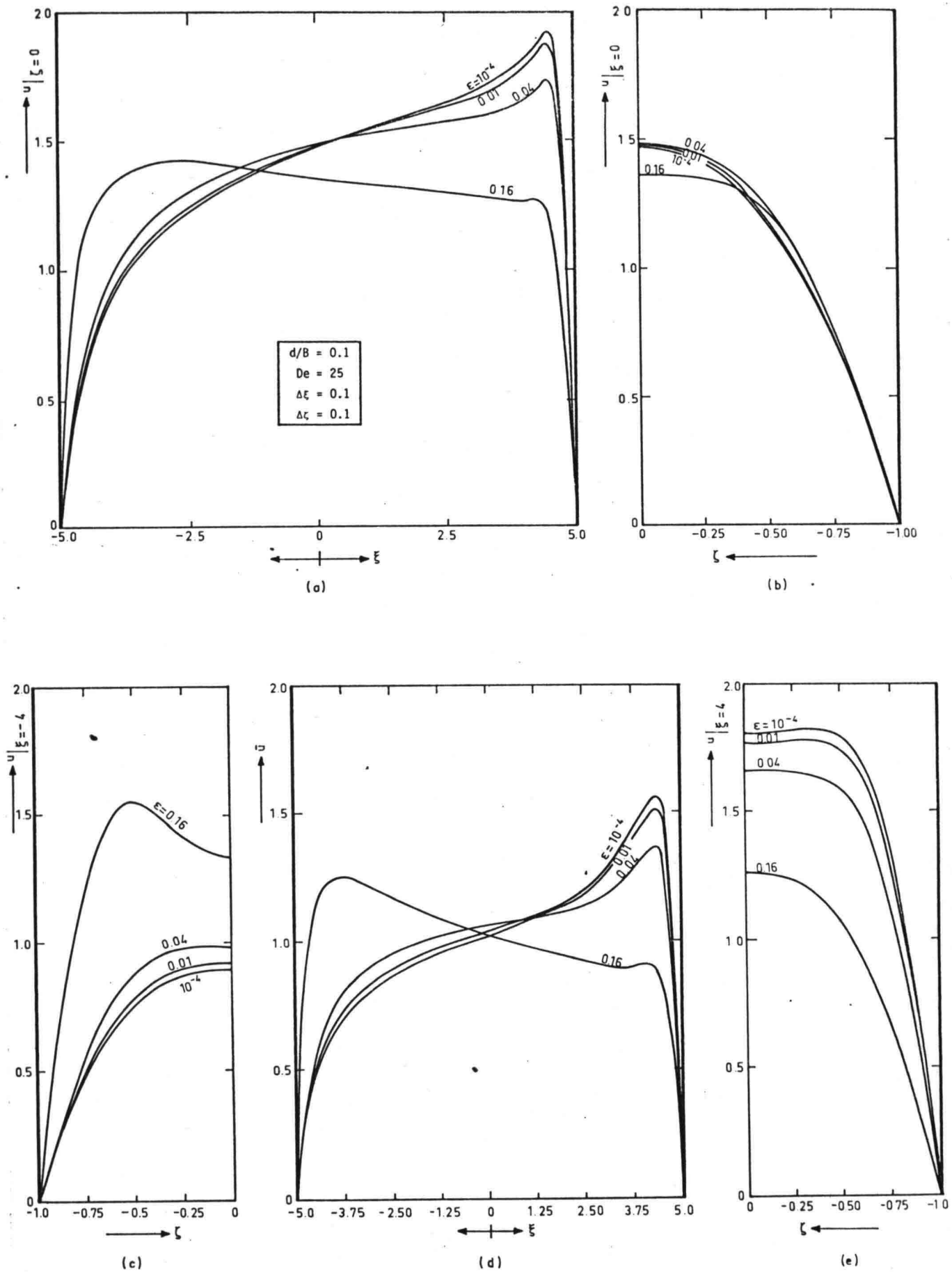


Figure 16. Influence of the curvature ratio on the flow in a shallow channel
(a) Main velocity at the surface
(b) Main velocity in the centreline
(c) Main velocity near the inner wall
(d) Mean velocity
(e) Main velocity near the outer wall

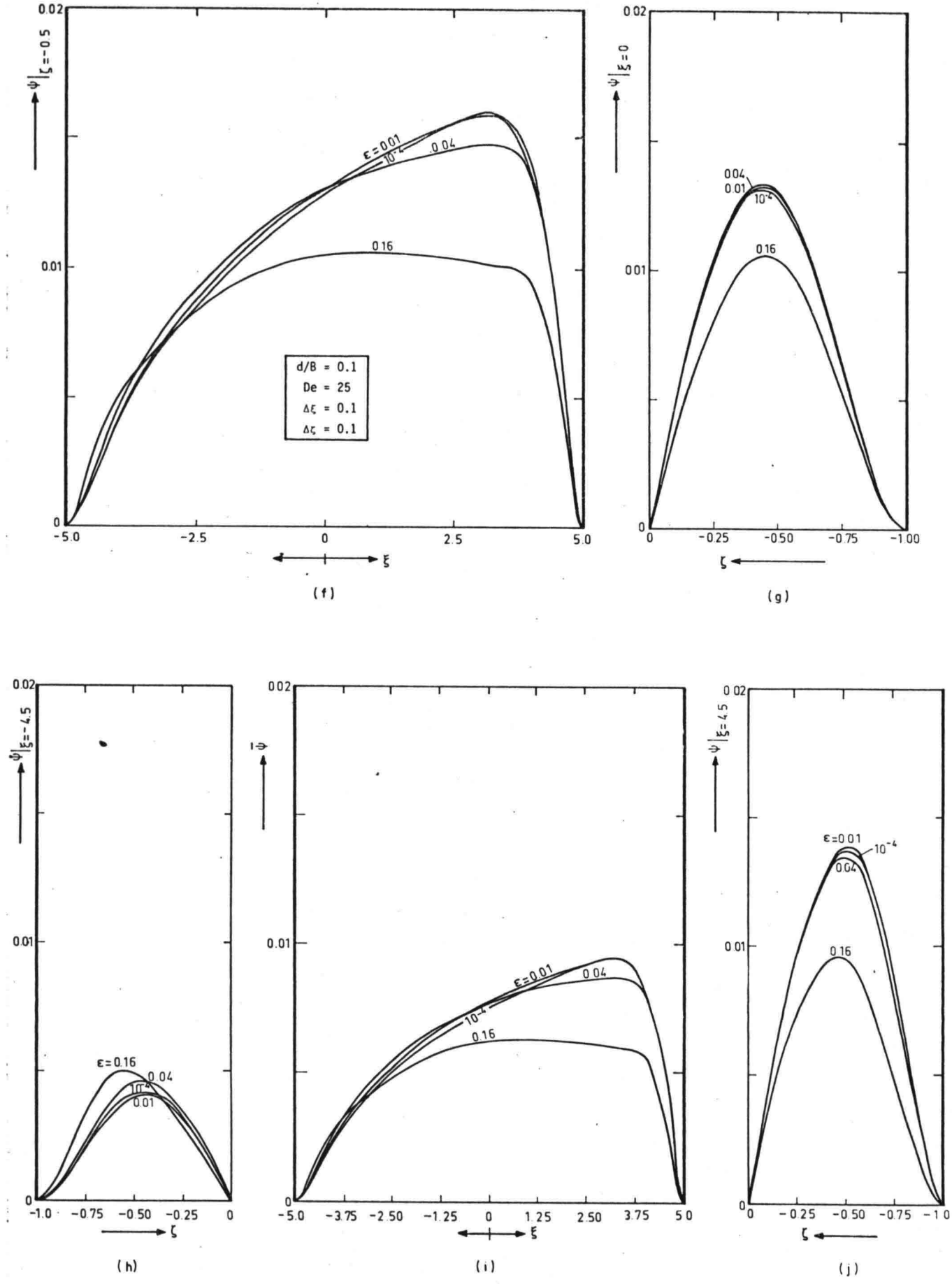


Figure 16. Influence of the curvature ratio on the flow in a shallow channel
(f) Stream function at half depth
(g) Stream function in the centreline
(h) Stream function near the inner wall
(i) Mean stream function
(j) Stream function near the outer wall

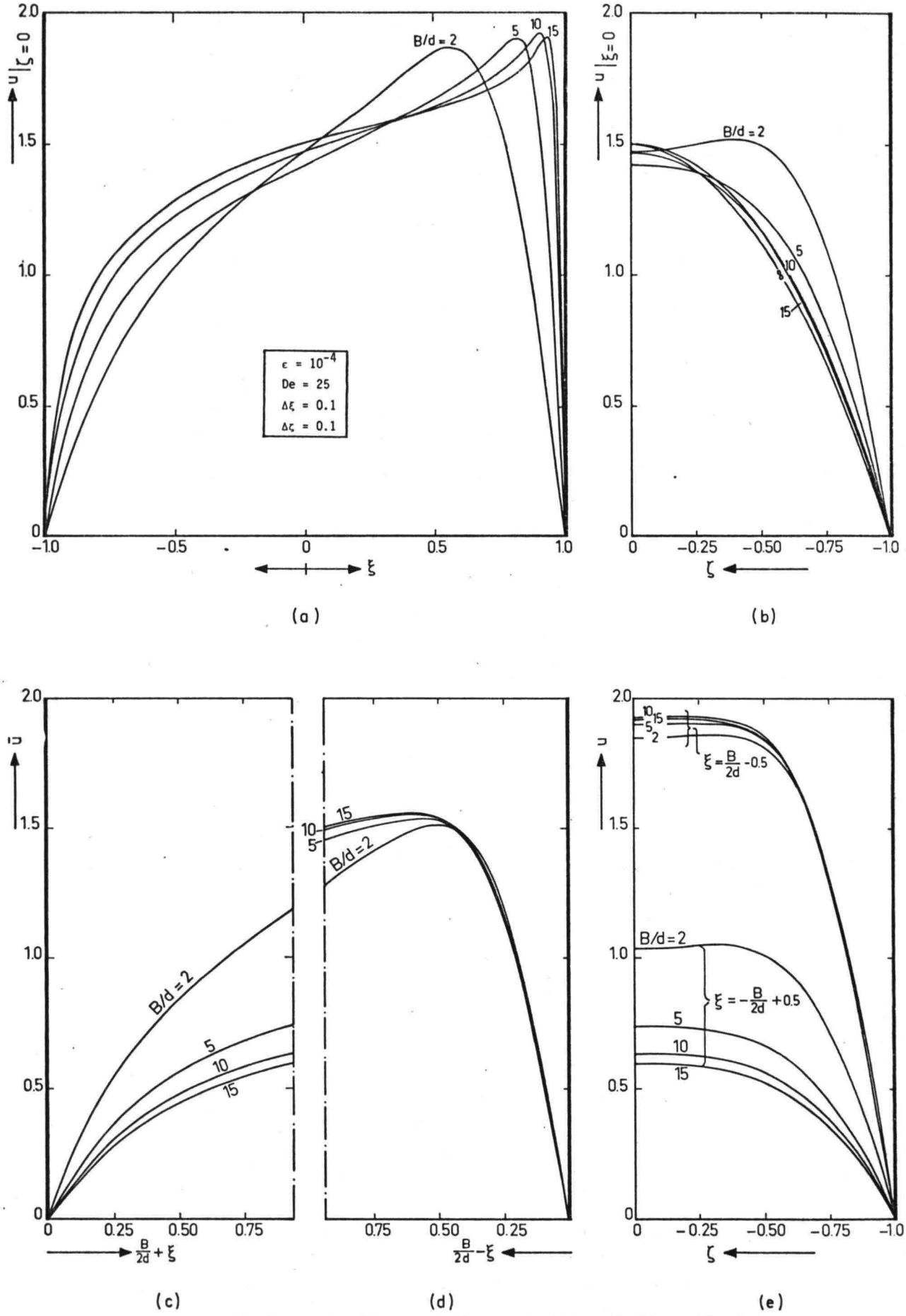


Figure 17. Influence of the channel aspect ratio:
(a) Main velocity at the surface
(b) Main velocity in the centreline
(c) Mean velocity near the inner wall
(d) Mean velocity near the outer wall
(e) Main velocity near the sidewalls

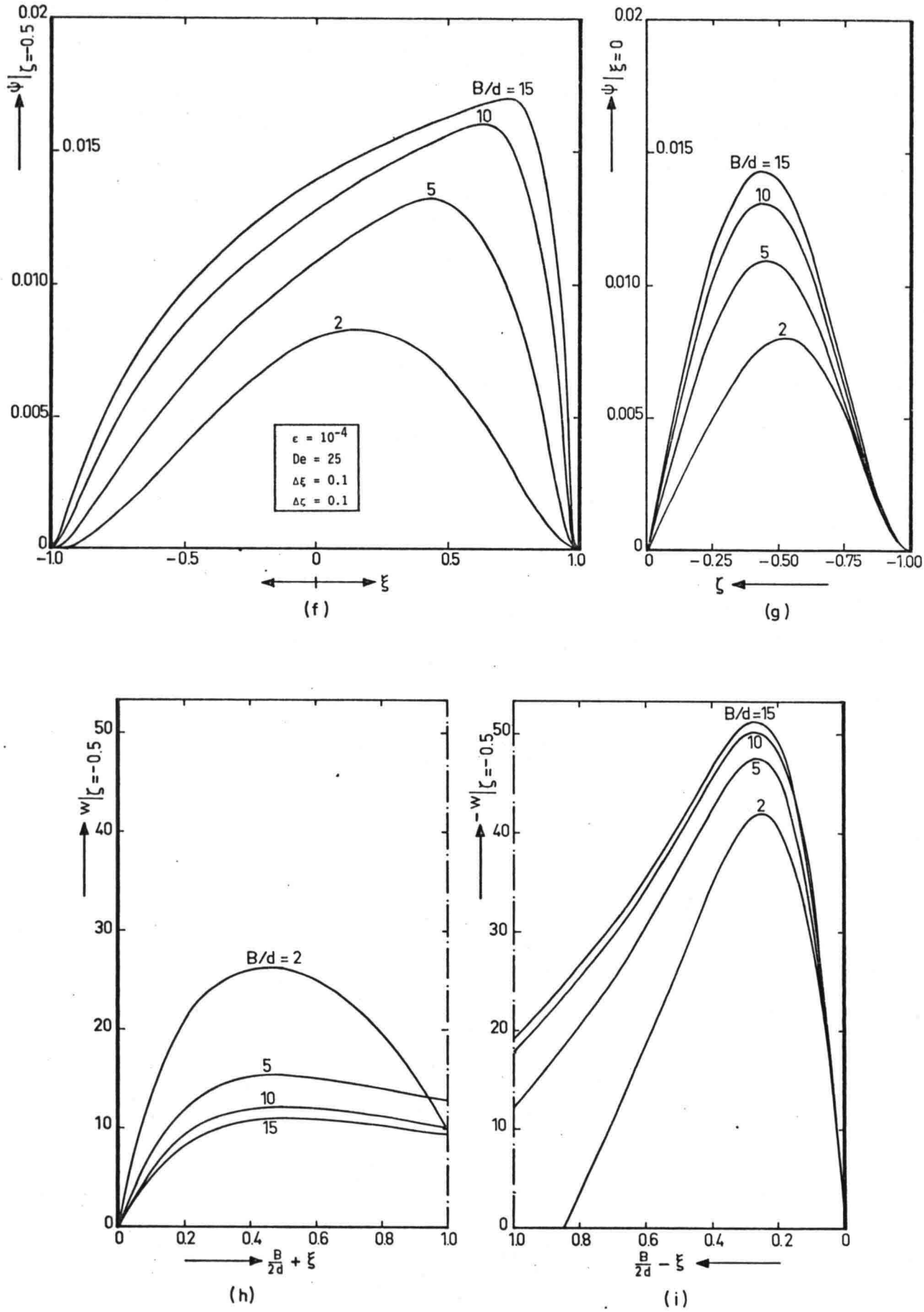


Figure 17. Influence of the channel aspect ratio.
(f) Stream function at half depth
(g) Stream function in the centreline
(h) Vertical velocity near the inner wall
(i) Vertical velocity near the outer wall

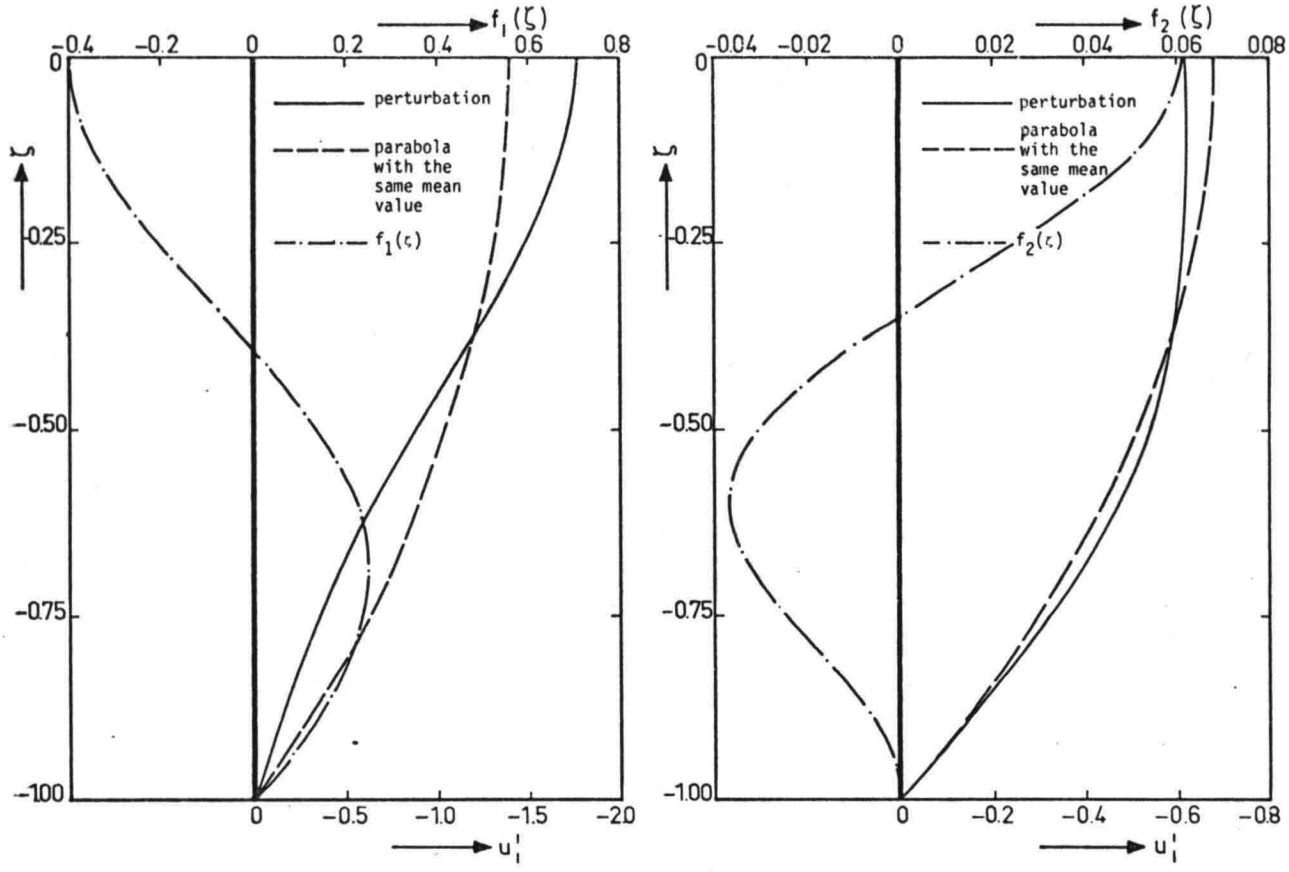


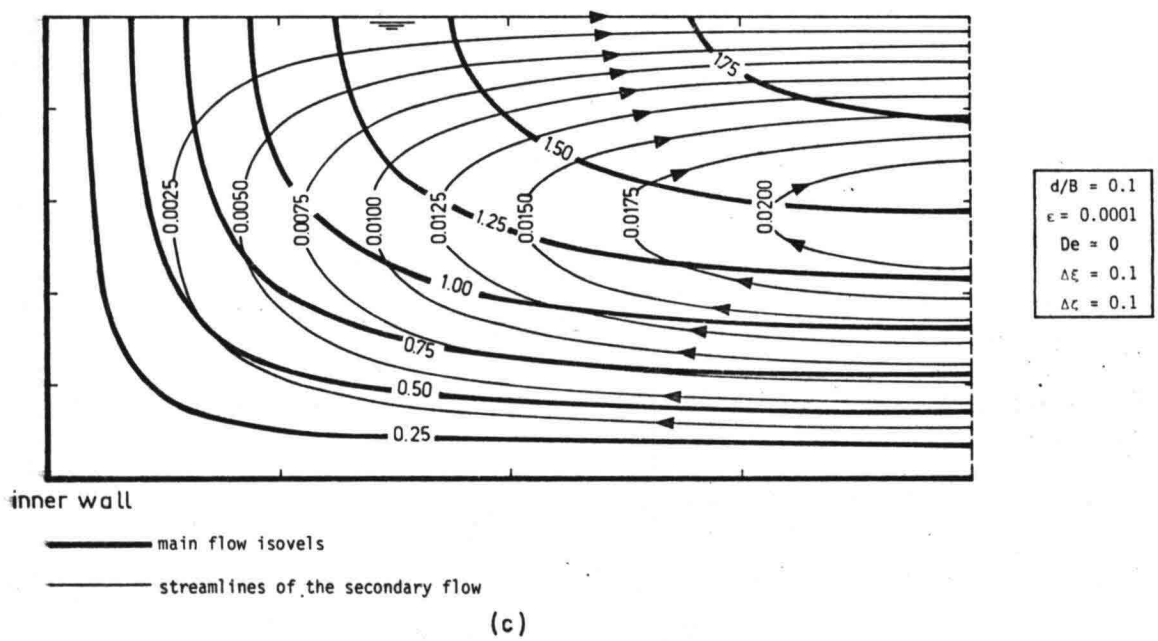


Figure 18. Perturbation of the main velocity due to advection
(a) Vertical distribution of the perturbation due to radial advection
(b) Vertical distribution of the perturbation due to vertical advection
(c) Main flow isovels and secondary flow streamlines

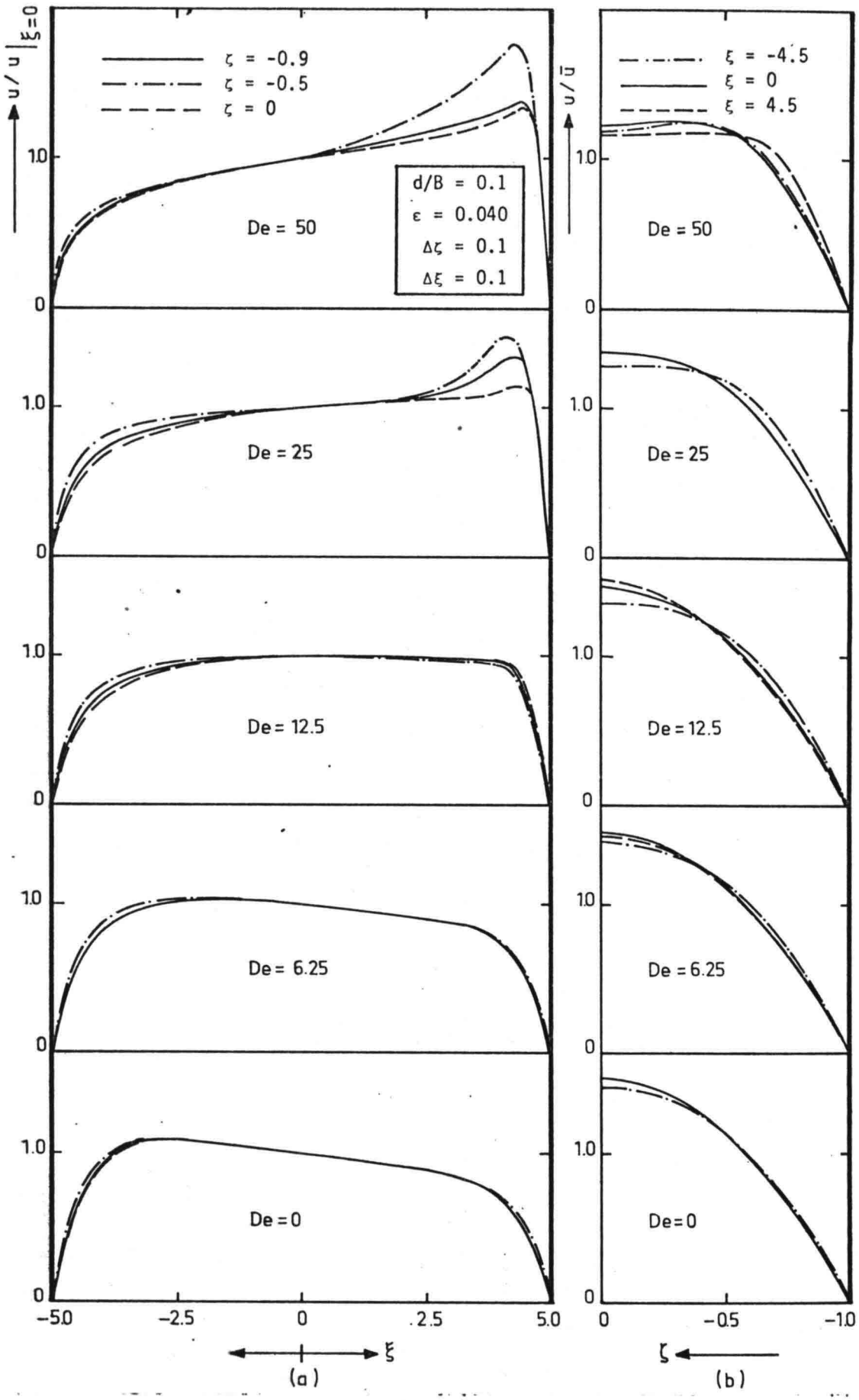


Figure 19. Similarity of the main velocity distribution
(a) Vertical similarity
(b) Radial similarity

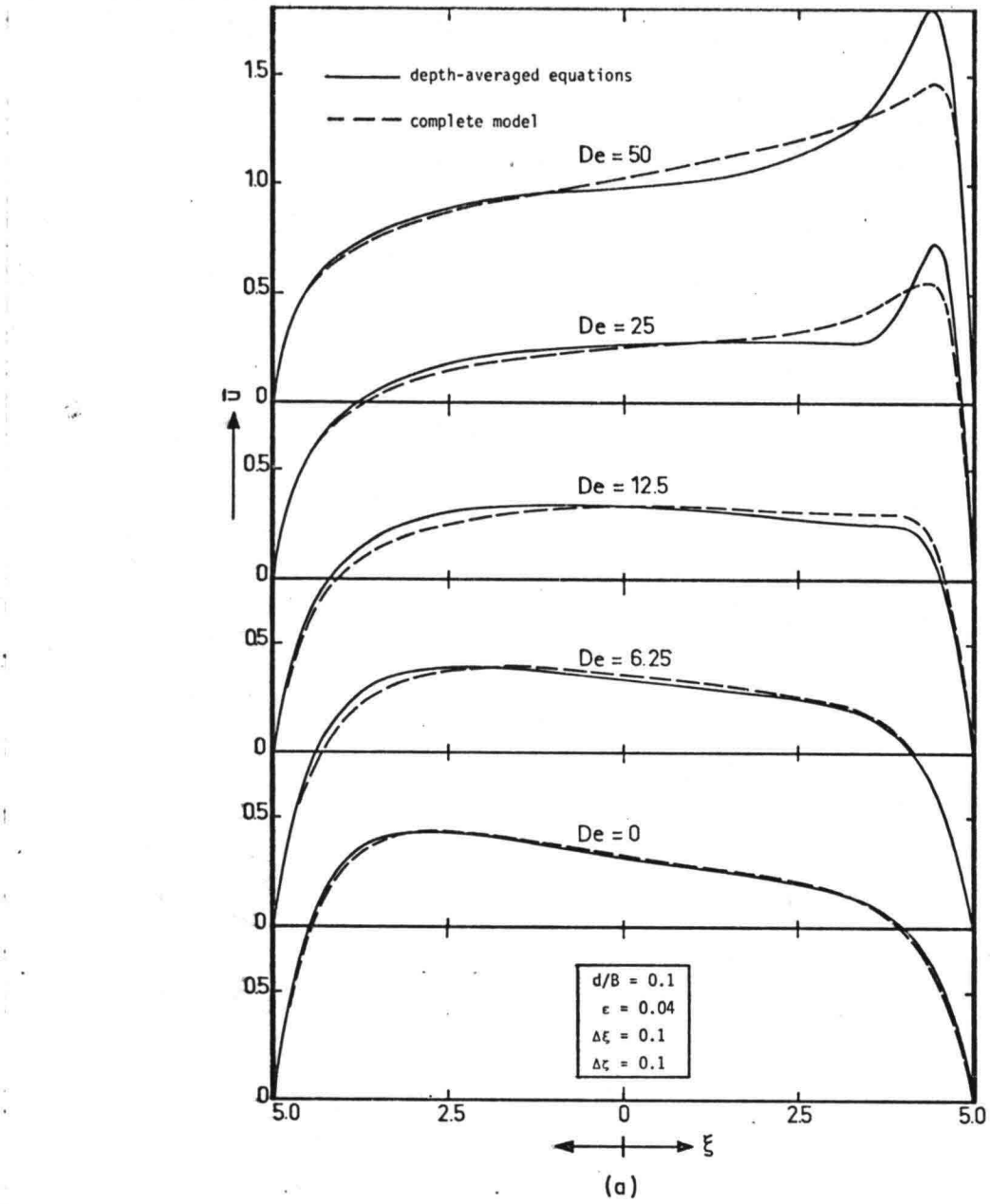


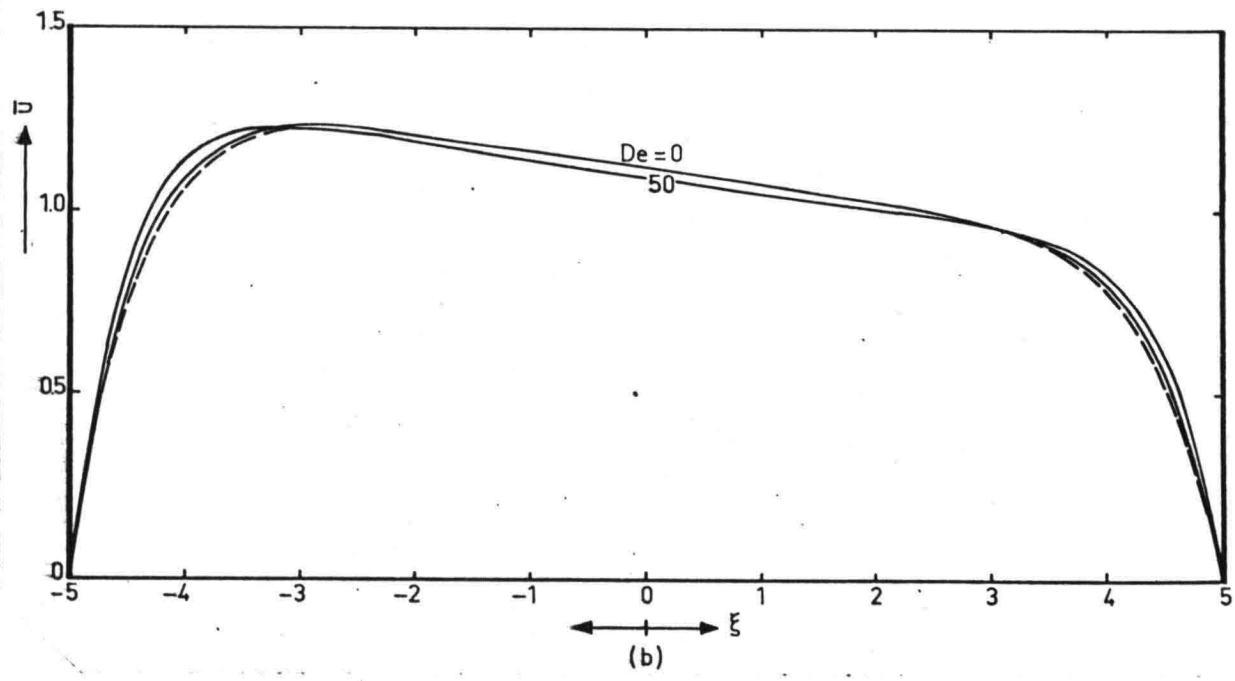


Figure 20. Depth-averaged computation of the main velocity
(a) All advection terms included
(b) All advection terms neglected

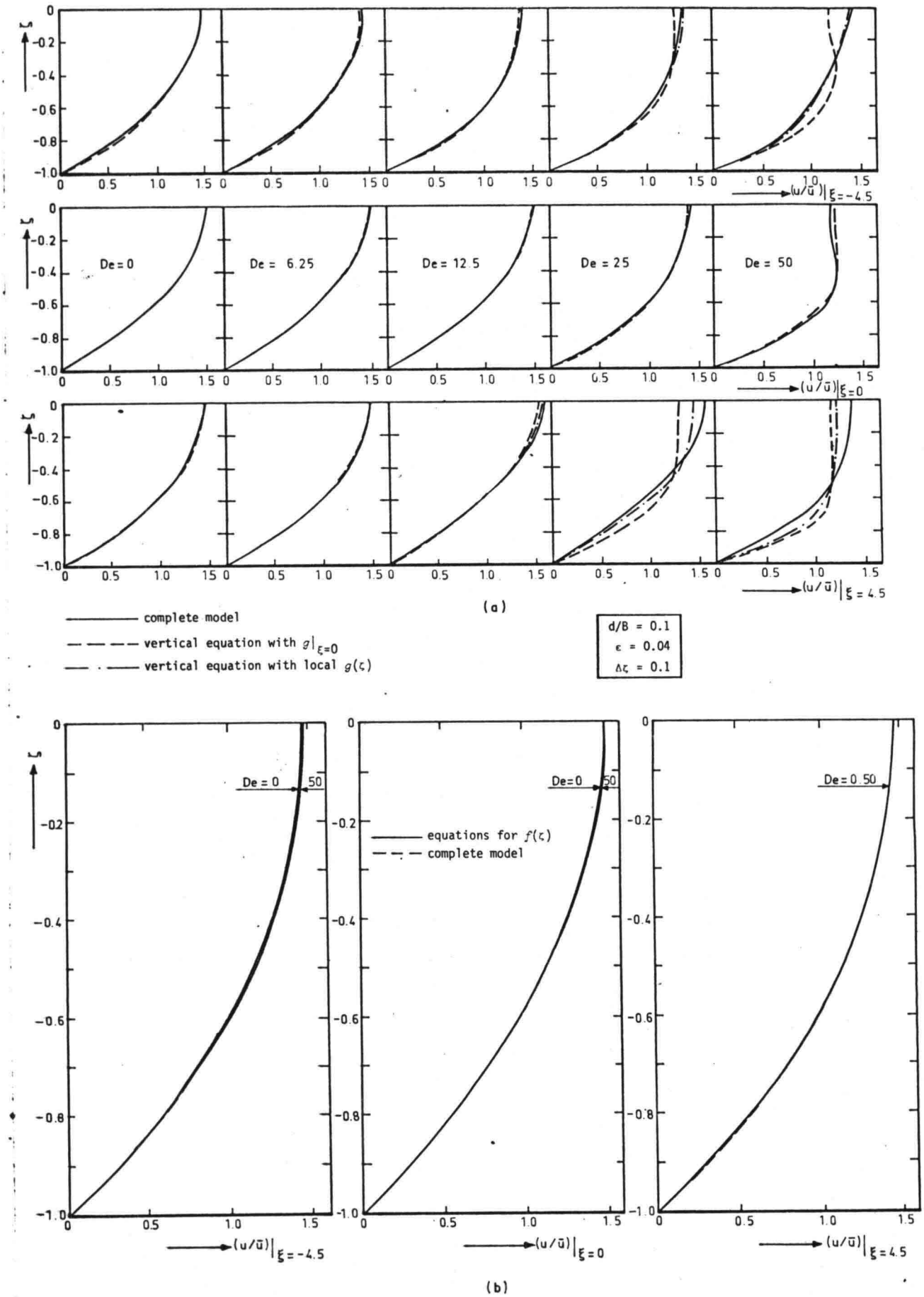


Figure 21. Separate computation of the vertical distribution of the main velocity
(a) All terms of the equation included
(b) All advection terms neglected

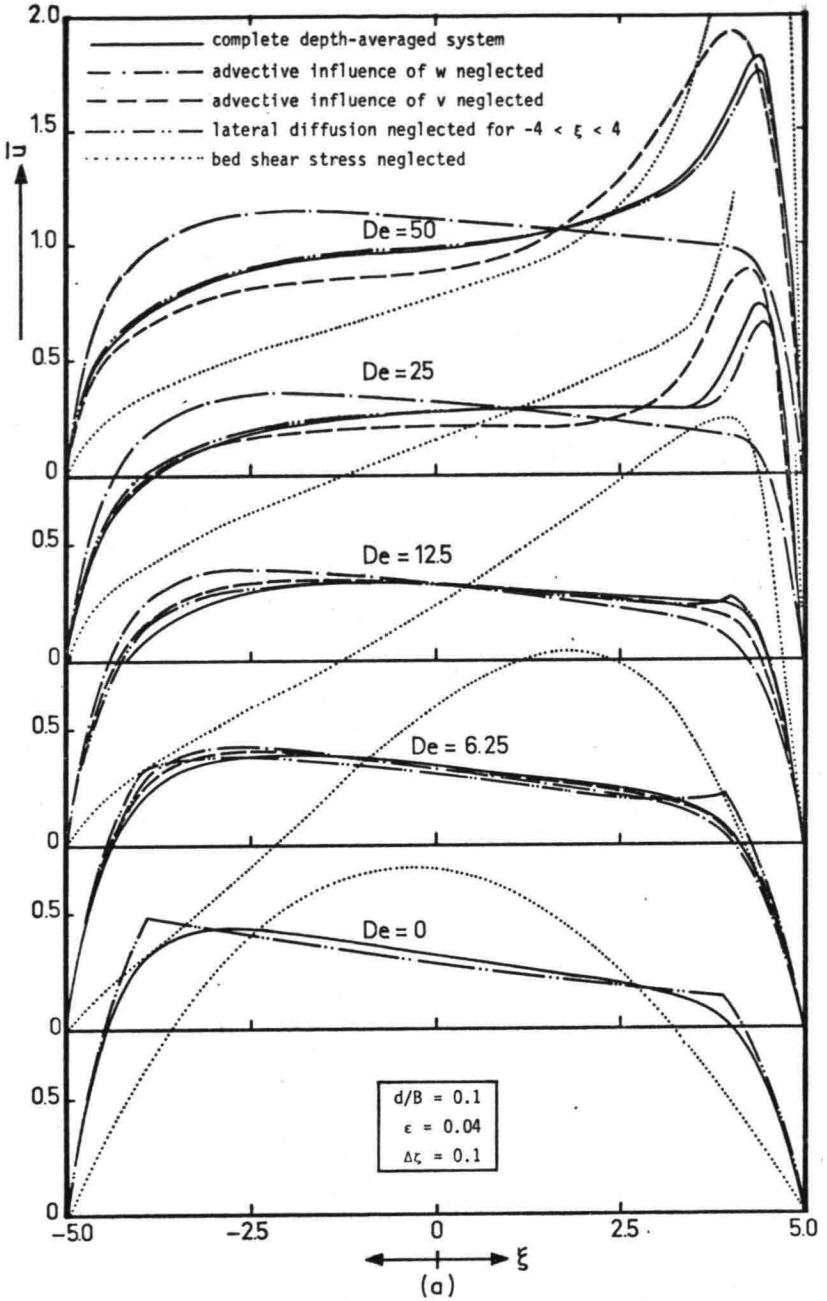


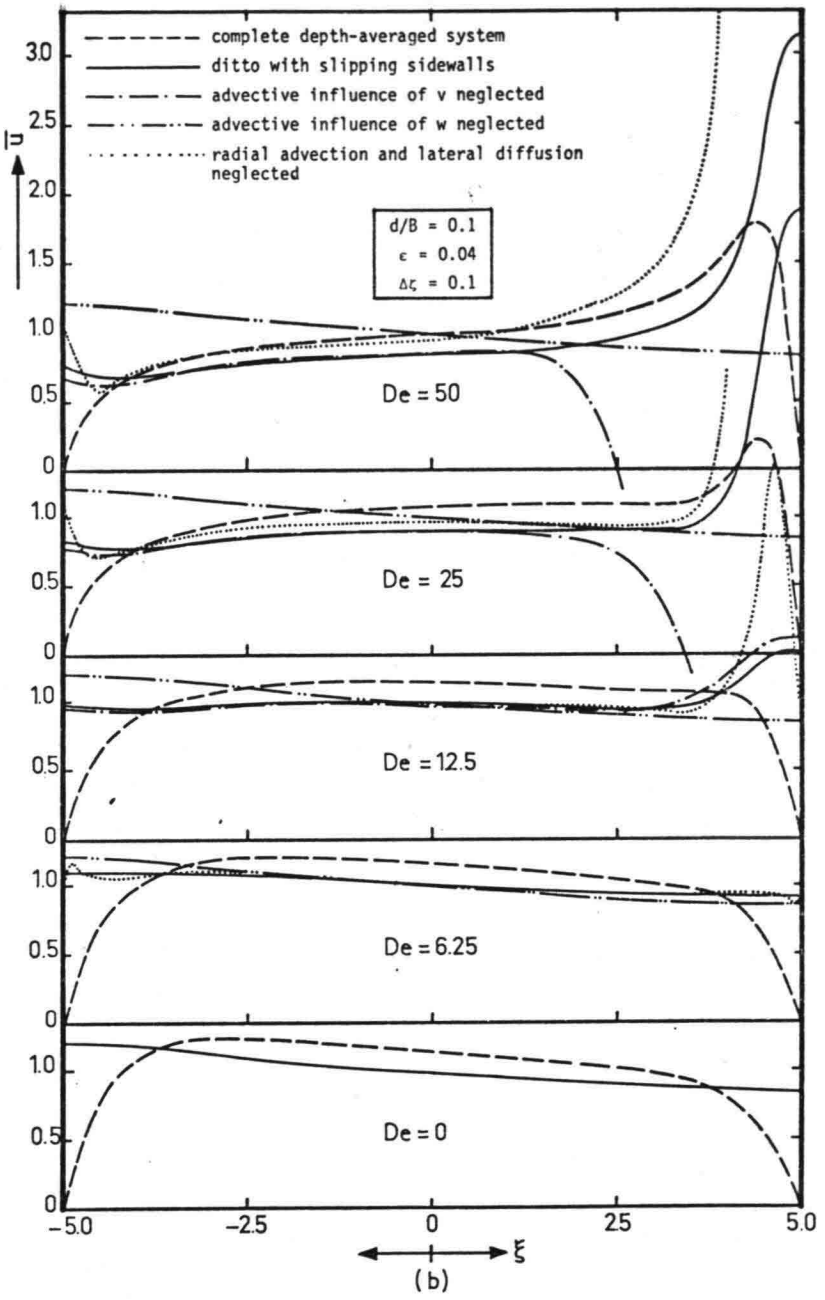


Figure 22. Analysis of the mean velocity distribution
(a) Separate influence of the secondary velocity components, lateral diffusion and the bed shear stress
(b) Separate influence of the secondary velocity components in case of slipping sidewalls

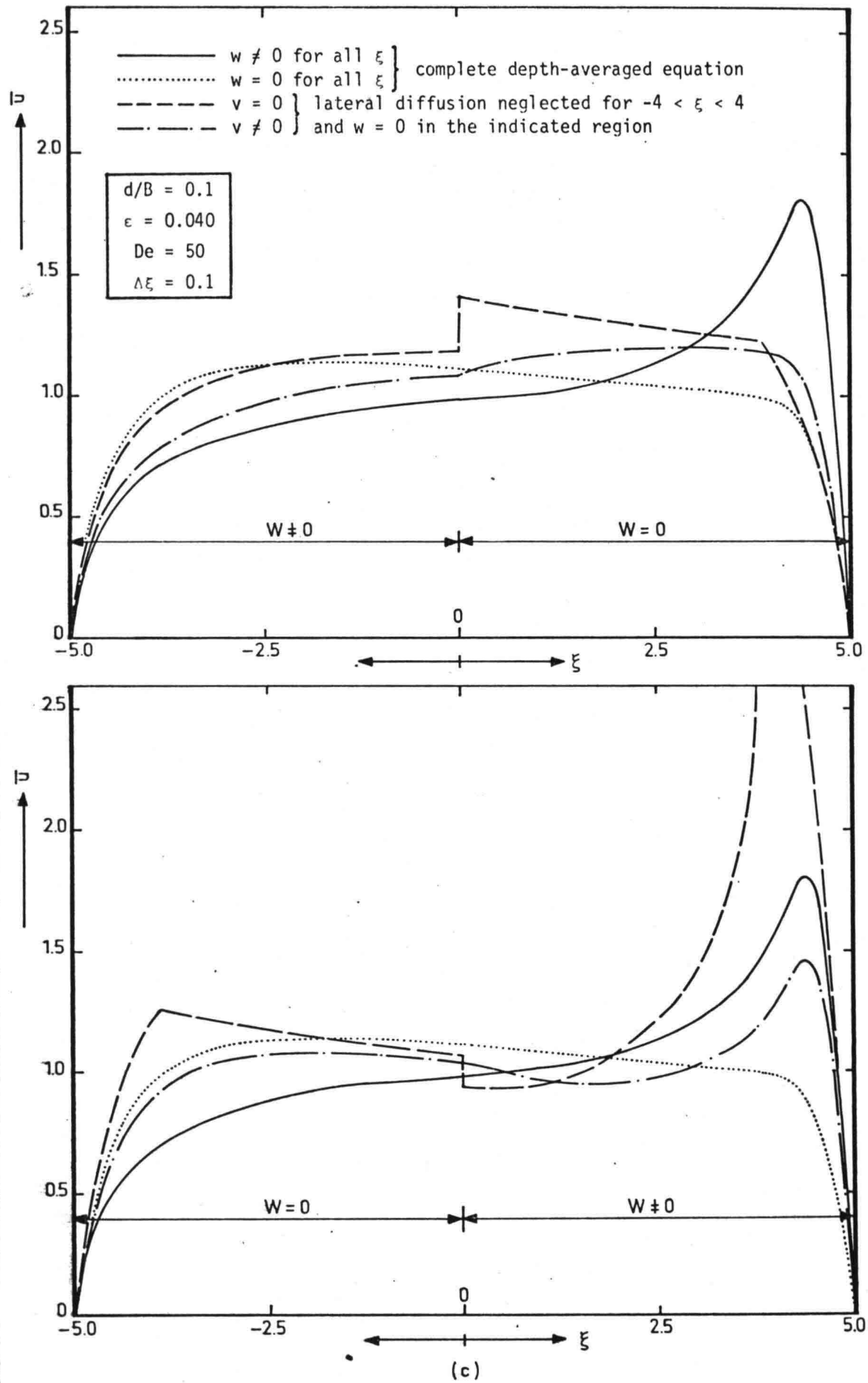


Figure 22. Analysis of the mean velocity distribution
(c) Retardation effect of radial advection

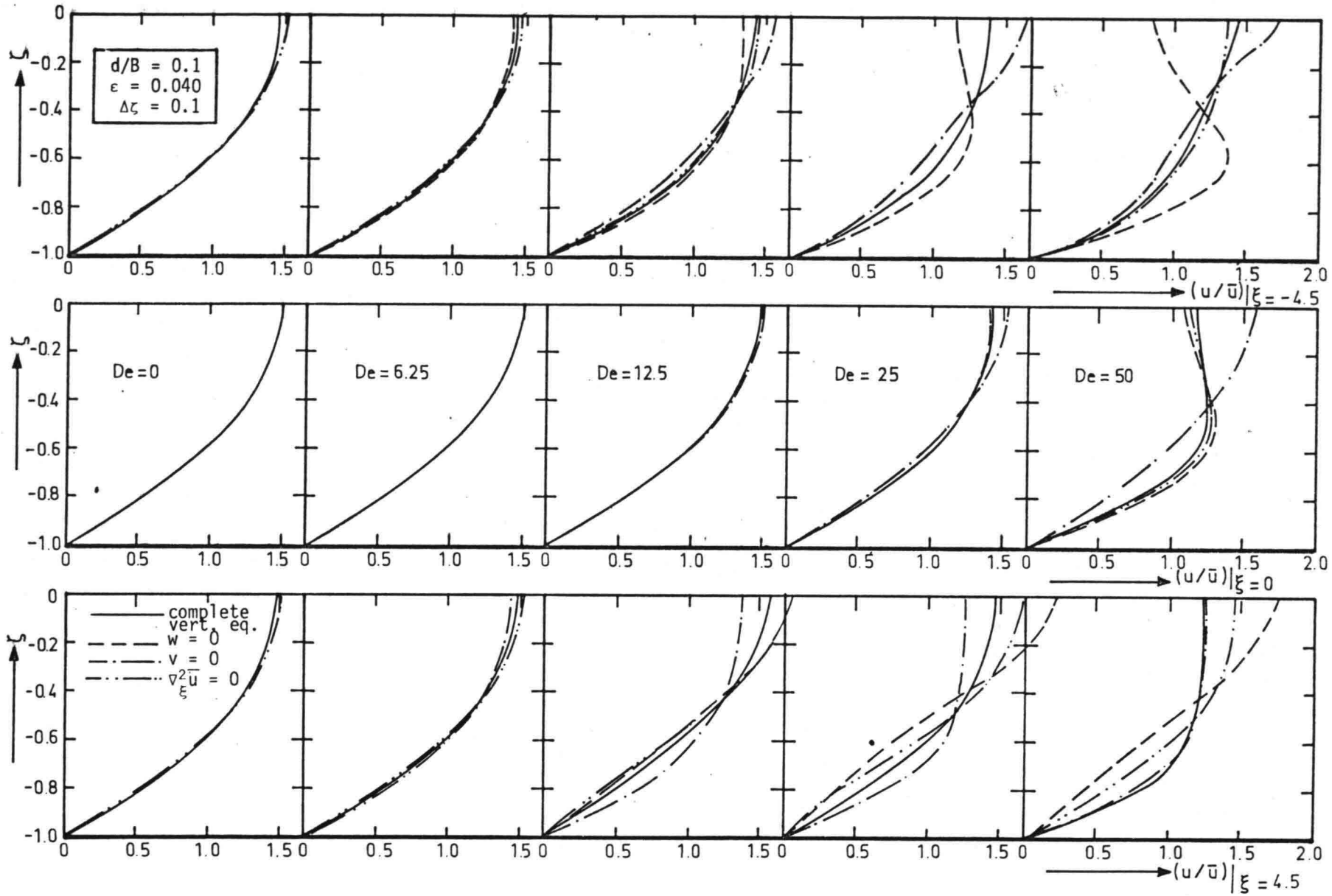


Figure 23. Analysis of the vertical redistribution of the main velocity

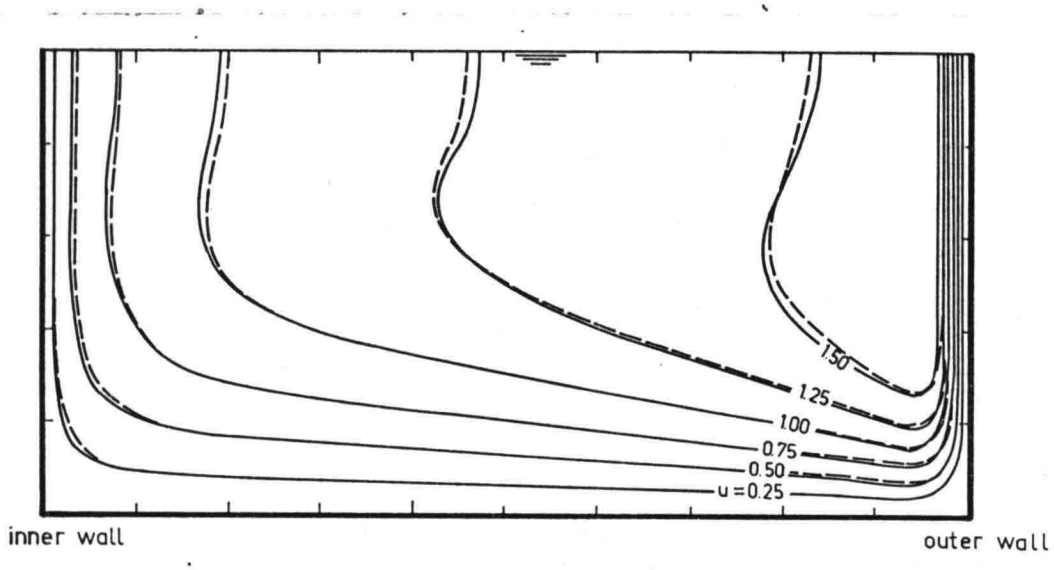


(a)

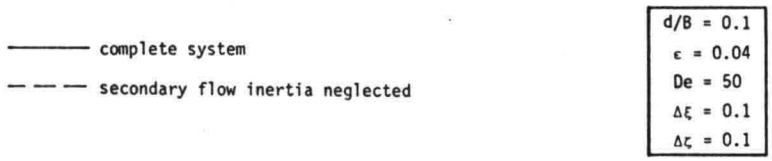


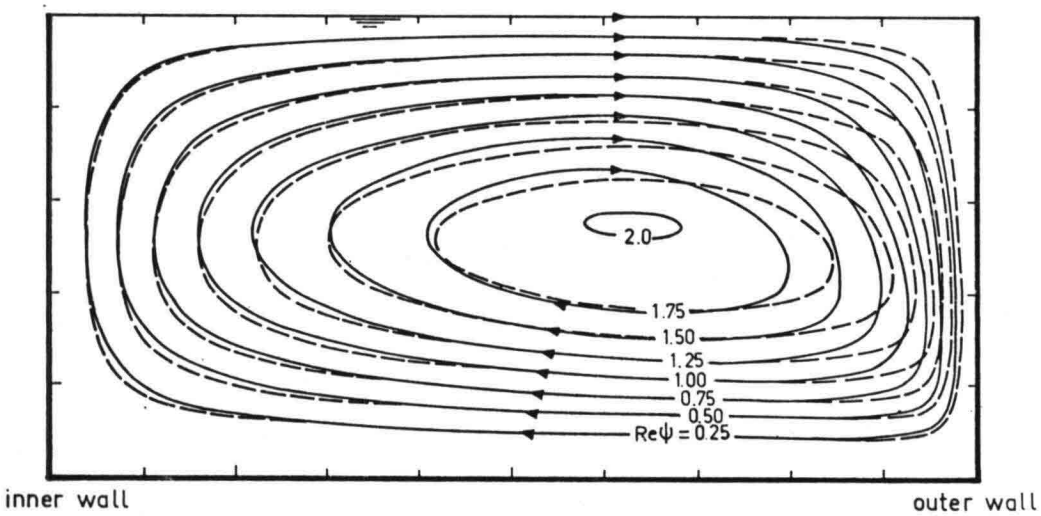


(b)

Figure 24. Influence of secondary flow inertia on the flow in a shallow channel
(a) Main velocity isovels
(b) Streamlines of the secondary flow

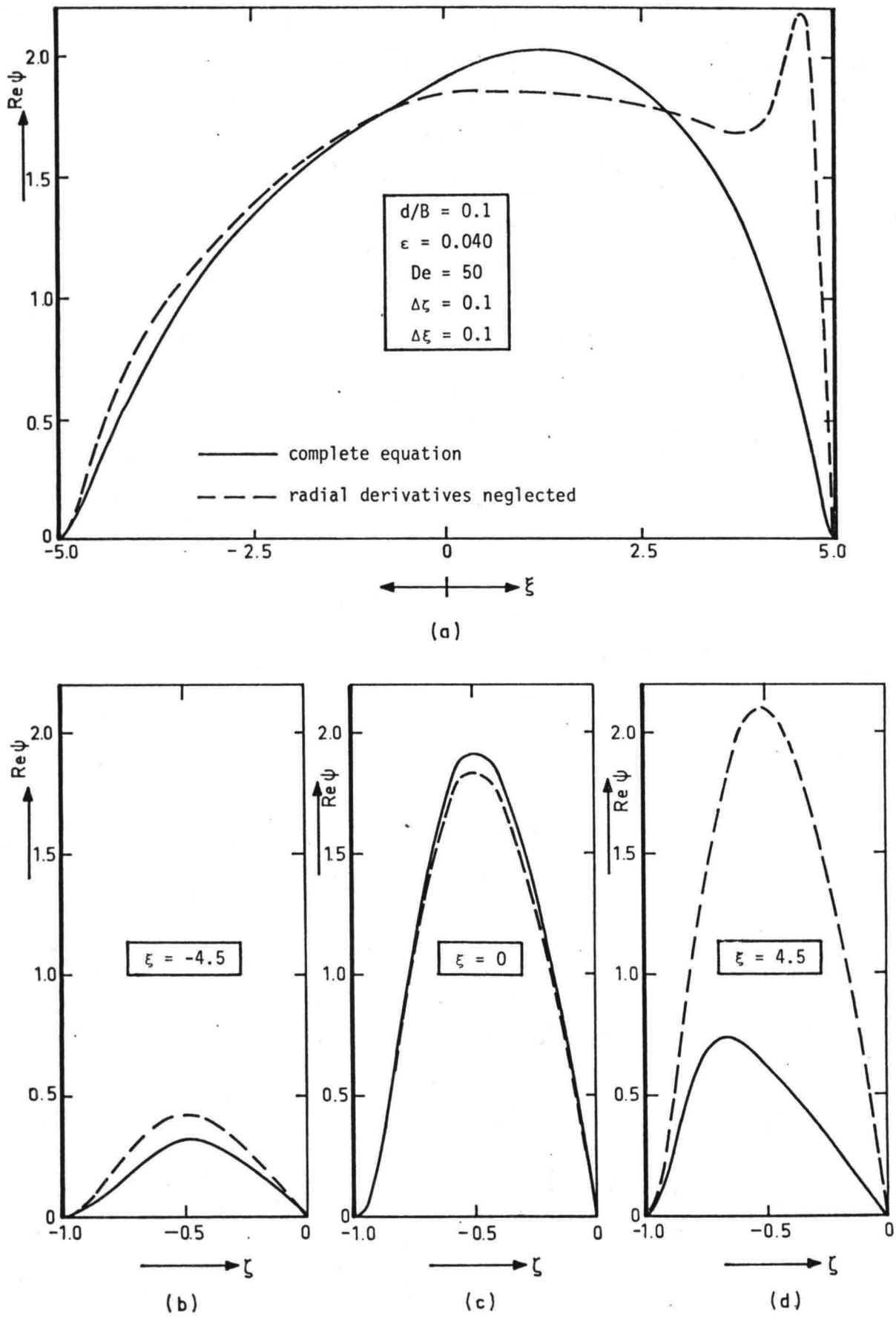


Figure 25. Influence of neglecting all radial derivatives in the stream function equation in case of a given main velocity distribution
(a) Radial distribution of the stream function at half depth
(b)-(d) Vertical distributions of the stream function

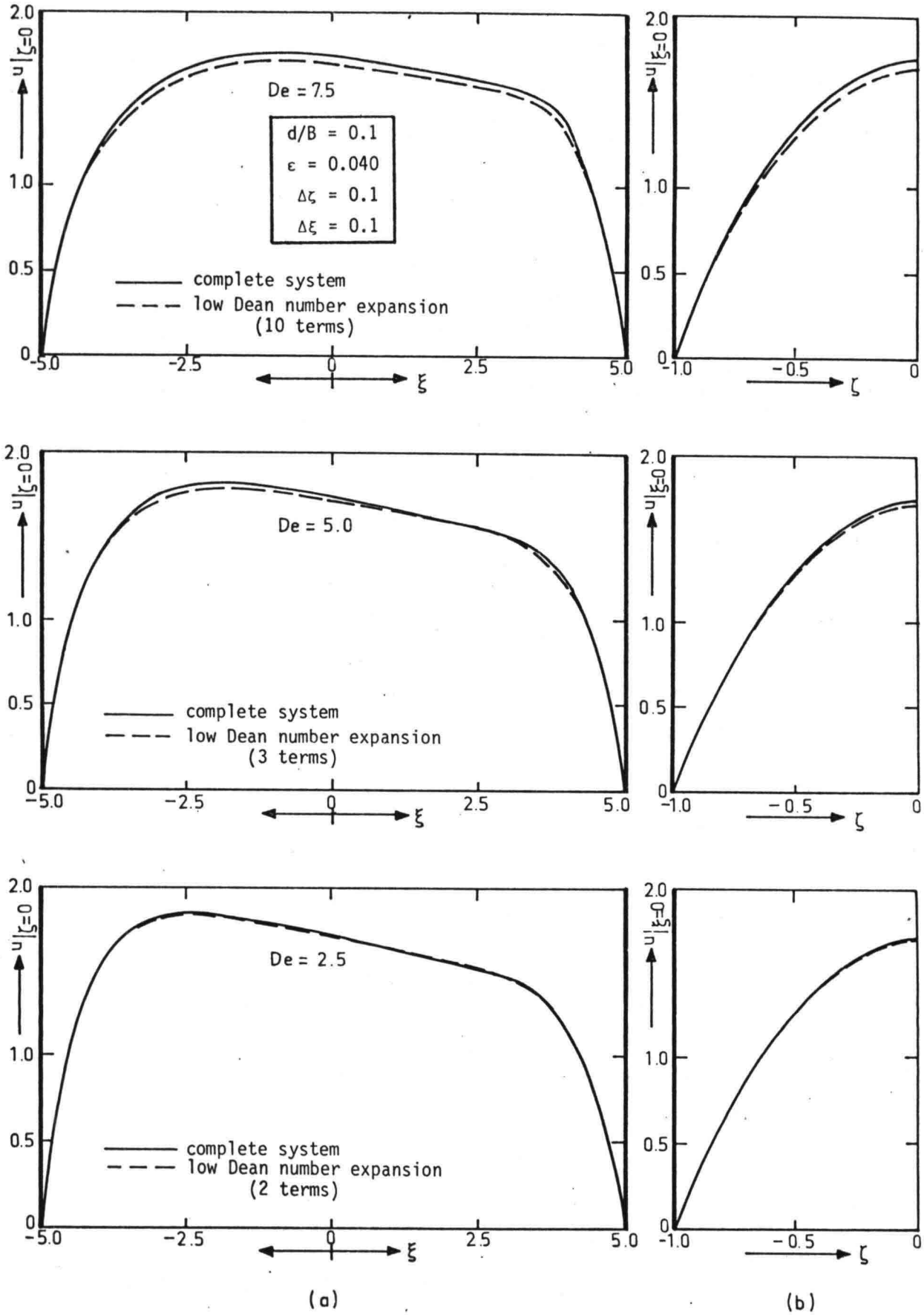


Figure 26. Successive approximation of the main velocity by low Dean number perturbations in the whole cross-section
(a) Main velocity at the surface
(b) Main velocity in the channel axis

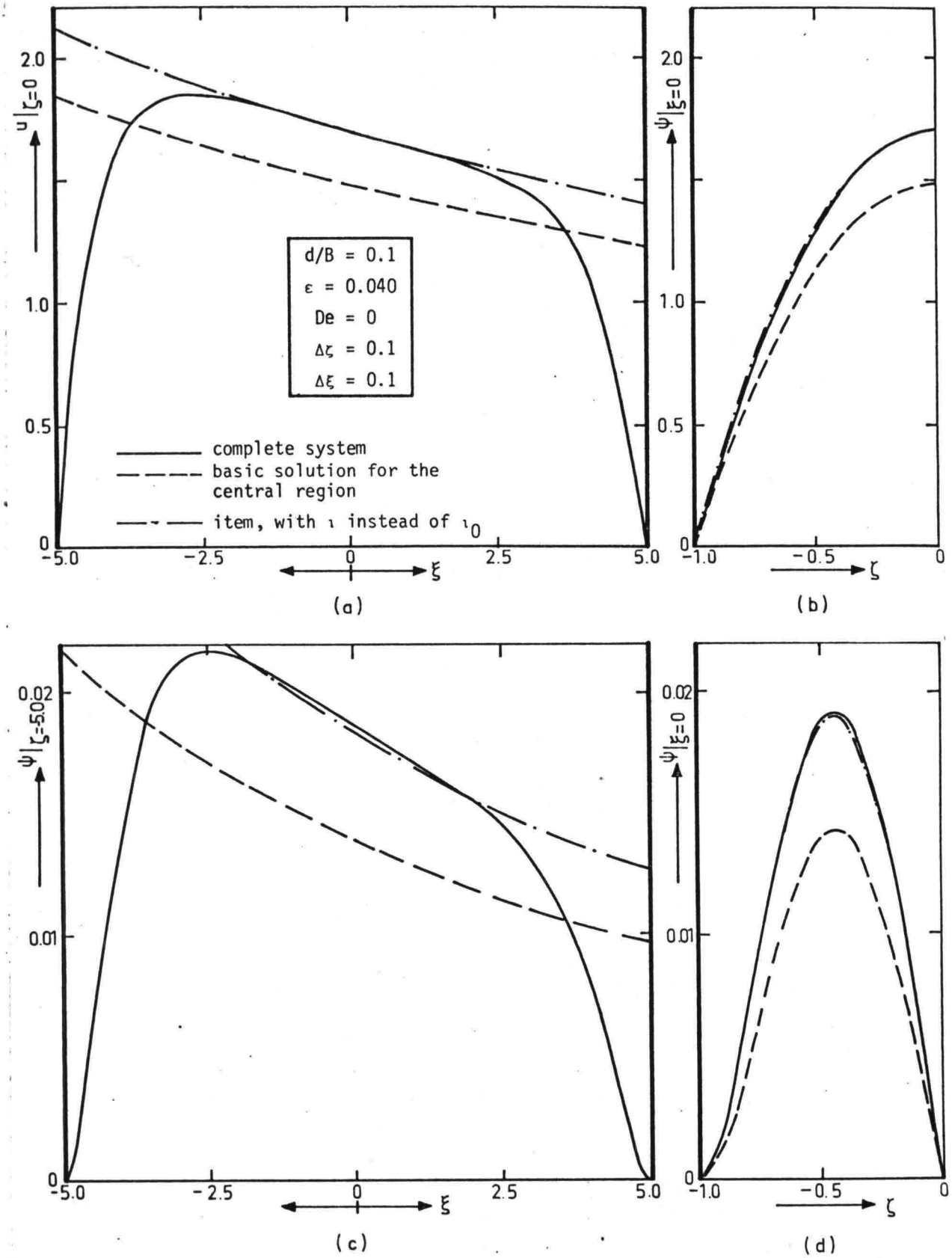


Figure 27. Basic solution for the central region
(a) Radial distribution of the main velocity at $\zeta=0$
(b) Vertical distribution of the main velocity at $\xi=0$
(c) Radial distribution of the stream function at $\zeta=-0.5$
(d) Vertical distribution of the stream function at $\xi=0$

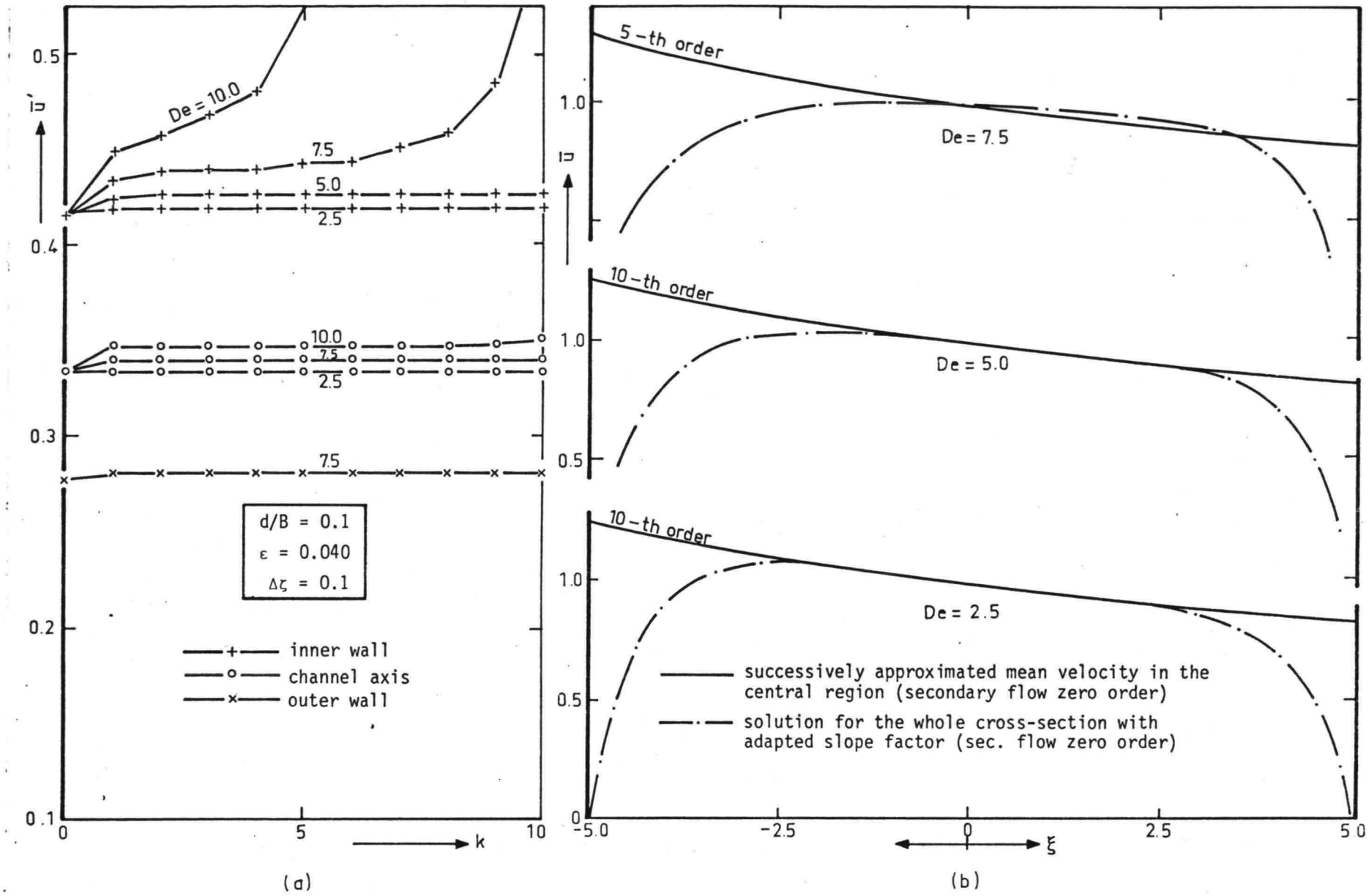


Figure 28. Successive approximation of the main velocity in the central region
(a) Convergence
(b) Mean velocity distribution

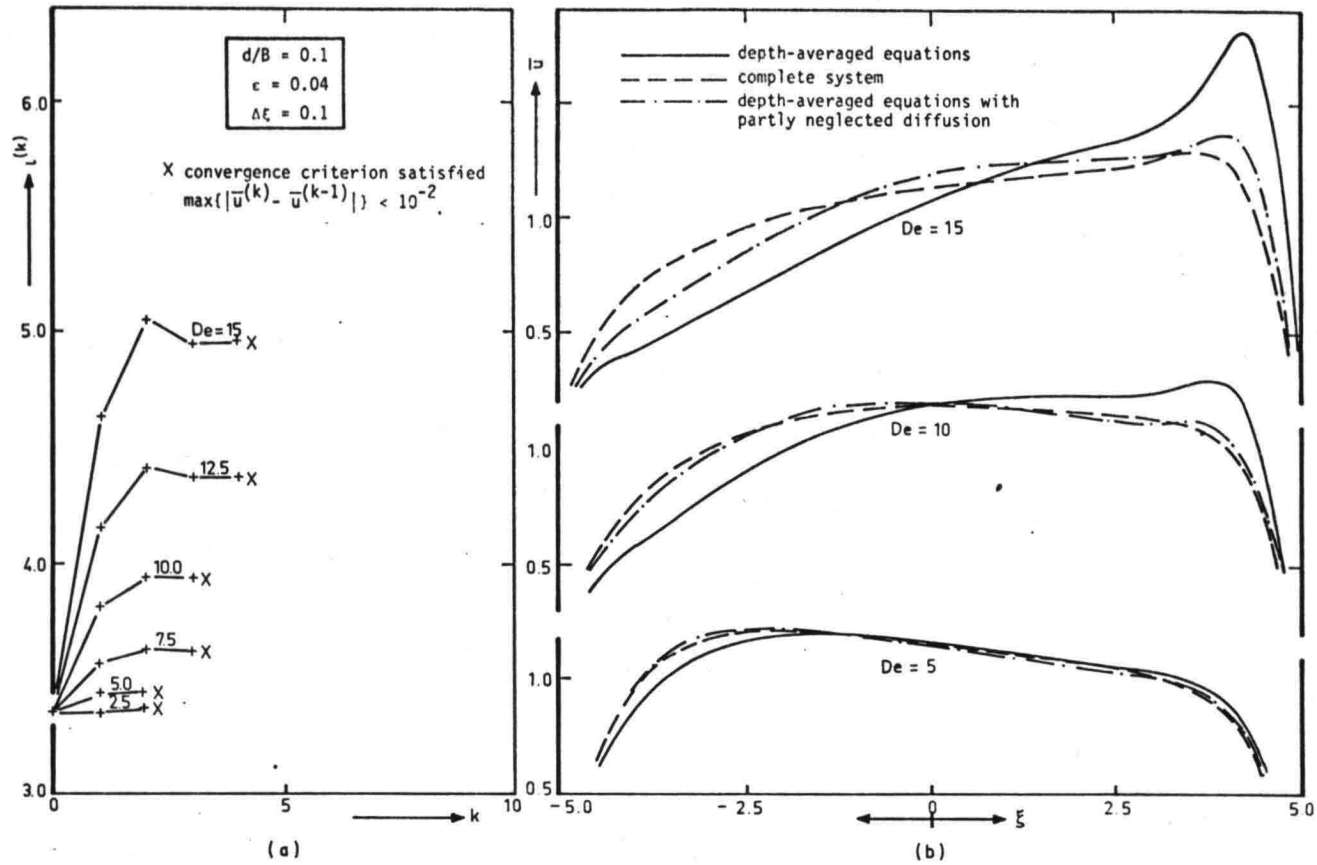


Figure 29. Solution of $\bar{u}$ from depth-averaged equations derived from the low Dean number expansion (zero order approximation of the secondary flow)
(a) Convergence of semi-implicit procedure
(b) Mean velocity distribution

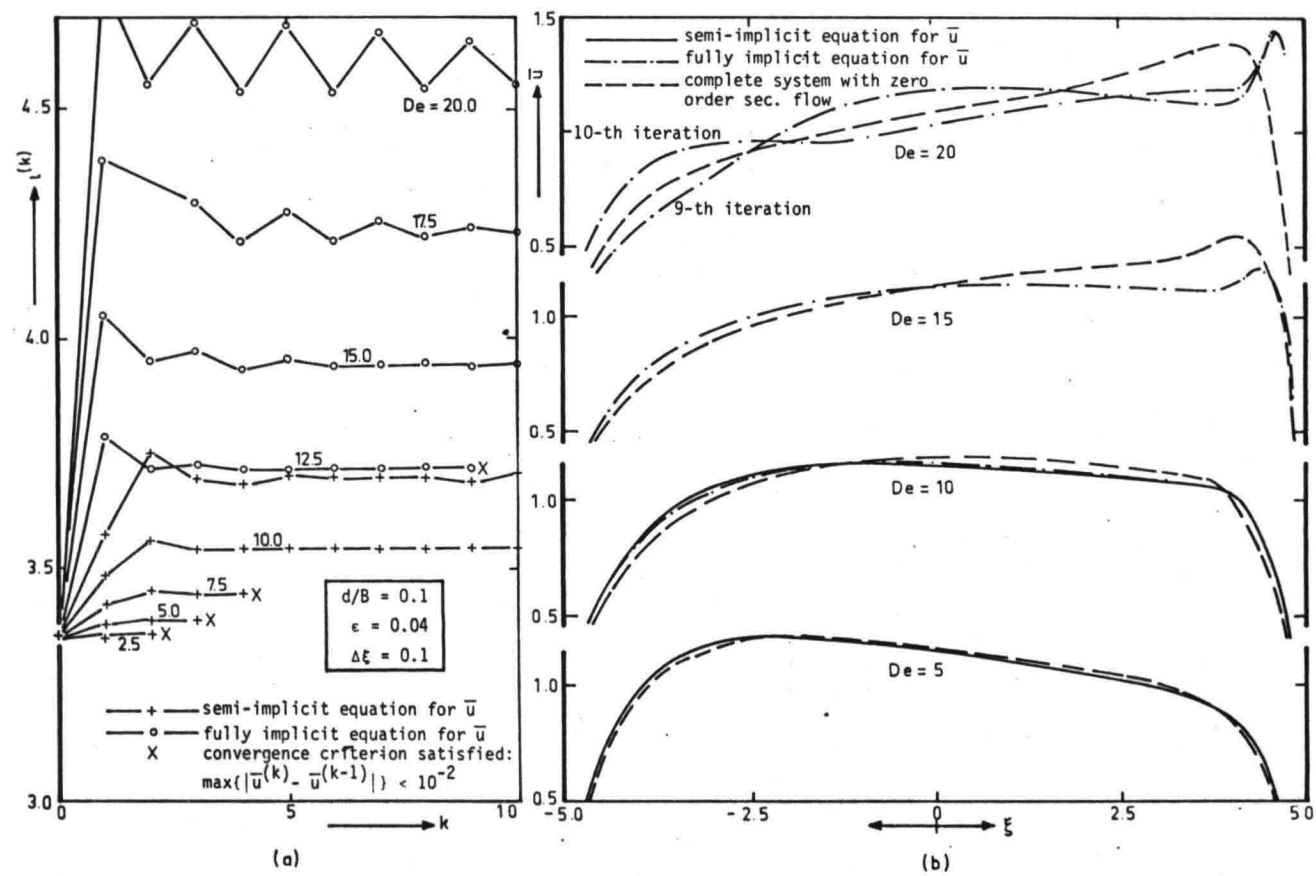


Figure 30. Solution of the depth-averaged equations derived from the low Dean number expansion (secondary flow updated in each iteration step)
(a) Convergence
(b) Mean velocity distribution

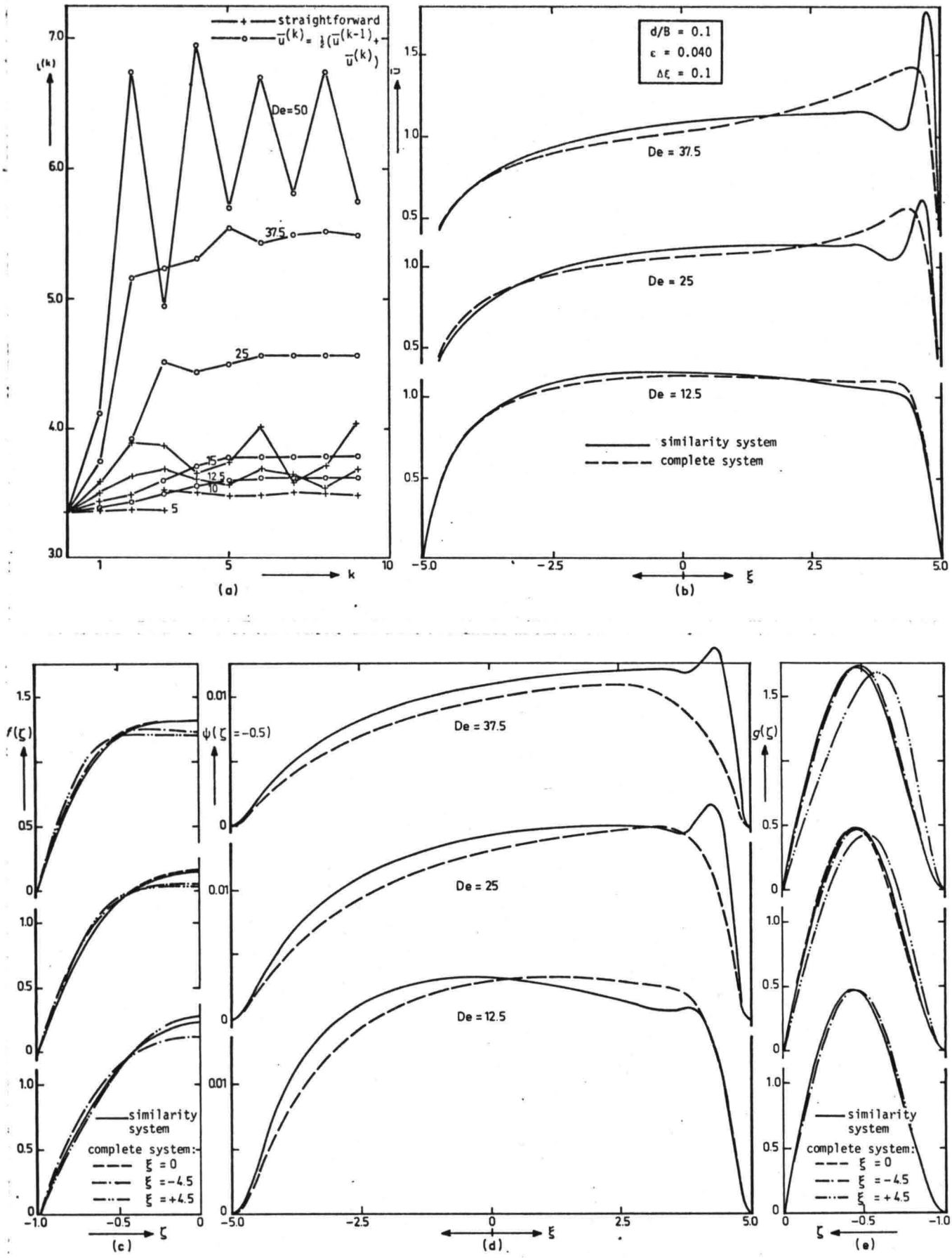


Figure 31. Similarity solution
(a) Convergence
(b) Mean velocity distribution
(c) Vertical distribution of the main velocity
(d) Stream function at half depth
(e) Vertical distribution of the stream function